High-Frequency Shallow Seismic Reflection Characterization of Overburden at an Abandon Pb-Zn Mine Beneath U.S. Highway 69 in Treece, Kansas Using Seismic Imaging and Vp/Vs Ratio

By

Joseph M. Fontana

B.Sc., Southern Methodist University, 2013

B.A., Southern Methodist University, 2013

Submitted to the graduate degree program in Geology

and the Graduate Faculty of the University of Kansas in partial

fulfillment of the requirements for the degree of Master of Science.

_____

Chair: Richard Miller

_____

Ross Black

_____

Jennifer Roberts

Date Defended: August 31, 2017

The thesis committee for Joseph M. Fontana

certifies that this is the approved version of the following thesis:

High-Frequency Shallow Seismic Reflection Characterization of Overburden at an Abandon Pb-Zn Mine Beneath U.S. Highway 69 in Treece, Kansas Using Seismic Imaging and Vp/Vs Ratio

_____

Chair: Richard Miller

Date Approved: August 31, 2017

Abstract

Overburden at an abandoned Pb-Zn mine beneath U.S. Highway 69 in Kansas was evaluated using P- and S-wave seismic reflection methods to estimate Vp/Vs ratio. Drilling reports indicate the mine works have lateral spans of unsupported roof rock as large as ~180 m vertically filled with up to ~30 m of water. Past borings encountered roof rock at depths ranging between 58 – 88 m beneath the highway right away. Historical records suggest the mined ore and the highly-fractured chert overburden at this location are part of the Mississippian Boone Fm. KDOT routinely investigates for indications of roof rock failure using elevation surveys and cross-hole seismic surveys. The project described in this thesis focuses on characterizing the fitness of the mine overburden. Two seismic reflection surveys were conducted within a 2.4 km segment of U.S. Highway 69 in extreme SE Kansas. The high-resolution P-wave allowed for interpretation of the the mine location and subsurface structure. Extensive preprocessing and data conditioning was required to accurately image the subsurface. A useful CMP stack was produced after combining detailed velocity analysis with surface consistent statics. A S-wave survey spanning the southernmost 1.6 km portion of the survey area intended to characterize the strength of the overburden and search for areas of elevated stress. Delineating reflections in both data sets allowed interpretation of the mine location. Lithology extracted from well data were roughly correlated to the seismic data to confirm the mine's signature and time depth for the data. Calculated Vp/Vs ratio were used to infer if lateral changes in rock velocities were sufficient to imply zones of elevated stress, or reduced strain. These data and analysis in this appraisal provide an excellent baseline study comparison point for future time-lapse studies designed to detect change in physical properties and seismic velocities, to determine if precautionary measures are necessary to minimize transportation hazards and public safety.

Acknowledgements

I would first like to thank my adviser, Rick Miller, for giving me the opportunity to work for him at the Kansas Geological Survey, and attend The University of Kansas. Without this opportunity, combined with his shared knowledge I would not be the geoscientist I am today, nor would my future opportunities be possible. The time and effort Rick puts into bettering his students and enhancing the geophysical world is unmatched. I had some incredible experiences in the field from Kansas, to Oregon, to Arizona working for Rick that were some of the best experiences in geophysics that I have ever had.

I would also like to thank my committee members, Ross Black and Jenn Roberts, for taking time out of their busy schedules to take on the task of an additional student. Ross shared his knowledge of seismic data processing and exploration as well as aided in thesis revisions. Jenn supported me throughout my time at KU, especially during my thesis revision process.

KGS Librarian, Nikki Potter, was extremely helpful tracking down papers for me. My co-workers at the Kansas Geological Survey especially Shelby Peterie, Julian Ivanov, and Mary Brohammer should also be recognized for their consistent help, guidance, figure generation, and dealing with my constant questions. I would also like to thank fellow students Dan Feigenbaum and Brett Judy for sharing their knowledge of seismic data processing and giving opinions throughout my time at KU. I would like to thank the Kansas Geological Survey's Exploration team, especially Brett Wedel, Jeremy Scobee, Joe Anderson, and Brett Bennett for their time and effort (and entertainment) through data acquisition. I would also like to thank my girlfriend, Katelyn Bourgeois, for her constant support throughout my graduate research. Lastly, I would like to thank my parents, Dwight and Melanie, and sister Madeline for supporting me throughout my academic career, and for always pushing me to be the best I can be.

Table of Contents

List of Figures

List of Tables

Introduction

The abandoned Webber-Barr lead (Pb) zinc (Zn) mine beneath U.S. Highway 69 west of Treece, KS (Figures 1 and 2) possesses the potential to threaten transportation and human safety. Drilling reports indicate that abandon mine workings lie approximate 58 - 88 m beneath the highway right of way, between 0.4 to 1.2 kilometers north of the Kansas/Oklahoma state line (KDOT, 2002). Within the Tri-State Mining District, the Webber-Barr mine is one of hundreds of mines. With over 1,500 open mine shafts and approximately 500 collapse features in the district (McCauley et al., 1983; McFarland and Brown, 1983; Dressel et al., 1986; Luza, 1986), mines in this area have been classified as safety hazards representing a risk for subsidence (Nairn et al., 2005). Within the ~0.2 km^2 area of Treece, 17 sinkholes have been correlated to mine voids left from local ore mining (McCauley et al., 1983; Luza 1986; Brady et al., 1989) (Figure 3).

Sinkholes formed from void migration around the world threaten transportation, infrastructure, property, and human safety (Beck et al., 1999). Surface subsidence resulting from overburden load exceeding the roof rock strength of a void forms a sinkhole at rates and dimensions that depend on lithology, depth of the void, size of the void, bulking factor, and continuity of overburden (Miller et al., 2006).

As a result of potential threats posed by sinkhole formation and water contamination resulting from historical mining in this area (Brady et al., 1989), the Kansas Department of Health and Environment (KDHE) and Environmental Protection Agency (EPA) combined to buy out and relocate the residents of Treece in 2009, for a total of $3.8 million (KDHE, 2016).

The Webber-Barr mine workings and overburden geology indicate a potential risk to sinkhole development through vertical mine void migration to the surface. Well reports and mine maps indicate the Webber-Barr Mine geometry is characterized as having up to 200 m of laterally unsupported roof rock and water filled rooms with heights up to 30 m (KDOT, 2002). Historical records suggest the mine roof is composed of a structurally altered (i.e. fractured and faulted) cherty limestone (Williams and Frederickson, 1985) and is overlain by Pennsylvanian and Mississippian aged shale and limestone units (McKnight and Fisher, 1970). The local geology combined with the mine geometry and documented surface subsidence in this area suggests failure of the mine roof is possible and could result in vertical migration of the mine void to the ground surface, resulting in a sinkhole.

Once the world's leading region for zinc production, early studies of The Tri-State Mining District exclusively focused on exploration and discovery of ore (Hambleton et al., 1959). More recently geologic and environmental studies have investigated surface stability, water quality, and soil chemistry (Weidman, 1932; Hambleton et al., 1959; McKnight and Fischer, 1970; Brady et al. 1989; Nairn et al., 2005; Pfeiffer et al., 2009) For the Kansas Department of Transportation (KDOT), studies targeted public safety along U.S. Highway 69 from the KS/OK border north to the Miami Trough specifically over the Webber-Barr mine. High-resolution elevation surveys of the highway surface are routinely conducted and have reported no significant change in elevation prior to this study in 2016. In 2002, KDOT commissioned a borehole study designed to penetrate the mine interval immediately adjacent to the highway. Geological logs of the rock units overlying the mine workings as well as the mine locations were documented. In conjunction with the borehole lithology study, a cross-hole tomography survey was undertaken to measure the velocity of the limestone unit overlying the

mine to see if any lateral velocity changes were present. This cross-hole study was repeated in 2009 as a time-lapse survey highlighting any changes since the initial survey (Pfeiffer et al., 2009). Changes in these compressional (P-wave) velocities could indicate changes in increased stress in the limestone roof rock. Results provided minimal to no evidence of change in the velocities, but continued monitoring of the area was adopted by the KDOT.

This seismic study was designed to delineate the mine overburden using near-surface high-frequency seismic reflection methods, and characterize the associated Vp/Vs ratio using seismic velocities from these surveys. Seismic imaging is used in engineering for a multitude of applications including locating and delineating voids in the subsurface (Schepers, 1975). Calculating the elastic moduli, defined by the seismic velocities, will allow differentiation between a water filled void and rock. These rock/void interfaces make superb reflecting interfaces (Miller and Steeples, 1991).

High-resolution near-surface seismic reflection studies have proven to be successful in imaging structure in the upper 100 m of the subsurface, delineating collapse features, and identifying characteristics and stages of sinkhole development (Steeples et al. 1986; Knapp et al., 1989; Miller et al., 1990; Miller and Steeples, 1991; Miller et. al, 1997; Miller and Henthorne, 2004; Lambrecht, 2006; Miller et. al., 2006; Miller, 2007; Rice, 2009; Bailey, 2014; Judy, 2015). A high-frequency compressional wave (P-wave) and shear wave (S-wave) surveys, were acquired on several dates from 2015 to 2016. Both P- and S-wave data were processed using unique processing flows, while applying traditional Common Mid Point (CMP) data processing workflows throughout (Steeples and Miller, 1998; Miller, 2007). These data were processed using extreme detail and high accuracy to generate traditional CMP stacked sections representative of true geology. 2-D reflection profiles from these surveys were used as imaging

tools to increase the knowledge and accuracy of the mine location and geometry, as well as identify areas that could represent a threat for mine roof failure.

This study included the acquisition and processing of coincident P-wave and S-wave data with the purpose of using their respective velocities matched to coincident intervals to generate a Vp/Vs ratio map. This allowed for characterization of a shallow and relatively thick mine overburden for the purpose of judging risk of failure and collapse.

Vp/Vs ratio is commonly used to indicate lithology, identify pore fluid, determine degree of consolidation, and estimate velocities (Lee, 2003). Changes in rock properties (bulk and shear modulus) from increased stress associated with elastic strain would result in a change in P- and/or S-wave velocities of a roof rock under excessive load (Miller et al., 2015). Past studies using Vp/Vs ratio vary from oil and gas exploration (Gaiser, 1996; Lee et al., 1999; Rojas, 2008; Lines et al., 2005), identifying lithological changes within a unit (Domenico, 1984), water table and aquifer estimations (Pasquet et al., 2014), to changes in roof stability (Maleki et al., 1993). This study demonstrates how to use seismic interval velocities of separate P-wave and S-wave surveys to calculate the Vp/Vs ratio in order to interpret the current state of the mine overburden. Past studies have used log data (Rojas, 2008), converted P- to S-wave data (Gaiser, 1996; Lines et al., 2005), refraction surveys (Pasquet et al, 2014), cross-hole tomography data (Maleki et al., 1993; Pfeiffer, 2009), laboratory measurements (Domenico, 1984), and earthquake tomography (Westman and Luxbacher, 2008) to get their velocity estimates for Vp/Vs ratio calculation. This study uses the seismic velocities of separate P- and S-wave near-surface high-frequency 2-D seismic data sets to generate a Vp/Vs ratio of the mine overburden.

This study successfully delineated the overburden, interpreted the approximate mine location beneath the highway, and calculated the Vp/Vs ratio of a set of the lithological units above the mine. Changes to the geologic structure in the seismic reflection data and/or the Vp/Vs ratio from this study to future studies could indicate changes in physical properties of the mine roof. Increased stress would suggest increased risk of failure of the mine roof depending on the location of the stress. If the failure was large enough and bulking factor, ratio of the volume of excavated matrial versus original in situ volume material, was low enough a sinkhole could development along a major U.S. highway. The findings of this study serve as a solid baseline study to future time-lapse studies.

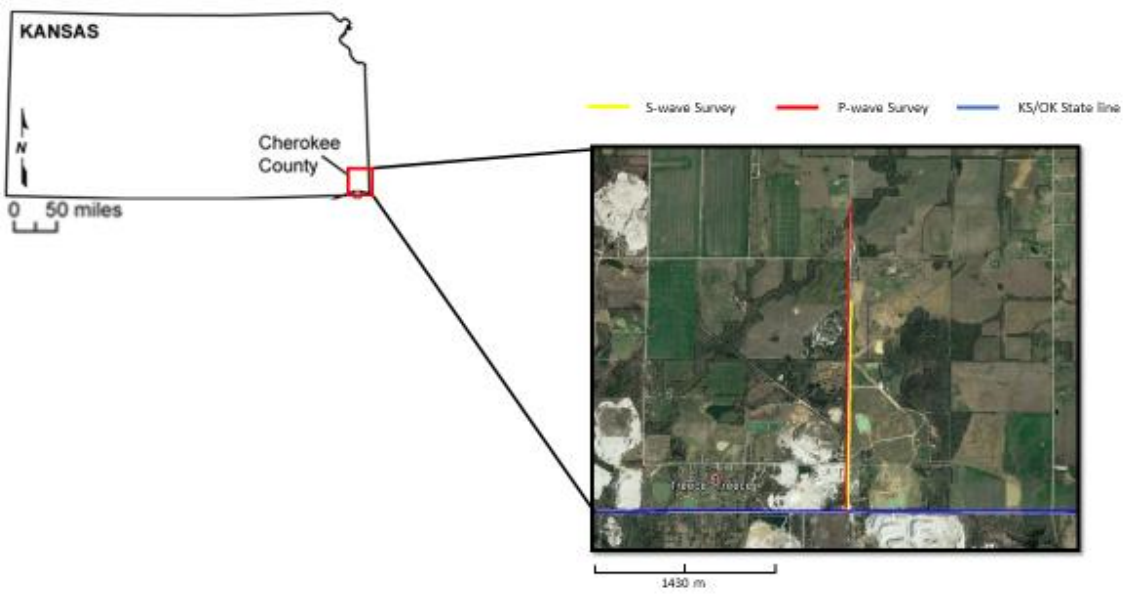

Figure 1: Location of Cherokee County (red box) marked on the state of Kansas (left). Zoomed in image of the field site location east of Treece, KS (right). The Kansas – Oklahoma state line is shown in blue, and the red (P-wave) and yellow (S-wave) lines represent the approximate locations of the survey lines over U.S. Highway 69.

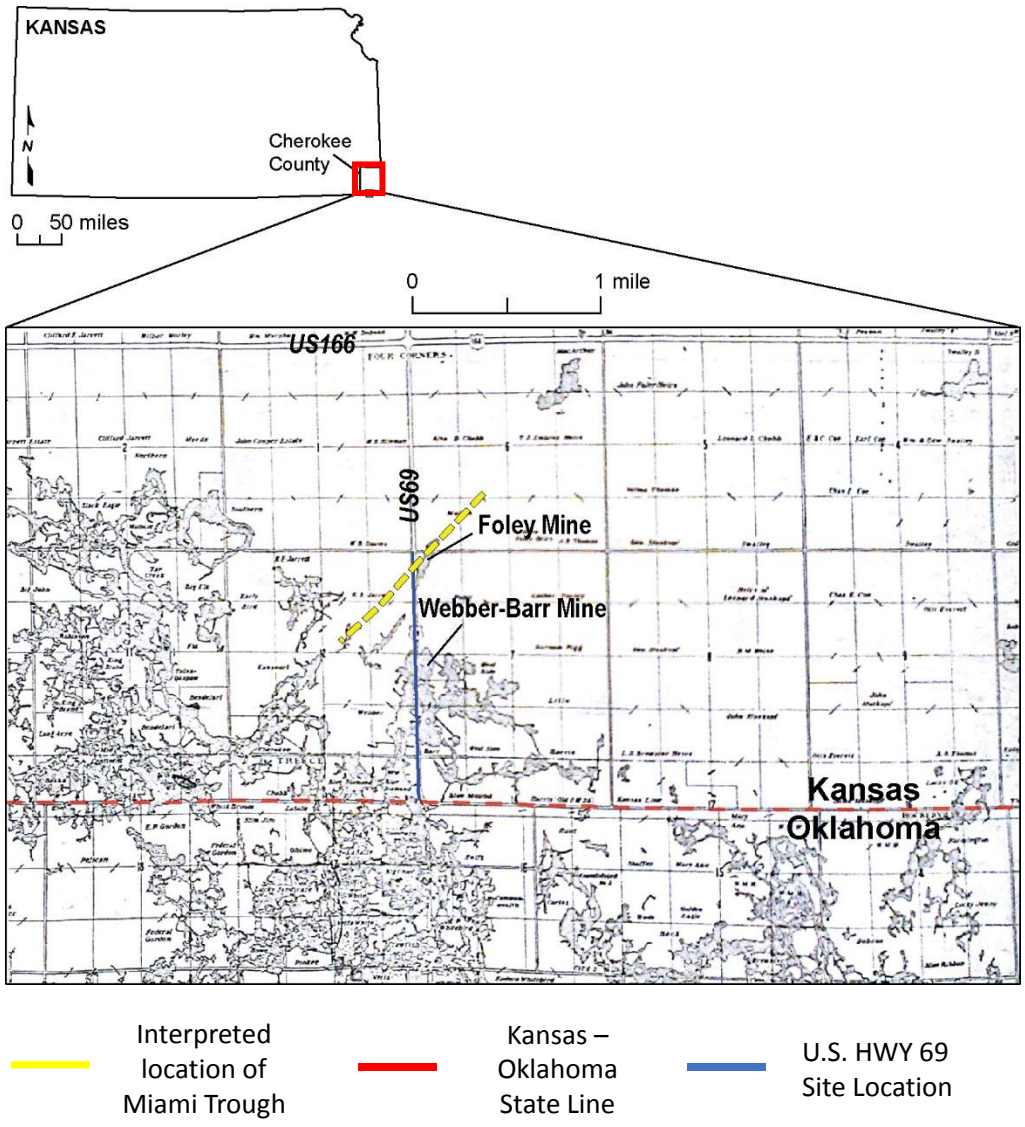

Figure 2: Location of Cherokee County (red box) marked on the state of Kansas (top). Zoomed in image of part of the Tri-State Mining District (Bottom). The Kansas Oklahoma State line is shown in red, and the blue line represents the approximate location of the Survey lines over U.S. Highway 69. The Webber-Barr Mine identified in its proximity to U.S. 69 (Modified from Miller et al., 2015).

Figure 3: Collapsed mine northwest of the town of Treece, Kansas (photo from Wichita Eagle, 2009).

Field Site

For over a century the Tri-State Mining District was the largest producer of zinc in the world (Hagni, 1986) (Figures 2 and 3). Cherokee County, Kansas' most southeastern county, is in the Tri-State Mining District, which includes portions of Southeastern Kansas, Northeastern Oklahoma, and Southwestern Missouri. The field site for the high-frequency seismic data sets is 2.4 km from the town of Treece and along the north-south trending U.S. 69 Highway (Figure 2). The seismic surveys start near the KS-OK state line and run north to mile marker 1.5 (P-Wave) and mile marker 1 (S-wave). U.S. 69 runs through Cherokee county across the Tri-State Mining District and directly over the abandon Webber-Barr Pb-Zn Mine, which is located between mile markers ¼ and ¾ (Figure 3 and 5) (KDOT, 2002).

Geologic Setting

Quaternary alluvial silts, sands, clays, and gravels overlie limestones and shales of the Mississippian and Pennsylvanian throughout Cherokee County (McKnight and Fischer, 1970) (Figure 4). The Mississippian aged Limestones and chert units are the key mineralized zones of the Tri-State Mining district and are associated with the Ozark Plateau. The Ozark Plateau developed on the Mississippian aged cherty limestone, and are the oldest outcropping rocks in Kansas (McCauley et al., 1983). These Mississippian rocks are important oil producing units in much of Kansas. Additionally, in southeastern Kansas they are known mainly for their metalliferous deposits (Merriam, 1963). The surface of the Precambrian basement rocks sits approximately 550 meters beneath ground surface (BGS) in this area and is overlain by the Chattanooga Shale.

The Webber-Barr Mine is located in the Mississippian Boone Fm, which overlies the Chattanooga Shale unconformably. The Boone Fm is the mineralized zone in the Treece area and contains predominately the Osage and Maramec Limestones. Fossiliferous limestone, cotton rock, and chert, which is prevalent in nodules and interbeds ranging up to 18 m, make up the Boone Fm (McKnight and Fischer, 1970). Drilling reports indicate that these limestones range from hard to brecciated and cherty (KDOT, 2002). The Boone Fm is broken up into distinct members (McKnight and Fisher, 1970), and has been assigned a lettering system (Fowler and Lynden, 1932). The Joplin member, "M" bed, is categorized as the most important unit in the Boone Fm in regards to ore deposition. The upper Mississippian Chester series unconformably overlies the Boone and contains undifferentiated formations of limestone, sandstone, and shale (Seevers, 1975).

The Hale/Kearny Fm makes up the lower Pennsylvanian Morrow series, which is composed of alternating brown to black sandstone, dark shale, and fossiliferous limestone (McKnight ad Fischer, 1970). The Pennsylvanian aged Marrow and Cherokee, which contains the Krebs group sits uncomformably above the Mississippian rocks (Hambleton et al., 1959). The Cherokee is represented by the black coal, gray coal, and fissile coal packages of the Krebs Fm in the Des Moines Series (McKnight and Fischer, 1970). The geologic logs indicate that the upper ~ 100 m consists of Pennsylvanian aged shales, which range from weathered to firm, and are overlain by Quaternary alluvial silts and clays at the ground surface (KDOT, 2002).

The Miami Trough is the dominant structural feature in the Treece area (McCauley et. al., 1983). It is part syncline part graben and intersects U.S. 69 obliquely (Figure 5). Mineralization in this area and the Webber-Barr Mine in particular was strongly influenced by faulting associated with the formation of the Miami trough. The mineralized zone of the Webber-Barr Mine is bounded on the north by the Miami Trough (Figure 6). The NE/SW trough extends roughly 65 km and is 91 m deep and 300 m wide in the Treece area (McKnight and Fischer, 1970) (Figure 7).

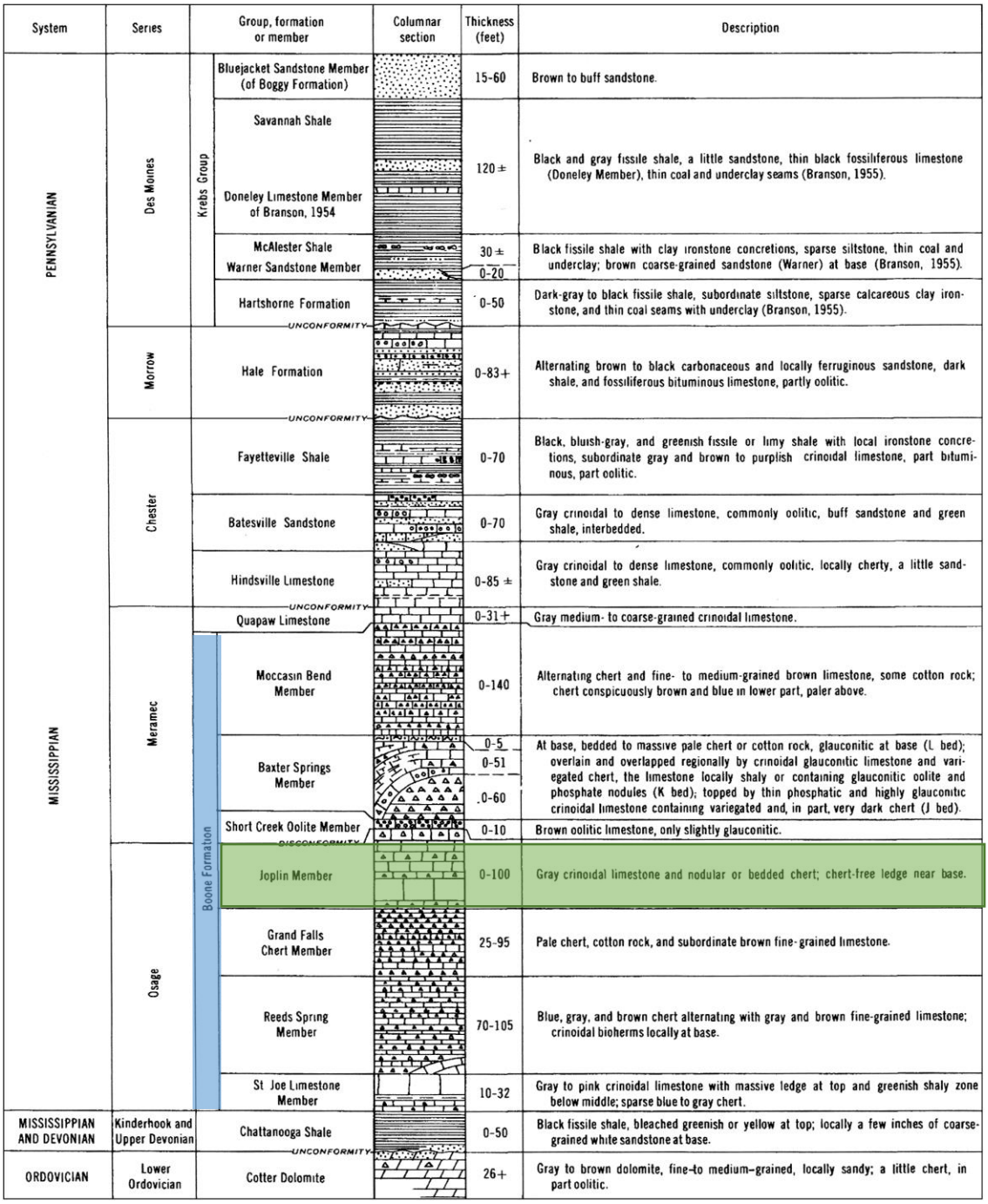

Figure 4: Stratigraphic column from McKnight and Fischer, (1970). The Boone Fm is highlighted in blue, while the Joplin Member, "M" bed, which is considered the most important bed in regards to ore deposition is identified in green.

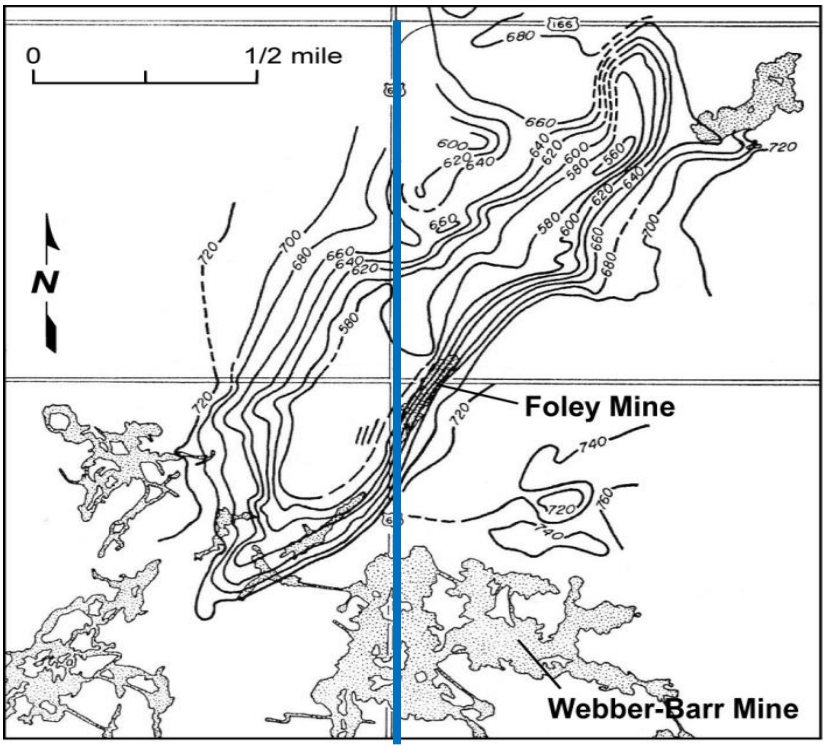

Figure 5: U.S. 69 is represented as the blue line. The Webber-Barr mine is identified and shaded in gray, while the Miami trough is represented by the contours north of the mine. The tightly spaced contour lines on the southern flank of the trough represents a narrow fault zone, which has likely bounded the north end of mineralization resulting in the location of the Webber-Barr Mine (Modified from Hambleton et al., 1959).

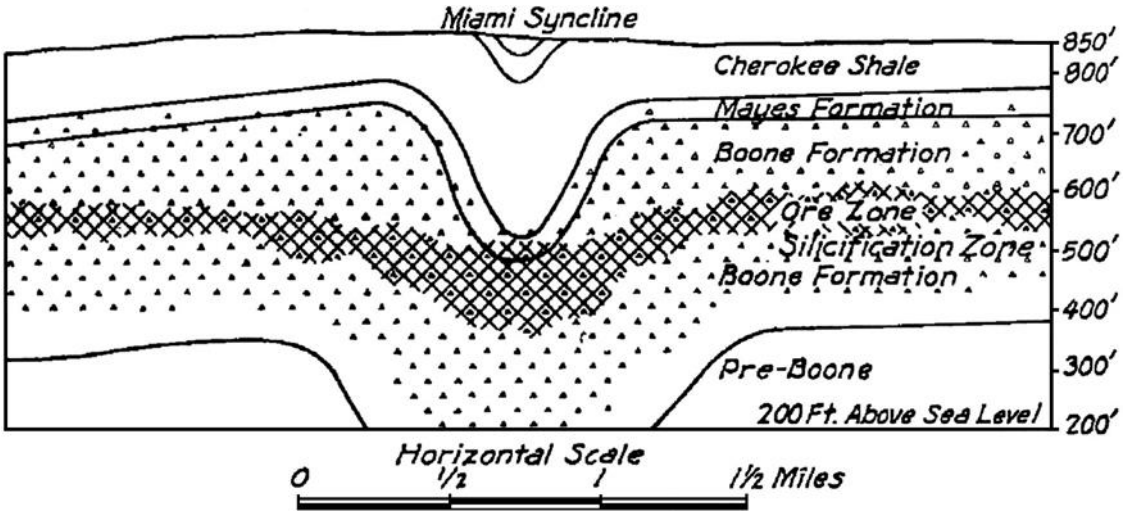

Figure 6: Illustration from Weidman (1932). This illustration represents the sillification zone within the Boone Fm in relationship to the overlying Mayes Fm (Chester Series) and Cherokee Shale (Krebs Group). The economic deposits of ore reside south of the trough.

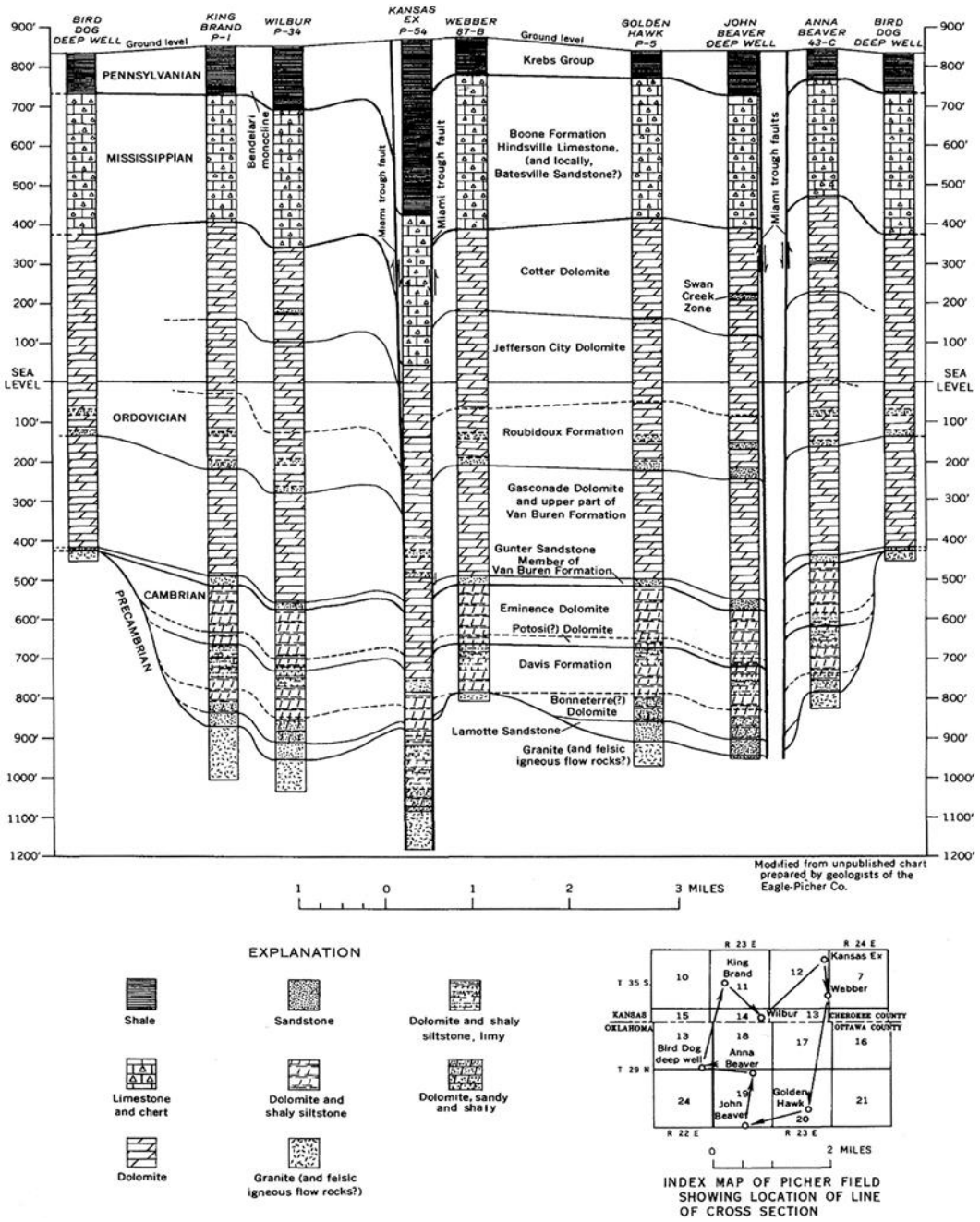

Figure 7: Correlated logs from a report by McKnight and Fischer (1970). The well correlation identifies the Miami trough between the Webber, Kansas EX, and Wilbur wells. The faulting of the trough is identified in the logs and from this report it is evident that the middle of trough lies at a depth of approximately 91 m.

Structural Formation and Ore Deposits

Faults associated with the Miami Trough bound the north end of ore accumulation zones in the Treece area resulting in the location of Webber-Barr Mine. The initial formation of the Miami Trough is a result of reoccurring failure in the Precambrian rocks. (McKnight and Fischer, 1970). Tectonic in origin, the Miami trough is well developed in the Precambrian basement igneous rocks, as identified in drilling reports (Figure 7), and could have possibly been modified later by collapse of the shallower carbonate rocks as a result of solutioning (McKnight and Fischer, 1970).

The presence of fractures within the Boone Fm significantly influenced the distribution of the ores within the rock (Weidman, 1932). The bodies of ore are in areas where flexing, shearing, and brecciating of the rock units took place pre-mineralization (Bastin, 1939). Warping and deformation (Figure 8) related to the formation of the Miami Trough resulted in extensive joint systems (McKnight and Fischer, 1970). Hydrothermal solutioning of deep-seated magma through the fractures in the Precambrian basement up into highly altered fractured permeable Mississippian Boone Fm rocks allowed for the accumulation of ore deposition.

The Boone formation had been prepared for mineralization through extensive deformation (fracturing), brecciation, and leaching in the Mississippian and Pennsylvanian. Timing of mineralization is unknown but is speculated to be during the Cretaceous or later (McKnight and Fischer, 1970). Mineralization occurred from mineral rich solutions gaining access to the voids and fracture zones in rocks by infiltrating them through the highly-fractured zones of an extensive joint system which acted as channels for fluids to travel through. The Boone Fm, specifically the Joplin member contains both the silification and mineralization

zones, with additional mineralized rock located in overlying Mayes Fm, which is part of the Hindsville limestone in the Chester series (McKnight and Fischer, 1970).

Deformation

When a material such as a rock behaves elastically, stress results in strain and when stress is removed it returns to its original shape (Lillie, 1999). This is the basis of Hooke's Law, which states, a given strain is directly proportional to the stress producing it (Sheriff and Geldhart, 1995). Once a material reaches a point where stress has been applied to a level that the material will never return to its original pre-stressed form, it has reached its elastic limit. Once a material reaches its elastic limit Hooke's law no longer applies, because the strain increases faster than stress and stress to strain is no longer proportional. At this point, the material undergoes deformation, where strain increases faster than stress. A rupture point is reached and failure occurs once strain exceeds the plastic limit (Figure 8).

Given what is known from the previous studies (KDOT, 2002; Pfeiffer et al., 2009) and known geology (McKnight and Fischer, 1970; Williams and Fredericksen, 1985) of this field area, some areas Boone Fm limestone could be passed their elastic limit. Deformation pre-Krebs (Pennsylvanian) in age deformed the ore bearing limestone resulting extensive brecciation (McKnight and Fischer, 1970). Additional deformation and brecciation occurred post-Krebs as a result of structural movement (McKnight and Fischer, 1970). These events are interpreted on the well report (KDOT, 2002) as the areas above the mine contain altered cherty limestone and brecciated limestone. With portions of the mine roof potentially past its elastic limit, the mine roof could continue to deform until reaching its rupture point, resulting in mine roof failure.

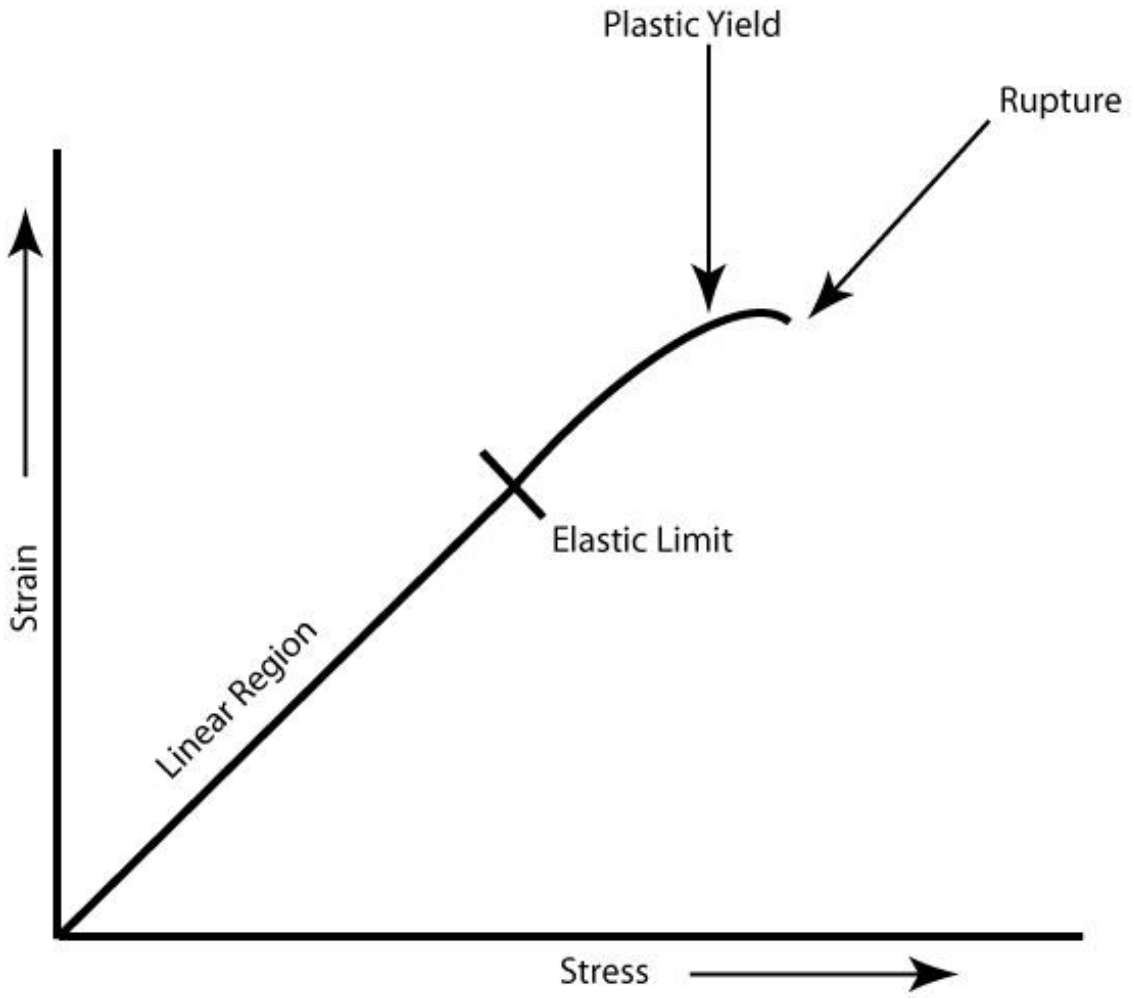

Figure 8: Stress vs. strain graph. Materials are only elastic up to a certain level of stress, upon a material reaching its elastic limit it begins to undergo deformation. The material will continue to deform as strain is now increasing faster than stress until it reaches rupture point, and the material fails.

Structural Concern

Sinkholes as a result of cavern roof failure within the Mississippian Limestones are common throughout the Tri-State Mining District (Hambleton et al., 1959). The high number of slump pipes reported near this area are a significant concern. Many have been mapped in outcropped Boone Fm located within 800 m of the Miami Trough (McKnight and Fischer, 1970). Slump pipes occur in this area coincidentally with extensive mineralization, which in this area are believed to have formed from spot solution of soluble limestone intervals, developing gradually as underlying layers were dissolved. Slump pipes are "small" (30 – 90 m radius) down dropped blocks, "pipes," which are fault controlled and are extremely problematic when they come in contact with mine roofs (McKnight and Fischer, 1970) (Figure 9). Slump pipes represent vertical zones of weakness and therefor increase the threat for failure and rapid migration of a void to the surface.

Highly altered cherty limestone overlying the roof of the Webber-Barr Mine represent a potential zone of structural weakness (Williams and Fredericksen, 1985). These Mississippian limestones have also been affected by natural fluids introduced to this field since the Mississippian. With mineralization, the limestone is susceptible to complete dissolution and replacement by fluid precipitation or collapse breccia (Hagni, 1986). Dissolution of the carbonate rocks could also decrease the structural integrity of the mine wall. The combination of the structurally unstable units overlying the mine roof as well as the proximity of slump pipes to the mine roof are a concern for roof rock failure.

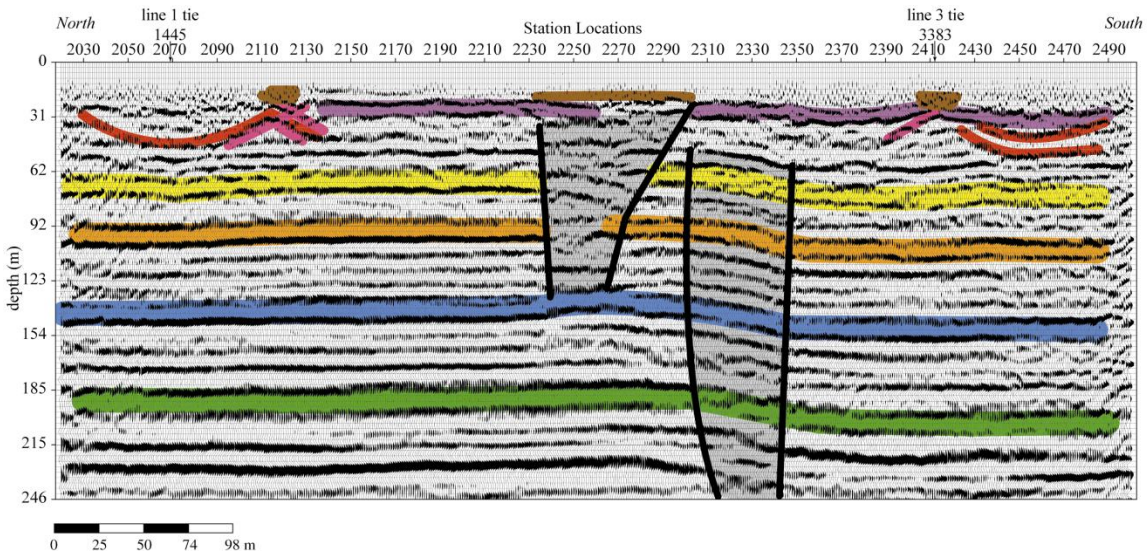

Figure 9: Features expected to be similar to slump pipes are shown in this seismic data. This data is a CMP stacked section over a faulted monocline and Karst subsidence feature. The associated features of this include diffraction scatter events (red), as well as alluvium filled collapse structures (black) (modified from Miller et al., 2015).

Sinkhole Fm

Sinkholes form as a subsurface void migrates to the surface upward until it reaches the ground surface. Subsidence rates at the surface as well as while the void migrates to the surface vary depending on the voids geometry, overburden load, and properties of the roof rock and overlying rock (Miller, 2007). Sinkhole formation can be gradual or catastrophic and is principally controlled by spans of unsupported roof rock and tensional strength of overburden. In this particular case, at Treece, a large water filled mine void (vertical zones up to ~ 30 m, with large unsupported roof spans, as much as 200 m) is present with a structurally altered roof rock. Seventeen collapse features are present in the Treece, KS area as a result of mining (McCauley et al., 1983; Brady et al., 1989). Failure of roof rock or overburden over the mine void in the Webber-Barr Mine could result in rapid migration of the mine void to the surface, forming a massive sinkhole in a matter of minutes.

The stress field over a mine will change as the unsupported roof span increases, consistent with the tensional dome (Davies, 1951) (Figure 10). An area of compressional stress

forms over the void in a tensional dome environment. Draping of surface rocks are a result of sag of overburden rock into the void over the area of compressional stress. The angle of draw is the maximum diameter of surface sag and is dependent on rock properties between the void and ground surface. Strain forms as compressional stress increases consistent with drape in the roof over the mine (Miller, 2007) (Figure10). The location where failure occurs is where the compressional stresses are the greatest over the void (Sofianos, 1996; Miller, 2007). If the roof rock has a low bulking factor, which is the ratio of change in rock volume, then the rock is weaker and more prone to failure. Collapsing or stoping of the overburden as the mine void migrates upward results in collapse breccia. Collapse breccia are remnant of roof rock failure which indicate upward migration of void (Miller, 2007). Once each rock layer in the overburden fails and the void successfully reaches the ground surface, the process will produce lines of failure along reverse fault planes defining the compressional failure of the subsidence feature. Normal fault planes define the secondary failure for an aging sinkhole as a result of extensional forces driven by gravity acting on overhanging blocks (Miller, 2007) (Figure 11).

Sinkhole formation has been documented within a mile of the Webber-Barr Mine. At the Webber-Barr Mine a portion of the approximately 50 – 80 m of overlying geological units above the mine and is comprised of a highly altered cherty limestone. Increased stress from stopping or spalling of roof rock could result in continued structural deformation of the mine roof to the point of failure. The combination of the overburden load and the structurally altered roof rock, gives this site the conditions needed for sinkhole development.

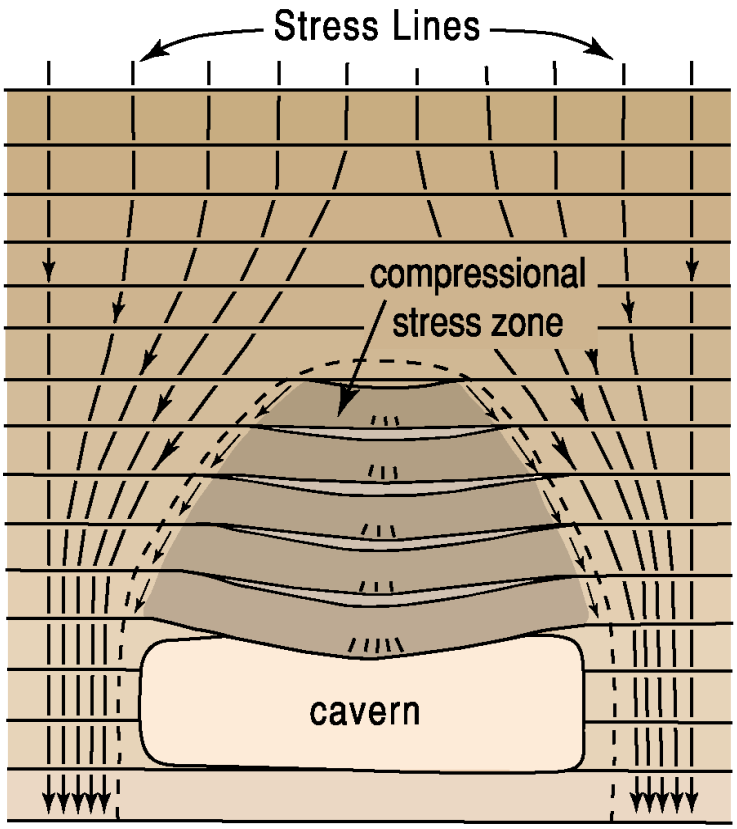

Figure 10: Davies (1951) depiction of a tensional dome and the associated distribution of stress lines around a cavern, void, in horizontal strata (modified from Miller, 2007).

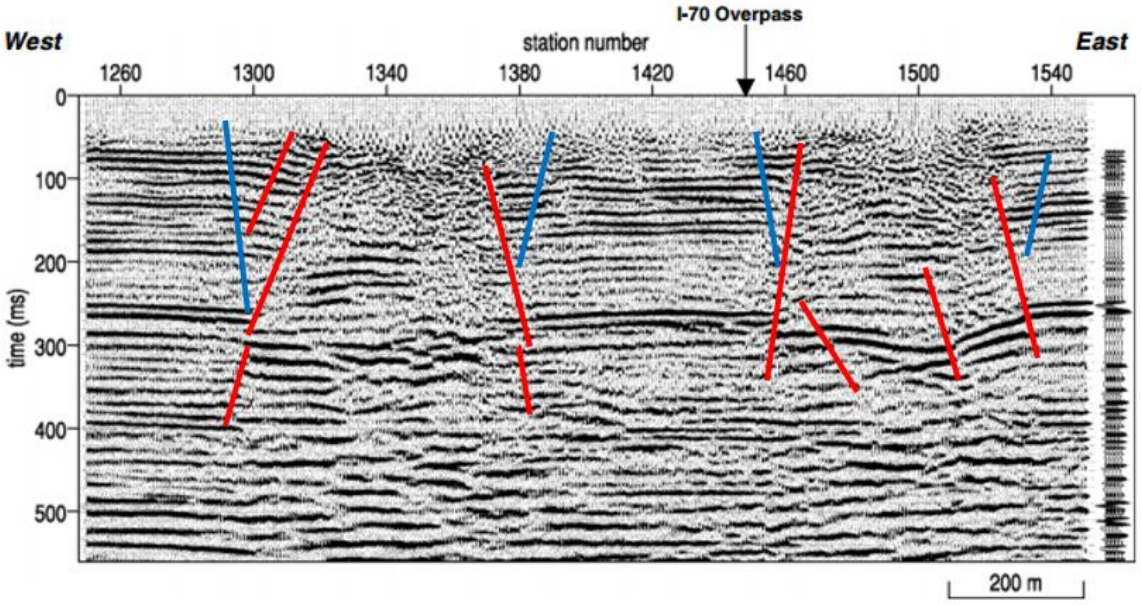

Figure 11: CMP stacked section over two dissolution sinkholes showing the reverse faulting from initial compressional failure (red) and the normal faulting from secondary extensional failure (modified from Miller, 2008).

Past Studies

Cross-hole tomography surveys, elevations surveys, and well studies have been completed in the last 15 years to investigate the geometry and failure potential of the Webber-Barr Mine. Evaluation of annual time-lapse elevation surveys prior to this study detected no change in surface elevation. KDOT (2002) drilled seventeen wells along the south bound lane of U.S. Highway 69. Wells 1 – 14, located in proximity to the Webber-Barr mine, are the most significant to this study (Table 1). Wells 15 – 17 lie north near the Foley Mine. Wells 1 – 14 were drilled to total depths ranging from ~ 80 m to ~ 96 m and were spaced anywhere from ~ 50 m to ~ 70 m apart. Geologic logs were developed at each well, that included identifying the rock units, rock composition, and noting if a void was present (Figure 12). This was the first study that attempted to quantify the mine roof and void size. The importance of these wells is that they identify the depth to the mine roof, the vertical extent of the mine, and the location at which the mine void is in proximity to the highway. Data from these wells have been and will continue to be useful for studies of this area. These data were used extensively in this study and roughly correlated with the seismic data to allow for the most accurate interpretation.

Cross-hole seismic tomography investigations were done in 2002 and again in 2009. The purpose of these cross-hole surveys was to do a time-lapse comparison of the velocity tomograms from the two surveys searching for change that might negatively impact void stability (Figure 13). Changes in the velocities over this seven-year period could be a symptom of increased stress. The two surveys produced near identical results except for between Wells 7 and 8, where there was a slight reduction in inverted velocity, and a high velocity in a previous low velocity zone. These observed changes were measured in the limestone unit above the mine and could represent an area where the rock materials have changed, but could also be related to

inconsistent acquisition parameters. Overall the velocity calculations from both surveys were very similar causing no immediate concern about changes in the overburden. Recommendations included further monitoring of the site through future tomography and possibly even downhole sonar surveys to map the mine workings. Additional work in the existing wells would require they be re-drilled and re-cased, due to casing failures (Pfeiffer, 2009).

Well	P-Wave Reflection Station	S-Wave Reflection Station	Comments
1	1187	1190	Mine detected 70 - 74 m
2	1214	1218	Mine detected 70 m
3	1238.5	1243	Mine detected 73 – 94 m
4	1262.5	1267	Mine detected 83 – 90 m
5	1282	1286.5	No mine detected
6	1311	1316	Mine detected 58 – 85 m
7	1335.5	1340	Mine detected 60 – 85 m
8	1368	1364	Mine detected 74 – 97 m
9	1384.5	1389	No mine detected
10	1408	1413	No mine detected
11	1436	1442	Mine detected 88 – 96 m
12	1456	1462	No mine detected
13	1481	1487	No mine detected
14	1505	1510	Mine detected 87 – 90 m

Table 1: Well locations along U.S. 69 Highway.

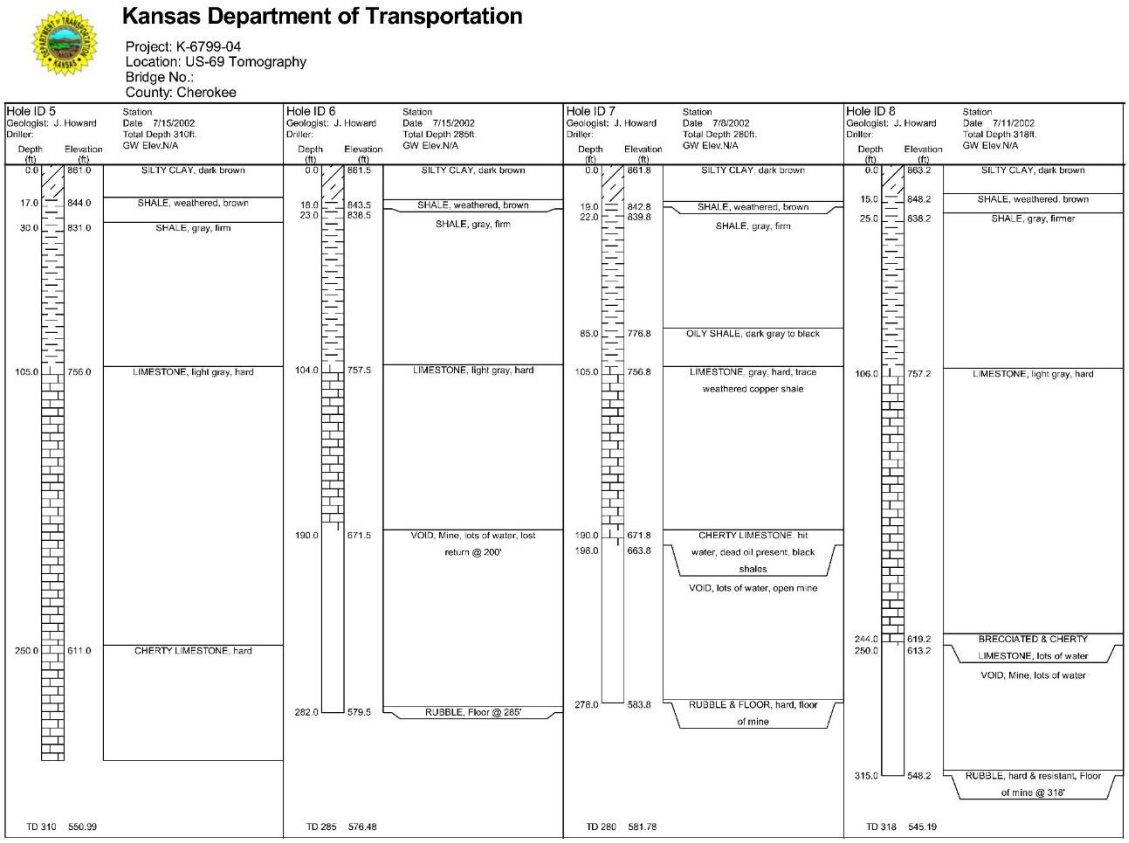

Figure 12: Example of the well report, Wells 5 – 8, from KDOT (2002) used to correlate well location with the stacked seismic reflection data.

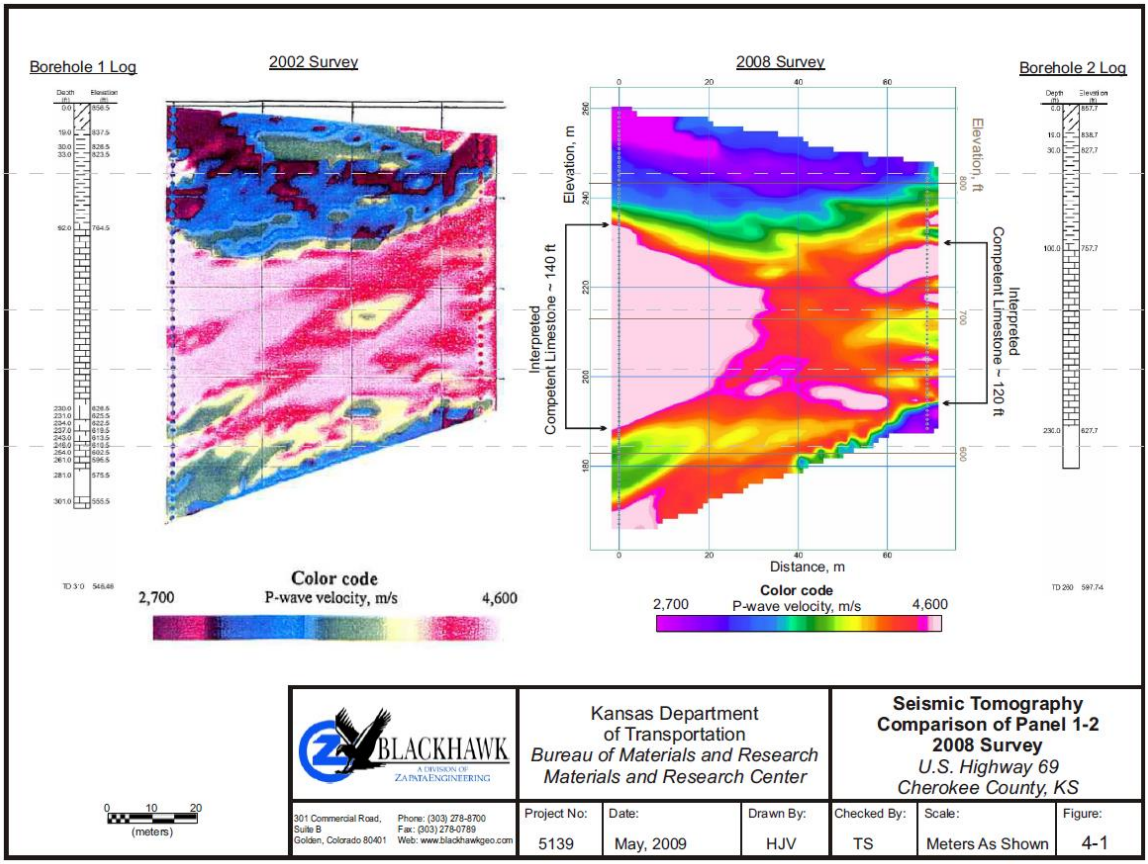

Figure 13: Example of the cross-hole tomography time-lapse study, Wells 1 – 2, from Pfeiffer et al. (2009).

MASW Study

Multichannel analysis of surface wave (MASW) data were acquired and processed over the same time period as the reflection data presented in this study. These data were used to investigate the shear wave velocities (Vs) in the upper 30 m of material overlying the mine. Lateral heterogeneity of Vs could signify changes in the shear modulus of the geologic units. Preliminary results from the MASW survey suggested the data allowed the generation of a 2-dimensional velocity profile of the shale units overlaying the mined limestone unit (Figure 14). Interpreted results of these data by Sarah Morton of the KGS, indicate a normal velocity structure in these upper units. When correlated with the well data, the MASW Vs profile correlates very well with the general lithological units on well logs. The relatively smooth 2-D MASW Vs profile shows no signs of increased shear moduli or change in geometry of the units in the upper ~ 25 m (Miller et al., 2017).

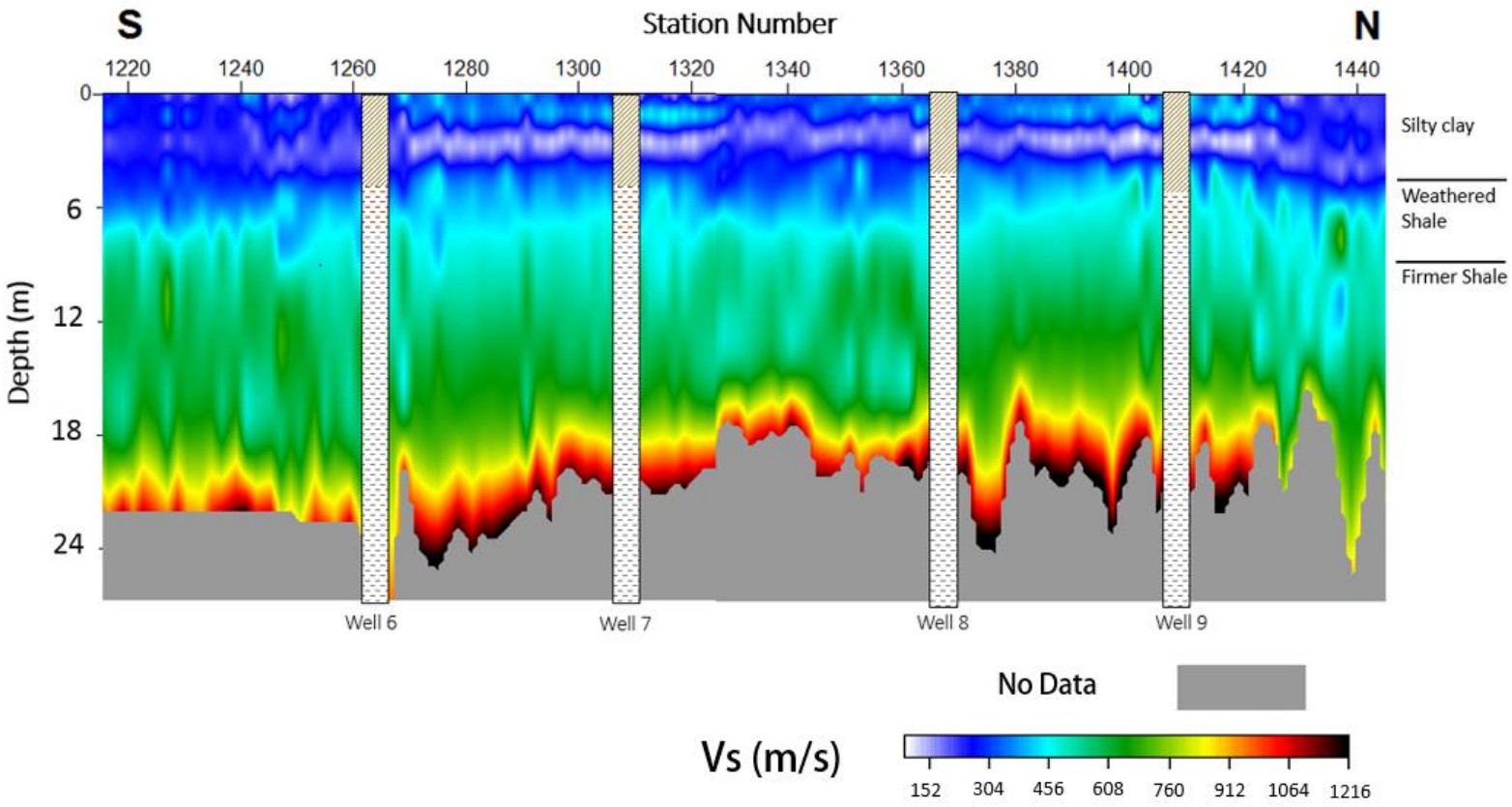

Figure 14: 2-D Vs profile of Wells 6 – 9. MASW results show expected increasing velocity with depth and Vs values for rock units in the well data. The Vs profile correlated extremely well with the lithology identified in the well logs. There were no signs of any abnormal velocity anomalies in the MASW data.

The Seismic Reflection Method

Changes in subsurface material affect data acquired and processed using the seismic reflection methods. Seismic reflections are a result of contrasts in acoustic impedance (Z) at material contacts. Acoustic impedance is a rock property that is the product of seismic velocity (V) and the density (ρ) of the medium it is traveling through.

$$Z = \rho V$$

Acoustic impedance contrasts between layers are used in the definition of the reflection coefficient (R), which determines the reflections amplitude and whether the polarity will be positive or negative.

$$R = (\rho_2 V_2 - \rho_1 V_1) / (\rho_2 V_2 + \rho_1 V_1)$$

For example, a high acoustic impedance overlying a low acoustic impedance will generate a negative reflectivity, while a low acoustic impedance overlying a high acoustic impedance will generate a positive reflectivity (Yilmaz, 1987) (Table 2).

Diffractions can be present in seismic data along with the reflections. They are a result of source scatter when a seismic wave contacts a discontinuity, such as fractures, faults, mine geometry (walls & pillars), and bed terminations.

Material	P-wave Velocity (m/s)	S-wave Velocity (m/s)	Density (kg/m^3)	Acoustic Impedance (10^4 kg/m^2s)*	Bulk Modulus (10^9 N/m^2)	Shear Modulus (10^9 N/m^2)
Air	320	0	1.0	0.0320	.0001	0
Water	1500	0	1000	150	2.2	0
Shale	3600	2600	2400	864	8.8	17
Sandstone	4300	2600	2500	1118	24	17
Limestone	5000	2900	2700	1450	38	22

Velocities are mean for a range appropriate for the material.
*Acoustic impedance is the product of the P-wave velocity density.

Table 2: Typical values for seismic velocities, density, acoustic impedance and elastic constants in air water and rocks present at this geological site. The velocities listed here fall within a range of velocities typical for that specific rock type. It can be expected for these values to be lower in fractured and faulted rocks (Modified from Lillie, 1999; Values from Kinsler et al., 1982).

High-Resolution

The P-wave seismic reflection data acquired in this study are considered to be high-resolution reflection data, there is no definition of what dominant frequency is considered high resolution for S-wave. Resolution is principally measured based on the minimum bed thickness that is distinguishable on the data set (Yilmaz, 1987), and is completely dependent upon the wavelength, the velocity divided by the frequency. Acquiring data that include more high frequencies allows for a higher resolution than conventional oil and gas seismic data (Widess, 1973). High-resolution frequencies are considered dominant 80 Hz and above, while conventional data routinely report dominant frequencies between 50 – 60 Hz (Sherriff, 2002). High-resolution is commonly the objective of near-surface seismic because of its ability to resolve thinner beds at shallower depths. Frequencies ranging up to several hundred Hz are essential for conducting a successful near-surface seismic reflection survey when resolving shallow targets is the objective (Pullan and Hunter, 1990). Higher frequencies are attenuated with true depth (Yilmaz, 2001). Conventional data collection is used when the focus is to image greater depths, in circumstances such as oil and gas exploration.

Elastic Waves and Elastic Constants

Seismic waves are elastic waves that propagate through the Earth (Yilmaz, 1987). The seismic method utilizes the propagation characteristics of these elastic waves (Sheriff and Geldhart, 1995). This study uses body waves (compressional (P-wave) and shear (S-wave) waves) to delineate the subsurface structure, measure rock velocities, and estimate the rock properties associated with the local site geology (Table 2). The velocity these waves move through the earth surface are dependent on density (ρ), and the elastic moduli: bulk modulus (k) and shear modulus (μ). These elastic constants are described as the strain of a given material under a specific type of stress (Lillie, 1999), directly relating the seismic velocities to the engineering world, and are defined as (Yilmaz, 1987):

Bulk Modulus (k) – the measure of incompressibility, the ability to resist being compressed; the ratio of hydrostatic stress over volumetric strain

Shear Modulus (μ) – rigidity, the measure of a materials ability to resist shear stress; the ratio of shear stress to shear strain

Lame's constant defines the relationship of these elastic moduli:

$$\lambda = k - \frac{2\mu}{3}$$

Using the bulk modulus (k), shear modulus (μ), Lame's constant (λ), and density (ρ) the velocities of P-wave (Vp) and S-wave (Vs) can be determined:

$$Vp = \sqrt{\frac{k + 4/3\mu}{\rho}} = \sqrt{\frac{\lambda + 2\mu}{\rho}}$$

$$Vs = \sqrt{\frac{\mu}{\rho}}$$

Seismic Velocities

Several conclusions can be made from the P- and S-wave equations (Yilmaz, 1987; Lillie 1999):

1) *Vs will always be slower than Vp when travelling through the same material.*
2) *Vs cannot travel through fluids and Vp will decrease through fluids faster than through rocks, because fluids have no shear strength ($\mu=0$).*
3) *The greater a rocks ability to resist compression, higher bulk modulus, the faster the Vp.*
4) *The greater a rocks ability to resist compression, higher shear modulus, the faster the Vs and Vp.*
5) *Vp and Vs are inversely proportional to density, which means rocks with lower density will a have higher velocity. Although in most cases when a rocks density is higher it is accompanied by higher bulk and shear modulus, therefore the velocity can be higher even when accompanied with higher densities.*
6) *Velocities tend to increase with depth due to deeper rocks being more compacted and cemented. They have higher shear and bulk modulus because they are more rigid and incompressible.*

By combining Vs with Vp the uncertainty in lithology can be improved (Yilmaz, 1987; Tatham & Stewart, 1993; Haines and Ellefsen, 2010). This is done by using the velocity ratio:

$$\frac{Vp}{Vs}$$

The higher the velocity ratio, the higher the Poisson's ratio. Vp/Vs ratio is directly related to Poisson's ratio (Castagna et. al, 1993). This has been used in oil and gas exploration as a

direct hydrocarbon indicator, such that a change in Poisson's ratio is related to a change in reflection amplitude (Ostander, 1984). Changes in bulk modulus, shear modulus, and density can be observed using Vp/Vs ratio. Understanding changes in the velocity ratio helps determine if there are any lithological or fluid based changes within the limestone unit above the mine (mine roof). Determining what is causing the Vp or Vs velocity to increase or decrease over time will give insight into what change has occurred in the rock properties (Table 3).

Areas of increased or decreased Vp/Vs ratio could imply an area of increased stress over a particular stretch of the mine roof compared to the rest. Depending on what causes a change in the Vp/Vs ratio, the Vp or the Vs changing, it can be determined whether the roof rock has areas of increase stress or if failure has begun. For example, an increased Vs would indicate a lower shear modulus in turn a higher area of stress. The Vp/Vs ratio from this study will be extremely helpful as a time-lapse tool. Changes in future studies of the Vp/Vs ratio would could cause for concern, because they would likely be indicative of higher stress over the mine roof, which would mean a greater risk of failure.

Vp	**Vs**	**Vp/Vs**	**Moduli Change**	**Stress Result**	**Overburden State**
increases	n/a	increases	Bulk Modulus increases	Increased stressed	Heightened potential for failure
n/a	increases	decreases	Shear modulus decreases	Increased stress	Heightened potential for failure
n/a	decreases	increases	Shear modulus increases	Yield has been reached	Failure has occurred
decreases	n/a	decreases	Bulk Modulus decreases	Relief of stress	Failure has occurred

Table 3: Changes to Vp/Vs ratio in future surveys would indicate changes in Bulk modulus and/or Shear modulus. This table indicates what changes in Vp and Vs could mean to the mine overburden.

METHODS

Reflection Data Acquisition

The KGS Exploration Services Group in conjunction with KDOT collected two seismic reflection data sets during two trips that spanned a total of eight days (Table 4) (Figure 15). Field conditions for both trips were ideal, with temperatures ranging from 21 to 30 degrees Celsius, minimal wind (< 8 km/h), and dry air, which allowed for optimal geophone coupling with the ground along the west road ditch. Cultural noise was present in the data as a result of the heavy traffic load on U.S. 69 highway and construction in the area. Both data were acquired and stored in industry standard SEG-2 format.

	P-wave	**S-Wave**
Date	08/2015	06/2016
Length of Profile	2.4 km	1.6 km
Frequency Sweep	25-300 Hz	15-150 Hz
Receivers	(3) 28 Hz vertical geophones	(1) 14 Hz horizontal geophones
Source Spacing	4.8 m	4.8 m
Receiver Spacing	2.4 m	2.4 m

Table 4: Reflection survey acquisition parameter comparison: P-wave vs. S-wave

Figure 15: Survey comparison, P-wave (red) vs. S-wave (blue). Both surveys first receiver started at 1001. The station was verified from one survey to another using GPS. Receiver 1001 is approximately just north location of the KS/OK state line (blue). The P-wave spans from 984 receivers (1001-1984), and the S-wave spans 625 receivers (1001-1624).

P-Wave Data Acquisition

The 2.4 km high-resolution compressional wave survey was acquired using a 600-channel rolling fixed-spread geometry. Three Sercel 28 Hz geophones in a 1 m array (Figure 16) were planted at each station on 2.4 m intervals to increase the signal-to-noise ratio (Myers et al., 1987). Geophones were planted in the west road ditch, in firm soil allowing the sensors 8 cm spikes to penetrate to the base of the geophone case for good coupling to the surface. For portions of the seismic line that crossed hard surfaces (i.e. intersections and in areas with road construction) rock plates were used in place of spikes. Rock plates do not couple as well as spikes but this approach avoided data dropouts.

An IVI MiniVib 1 was the seismic source. Three, ten second, 25-300 Hz linear upsweeps with a one second front and half second rear taper were imparted into the ground at each source station (Figure 17 and 18). Source stations were separated by 4.8 m, effectively every other receiver station, on the paved south bound lane. Source stations began 50 m south of the first receiver, to increase fold, and moved northward into the spread. Twenty-five networked, 24 bit, Geometric Geodes recorded data from up to 600 receiver stations for each shot (Figure 19). For each shot record a synthetic pilot trace and the ground force pilot were transmitted from the vibroseis and recorded at the seismograph. Each sweep was recorded and stored uncorrelated to allow signal enhancement and noise suppression during pre-correlation processing at a later date. A GPS data point was taken at every receiver location to ensure accurate spatial corrections during data processing and consistency for future surveys.

Data were acquired using fixed spread geometry that rolled increments of receivers from behind the source to in front of the source to maintain optimum offsets in front and back of the source. As the MiniVib moved midway into the receiver spread, receivers from the back of the

line were “rolled” to the front of the line and connected to the recording system defining the new fixed spread. During the 2.4 km survey 456 to 600 channels were actively recording during any given time of acquisition. This number of recorded channels varied as source operations continued as stations were rolled forward. US Highway 69 remained open and received high traffic volumes, consistent with normal load, the entire time of data collection. KDOT restricted traffic flow by closing the south bound lane and guided traffic back and forth along the North bound lane at controlled speed and quantity. The MiniVib source vehicle occupied the open lane. Well locations were logged and GPS data points were taken at their location to allow accurate correlation of seismic with well data. Analog field notes were heavily utilized for indicating dead phones, culverts, and shot stations skipped all key to allow for detailed and accurate preprocessing.

During the survey, damage to a seismic cable from an 18-wheeler caused a decrease from 600 to 456 recording channels. The first 144 channels were lost for a short period of time. This resulted in a decrease in fold for a small portion of the line. There was minimal effect on the resulting 2-D reflection profile even with a variation in total receiver count.

S-Wave Data Acquisition

The 1.6 km shear wave survey was conducted using a 612-channel rolling fixed-spread geometry. One Geospace 14 Hz shear component geophone was planted in S_H orientation at each receiver station spaced at 2.4 m. Geophones were secured to the west road ditch in hard soil using 7.3 cm spikes for coupling to the surface. Similar to the P-wave acquisition, rock plates were used in place of spikes across portions of the survey line that crossed hard surfaces was necessary (i.e. intersections and in areas with road construction). Source stations were spaced

every 4.8 m along the paved south bound highway lane. Source stations began at the first receiver station just north of the KS/OK state line (less than ¼ km from the border).

An IVI MiniVib 1 with a shear oriented mass was the source, and generated three, 10 second, 15-150 Hz linear upsweeps with half second tapers at each source station (Figure 17 and 18). Twenty-six, 24 bit, Geometric Geodes were used for data collection resulting in up to 612 recorded traces for each shot (Figure 19). The third trace in each shot record was the ground force pilot radio transmitted from the vibroseis to the seismograph. Traces one and two were not in use for this study. Each sweep was recorded and stored uncorrelated, allowing pre-correlation processing at a later date.

As the MiniVib moved through the 612-channel spread 24 receiver stations at a time were rolled from the back to the front of the line. During acquisition 288 to 612 channels were actively recording at any given time during the full 1.6 km survey. As the MiniVib occupied the south bound lane KDOT kept the highway open controlling traffic speed and quantity in the north bound lane. All well locations were logged to allow correlation with P-wave seismic data and well data. Inactive geophones, culverts, and unoccupied shot stations were to allow for appropriate correction during preprocessing. It was determined through analysis of the P-wave data set that a shorter 1.6 km survey was adequate for imaging of the mine void areas.

Figure 16: Receiver Station with 3-28 Hz geophones planted in approximate 1 m arrays.

Figure 17: IVI Mini 1 Vibroseis.

Figure 18: IVI Mini 1 Vibroseis' plate used to induce P-wave energy with a linear upsweep.

Figure 19: Gator housing the 600 channel Geometrics seismograph where data collection was controlled.

Vibroseis Correlation

The vibroseis method was used to acquire both P- and S-wave reflection surveys. It has proven to be the most effective and efficient way to collect high-resolution near-surface seismic reflection data in this kind of setting and depth of interest. Advantages of the method include the ability to control frequencies and high repeatability. This method relies on a source transmitting an amplitude and frequency into the ground across a time period (Ristow and Jurczyk, 1975). The earth generates a response to the source resulting in the sensor responding to a sinusoidal ground motion. Convolution (*) between the acoustic impulse response, reflectivity, r(t), and the vibroseis sweep, s(t), with the addition of uncorrelated noise, n(t), results in the uncorrelated seismogram, x(t). This is represented by the basic seismic convolution model for a seismic source equation (Brittle et al., 2001):

$$x(t) = r(t) * s(t) + n(t)$$

The resulting recorded trace from the source will have an implanted sweep in the data which is removed by cross-correlation. Cross-correlating (◊) the vibroseis pilot trace, drive, or a synthetic with the raw trace, removes the sweep, and results in the frequency regulated sweep to collapse. It is then replaced with a zero phase Klauder wavelet, k(t), which convolves onto the reflectivity sequence (Yilmaz, 2001). Cross-correlation is portrayed by (Brittle et. al, 2001):

$$x_{cc}(t) = r(t) * s(t) \lozenge s(t)$$

The Klauder wavelet is defined as the cross-correlation of two identical sweeps, the equation can be simplified to:

$$x_{cc}(t) = r(t) * k(t)$$

Seismic Reflection Data Processing

Software developed at the KGS including SeisUtilities, LWSeis, WinSeis, and SurfSeis, were used to process all seismic data in this study. Surfer (Golden Software) was used to display the velocity map generated with KGS software. Architecture, sequence, and detail of processing steps used to generate the final CMP stacked sections were consistent with common work flows used in traditional 2-D high-resolution near-surface CMP processing methods (Steeples and Miller, 1998; Miller, 2007). Each data type was processed using a customized flow and parameters unique and specifically tuned to ensure for the most representative stacked section for each (Figures 20 and 21). All data were stored in industry standard SEG-2 format.

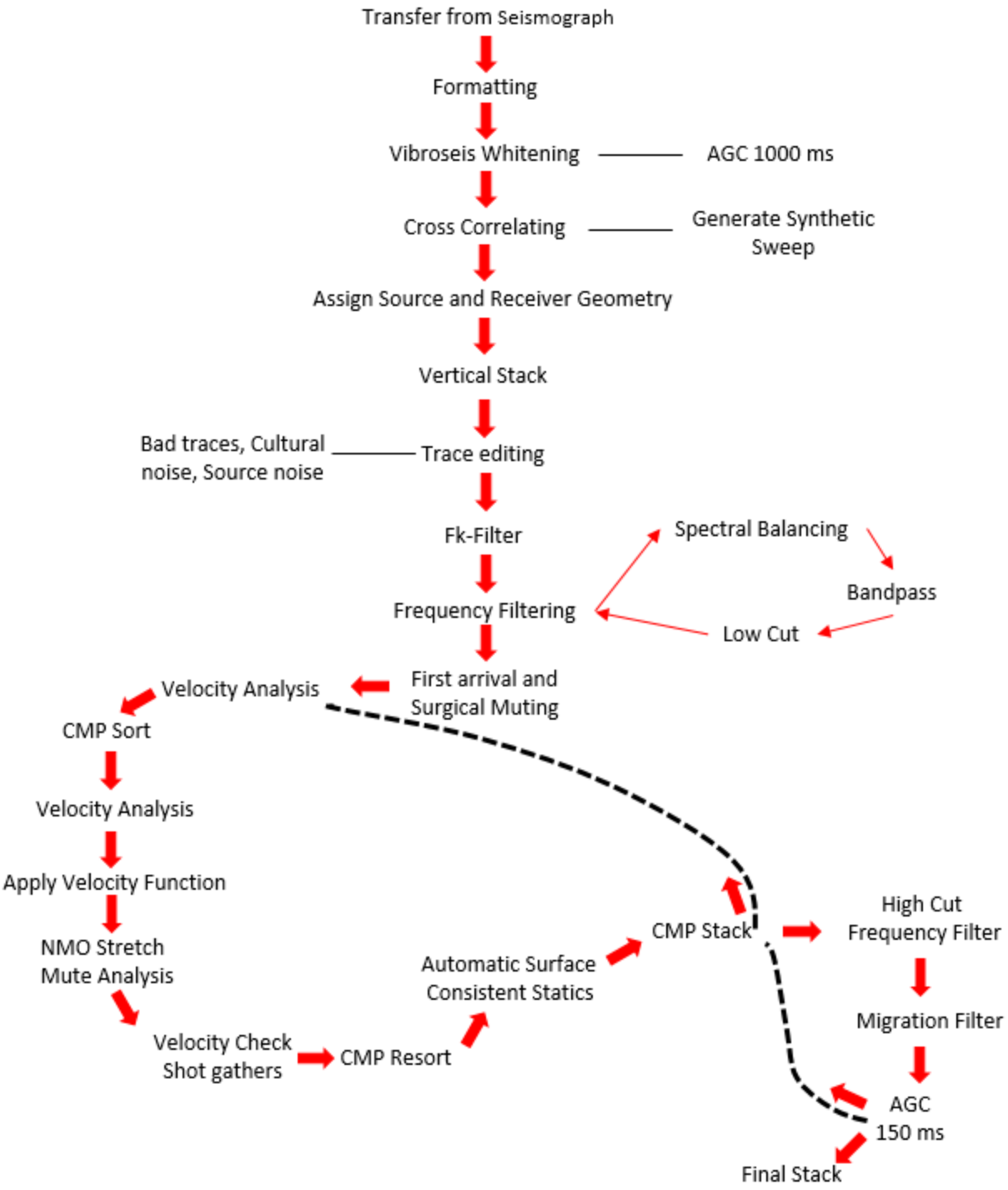

Figure 20: P-wave processing flow

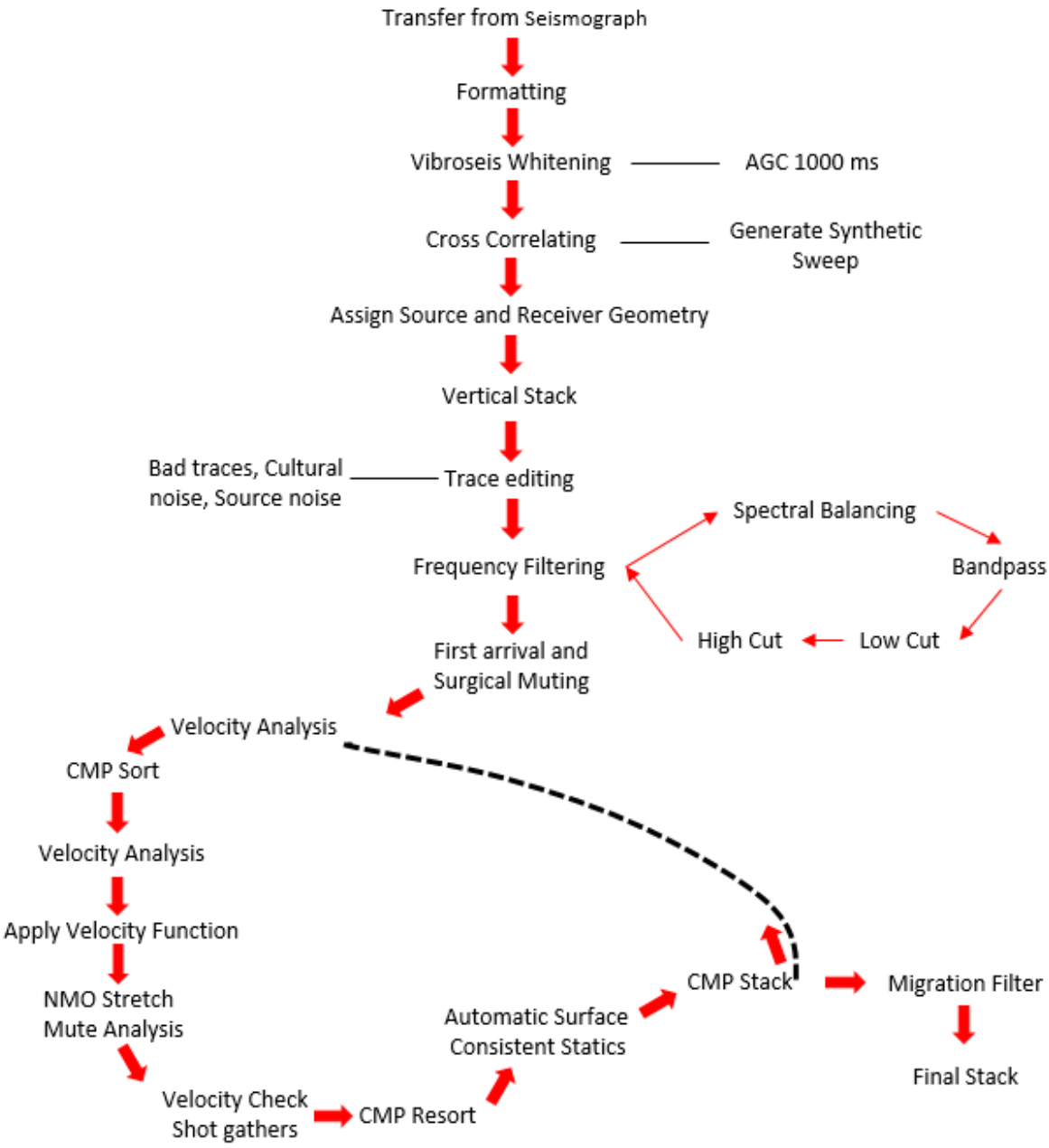

Figure 21: S-wave processing flow

P-Wave Data Processing

State of the art processing steps were used to ensure for the most accurate final stacked section. Data were converted from SEG-2 to a modified SEG-Y format. Pre-processing steps tailored for these data helped suppress noise and reduce unwanted signal, resulting in optimum signal-to-noise ratio. High ambient noise, as well as narrow bandwidth coherent noise generated by the source, can plague near-surface seismic data. This can lead to reflections being masked by noise and a decrease in resolution (Doll and Coruh, 1995). Past studies indicate vibroseis whitening (VSW) improves trace to trace waveform consistency, enriches the post correlated signal bandwidth and improves signal-to-noise ratio (S/N), suggesting it should be routinely applied to high-resolution CMP data (Lambrecht et al., 2004; Lambrecht 2006; Judy 2015). VSW improves the data by equalizing low and high amplitudes through applying a floating gain control over the full frequency spectrum. This can drastically improve data resolution and the apparent continuity of waveforms from trace to trace (Klemperer, 1987; Lambrecht et al., 2004) and increase the amplitude of the high frequency portion of the spectrum (Coruh and Costain, 1983). VSW was applied to these data by applying a one second automatic gain control (AGC) before cross correlation.

The raw recorded field traces represent the convolution between the vibroseis sweep and the reflectivity of the earth. A synthetic sweep matching the vibroseis drive signal was cross correlated with the recorded traces to generate correlated traces. Field geometry was applied, assigning the correct source and receiver locations to the correlated traces. Trace editing was done to remove dead, noisy, and low signal-to-noise traces on individual shot records. Shot records with high amplitude noise or inconsistent quality were omitted from the vertical stack.

High quality traces from multiple shots recorded at each station were vertically stacked to increase S/N of coincident recorded traces at each shot point (Figure 22).

These data were plagued with noise, due for the most part to the high traffic volume. The complex nature of the highly faulted and fractured subsurface, mine geometry also complicated the wavefield. Identifying reflections in the raw correlated and stacked shot records was difficult due to the presence of noise. Reducing this high level of noise required extensive data conditioning (e.g. frequency filtering) to target improvement of the amplitudes and coherency of reflections, and suppress noise. An F-K-filter was applied to reduce noise in the upper 150 ms (Figure 23). High frequency components of a propagating seismic wave attenuate more rapidly than low frequencies due to energy dissipation and absorption losses. This attenuation of the high frequencies result in narrowing of the band and drop in dominant frequency (Judy, 2015). Spectral balancing addresses this selective attenuation by enhancing shallow reflections, improving overall resolution. Spectral balancing was applied to these data consistent with sweep frequency range (25 - 300 Hz). This approach enhances higher frequencies and flatten the amplitude spectrum across the entire data set. This approach was designed to increase the effective bandwidth and therefor resolution. A bandpass and low cut filter were then utilized to attenuate additional noise and surface waves allowing further noise suppression, thus improving S/N and clarity of reflections on shot gathers (Figure 24).

Precise muting is a crucial step in any seismic data processing flow. First arrival muting was applied to remove high amplitude first arrival energy. This noise can mask reflections on NMO corrected and stacked sections (Figure 25). A surgical cone mute was then designed and applied to remove unwanted coherent noise, ground roll, and air wave energy present in this data within the noise cone (Figure 26). Some reflection events in this data set were in the 40 – 50 ms

range making distinguishing them from first arrival energy a challenge. Extreme caution was necessary to ensure the correct interpretation of all energy types (Steeples and Miller, 1998; Miller, 2007).

Detailed velocity analysis allowed Normal Moveout (NMO) velocity corrections to be applied in route to an interpretable first brute stack of the subsurface. Further analysis included the use of constant velocity panels (Figure 27). The final velocity function was developed using spatial groupings of 25 CMPs and a focus on time depths in the upper 200 ms. Stacking velocities ranged from 1,600 m/s to 2,875 m/s. These are reasonable velocities for the documented structural altered subsurface and lithological intervals in this area.

The highly altered subsurface combined with the mine geometry were responsible for a variable lateral velocity field across the entire data set. These high variable velocities resulted in static issues. To address these static issues, automatic static corrections were applied with a maximum static shift window of 3 ms. These subwavelength shifts allowed trace by trace reflection arrival times to shift to their correct temporal location without artificial enhancement to coherency. Velocity analysis was combined in a cyclic fashion with automatic surface consistent statics to generate a meaningful common midpoint stack.

Reflections must be tracked through the entire processing flow to prevent the likelihood of artifacts in the data (Miller et al., 1997). Reflections on the CMP stacked section were correlated back to the original hyperbolic reflection events on shot records and CMPs (Figure 28). NMO quality checks were performed by resorting the data back to shot records and CMPs with NMO corrections applied, to ensure the proper NMO velocity had been used in the velocity function. The flatness, or linearity, of the previously hyperbolic events are a measure of the

accuracy of the NMO velocity function. The quality checks can also aid in determining proper NMO stretch mute (Miller, 1992). A 25% NMO stretch mute was used and is sufficient and reasonable for this near-surface data set. Upon completion of NMO quality checks, a final high cut filter was applied to the CMP stacked section to reduce background ambient noise.

Both time and depth poststack migration methods are standard parts of a work flow when processing near-surface seismic reflection data (Bradford et al., 2002). Migration improves the accuracy of the data by re-locating reflecting points to their proper location. For example, in this particular data set a proper migration could have moved the reflections to match the reflectors and removed in the plane diffractions and scatter present in the P-wave stacked section. Critical to migration is an accurate velocity function to properly correct the dataset. Due to the highly variable velocity function at this site, in part due to the structural deformation and minimal reflectors in the shallow subsurface, traditional reflection data migration proved incapable of accurately correcting the optical distortion in this dataset.

Identifying complexities of varying lateral and vertical velocities sometimes associated with the near-surface can prove to be unrealistic when trying to migrate the data properly (Ivanov et. al., 1998). F-k migration is not recommended for near surface reflection seismic data because of how severely it can reduce the bandwidth to a large part due to the limitation on how the velocity is applied in making the projections (Ivanov et. al., 1998). Also, migration is sometimes skipped on near surface reflection data because changes in reflection points with lower velocities can be minimal (Black et al., 1994). The presence of reflections that were laterally inconsistent across the data set combined with the complexities associated with the highly altered near-surface geology and mine geometry where key factors that inhibited

assignment of a proper migration velocity function which would improve accuracy of the resulting CMP stacked image.

An F-k migration filter was used to enhance wavelet coherency (Ivanov et. al., 1998) and reduce much of the out of the plane scatter. The F-k migration filter allows for preservation of high frequencies while enhancing data quality through increasing signal-to-noise ratio by attenuating high-frequency random noise in the F-k domain. It improves data coherency without dramatically narrowing the bandwidth of reflections and reduces high frequency random noise by defining a significantly larger trace spacing which allows for all data to be retained as opposed to deleted (Ivanov et. al., 1998). A three velocity-time function was defined at every 25 CMPs and a trace spacing of 24 m (ten times the acquisition receiver spacing, 2.4 m) to generate the correction function for the migration filter. That velocity function was also used for producing a depth converted section.

A final AGC (150 ms window) was then applied to the migration filtered depth-converted stacked section to improve both the signal-to-noise ratio and the ability to interpret the 2-D seismic cross-section (Figures 29 and 30).

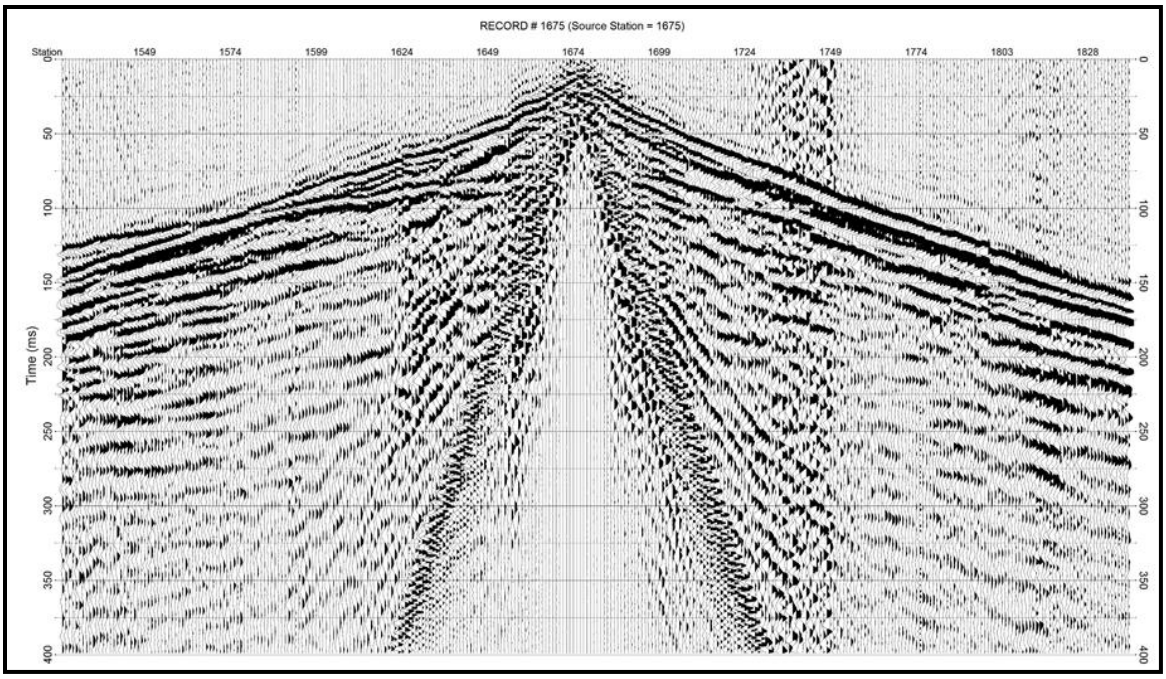

Figure 22: Representative P-wave shot record that has been vertically stacked with pre-correlation vibroseis whitening applied. A hyperbolic event (reflection) is observed at ~75 ms.

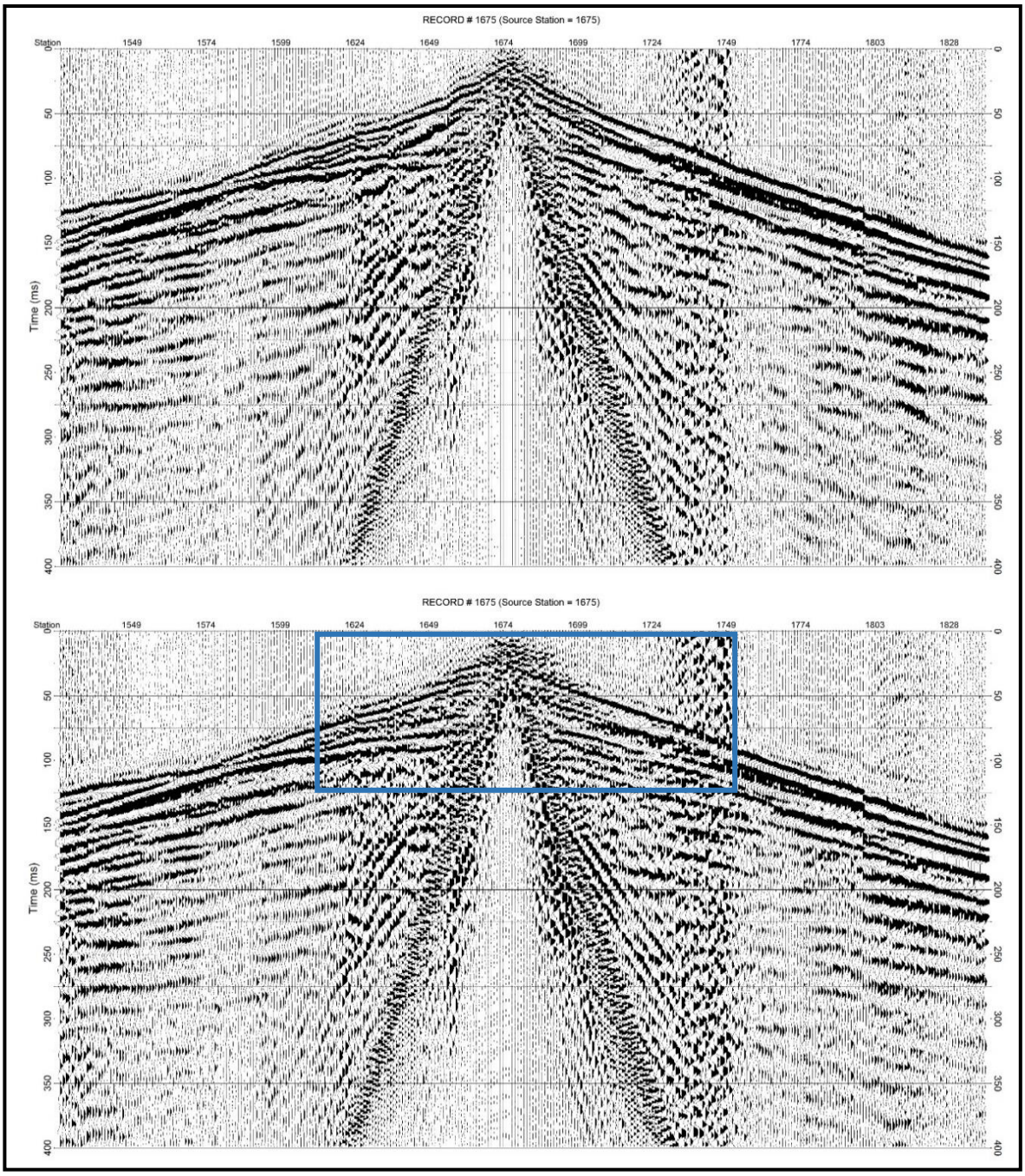

Figure 23: (Top**)** Representative P-wave shot record that has been vertically stacked with pre-correlation vibroseis whitening applied. (Bottom) The representative shot gather from above with an additional F-K filter applied. The upper 150 ms showed the best results of the F-K filter increasing the signal-to-noise (blue). The coherency of the reflection at 75 ms is drastically improved as a result of the filter.

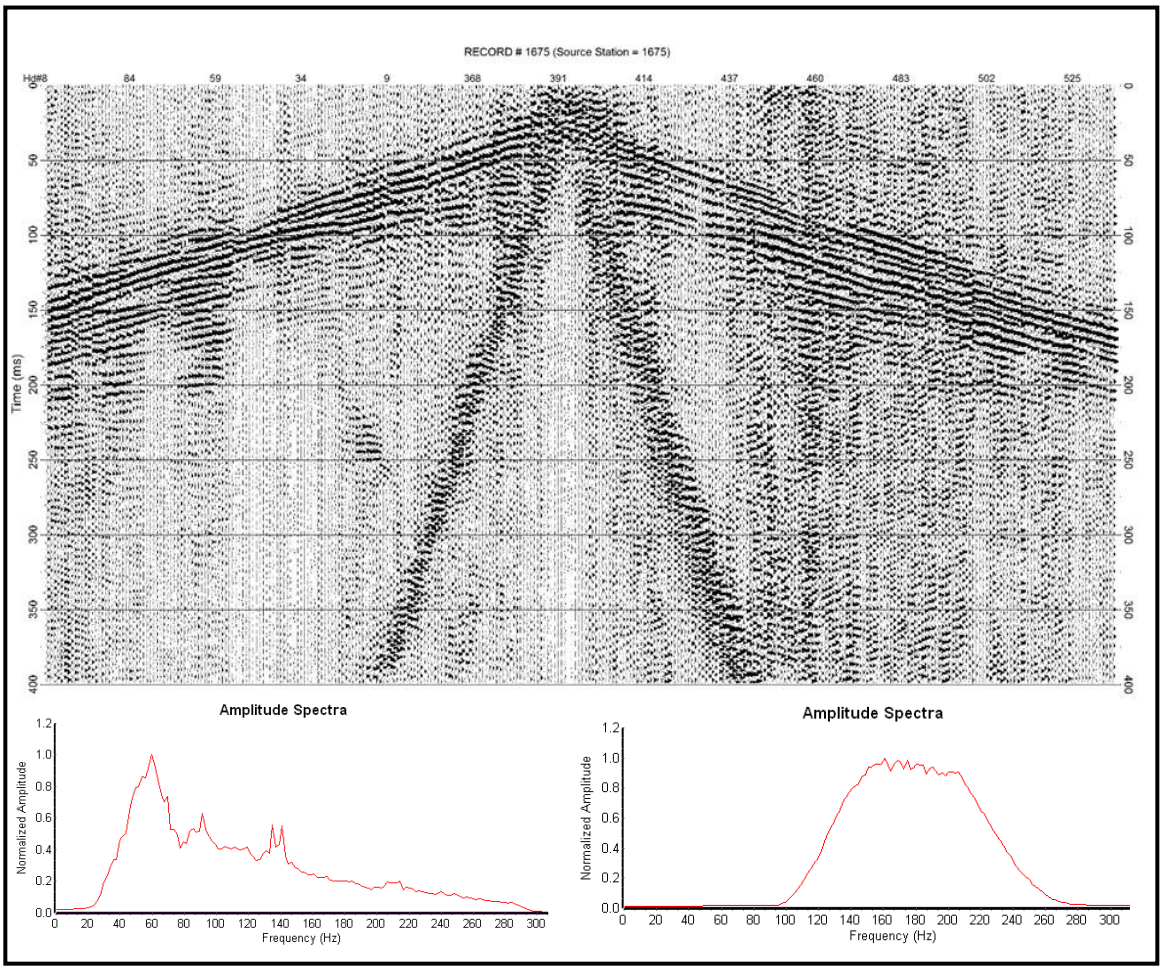

Figure 24: (Top**)** Representative P-wave shot record with frequency filtering and spectral balancing applied. (Bottom left) Amplitude spectrum before spectral balancing and frequency filtering. (Bottom right) Amplitude spectrum after spectral balancing and frequency filtering. Cutting out some of the low frequencies (<100) helped reduced some of the high amplitude energy in the shot records, which were masking reflections.

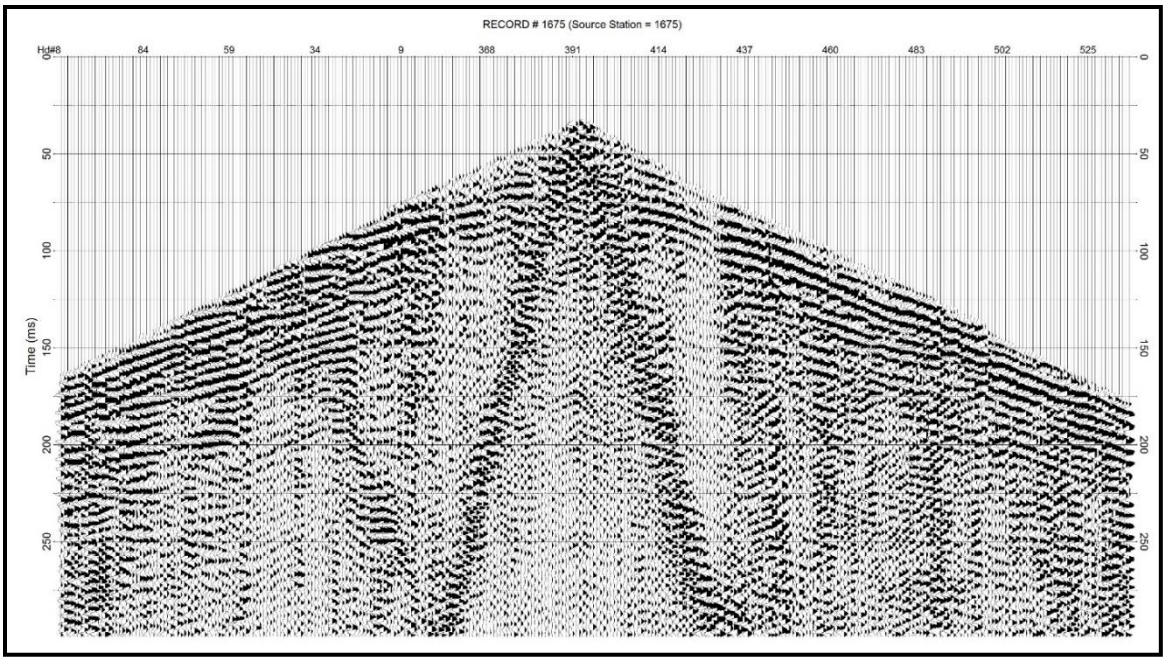

Figure 25: Representative P-wave shot record with first arrival muting applied.

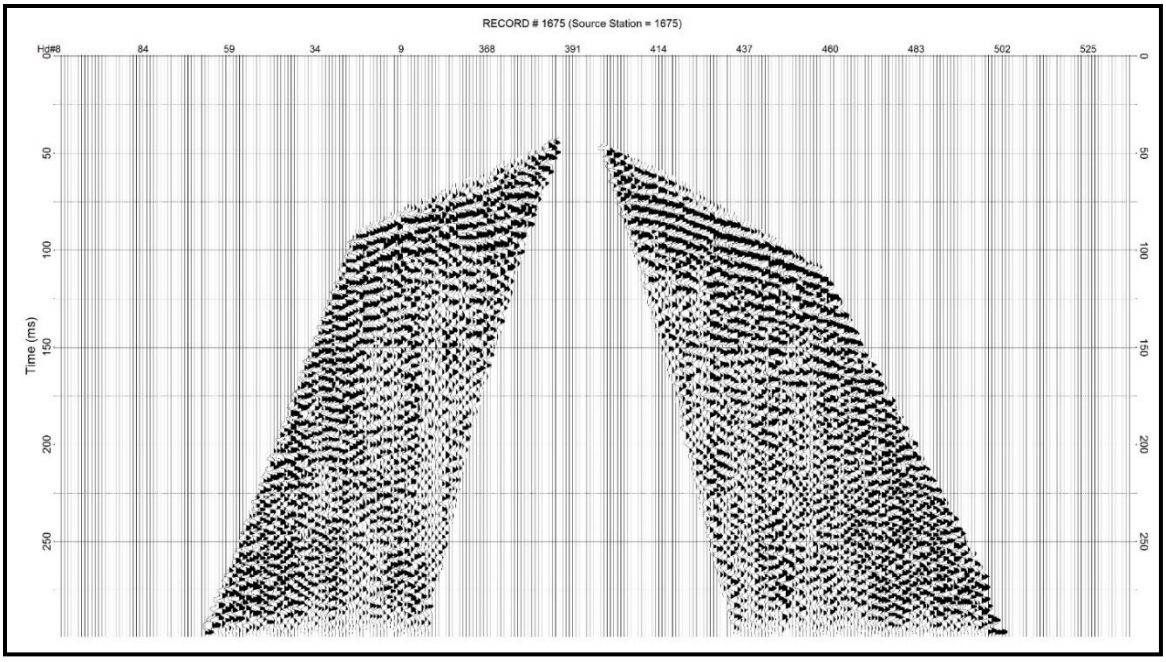

Figure 26: Representative P-wave shot record with additional first arrival muting and surgical cone mute applied.

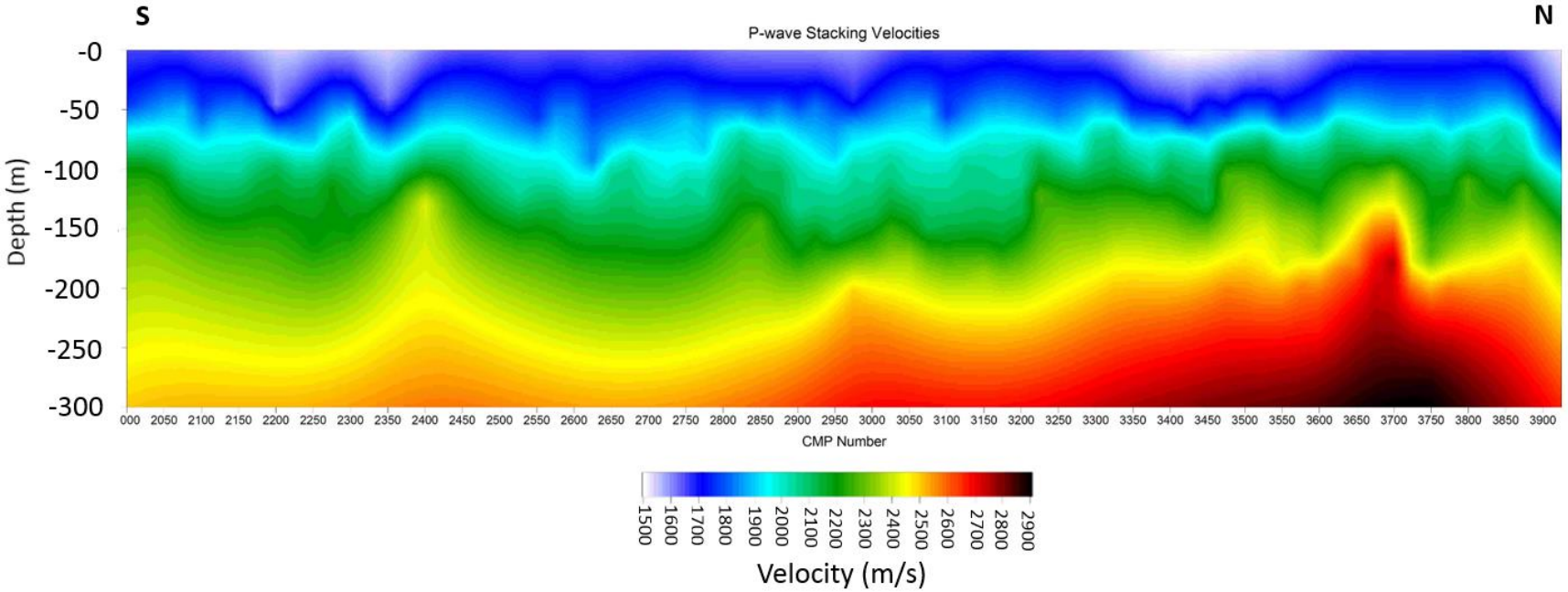

Figure 27: Plotted stacking velocities of the entire P-wave line used for NMO corrections. Notice the lateral variability in the velocity function due to the altered subsurface. Also, notice the increased velocities on the north end, which are associate with the Miami trough. The teepee like feature of increased velocity around CMP 2400 is a result of interpolation of the picking velocities. A velocity near -125 m was picked near CMP 2400 resulting in this anomalous increase on the velocity profile.

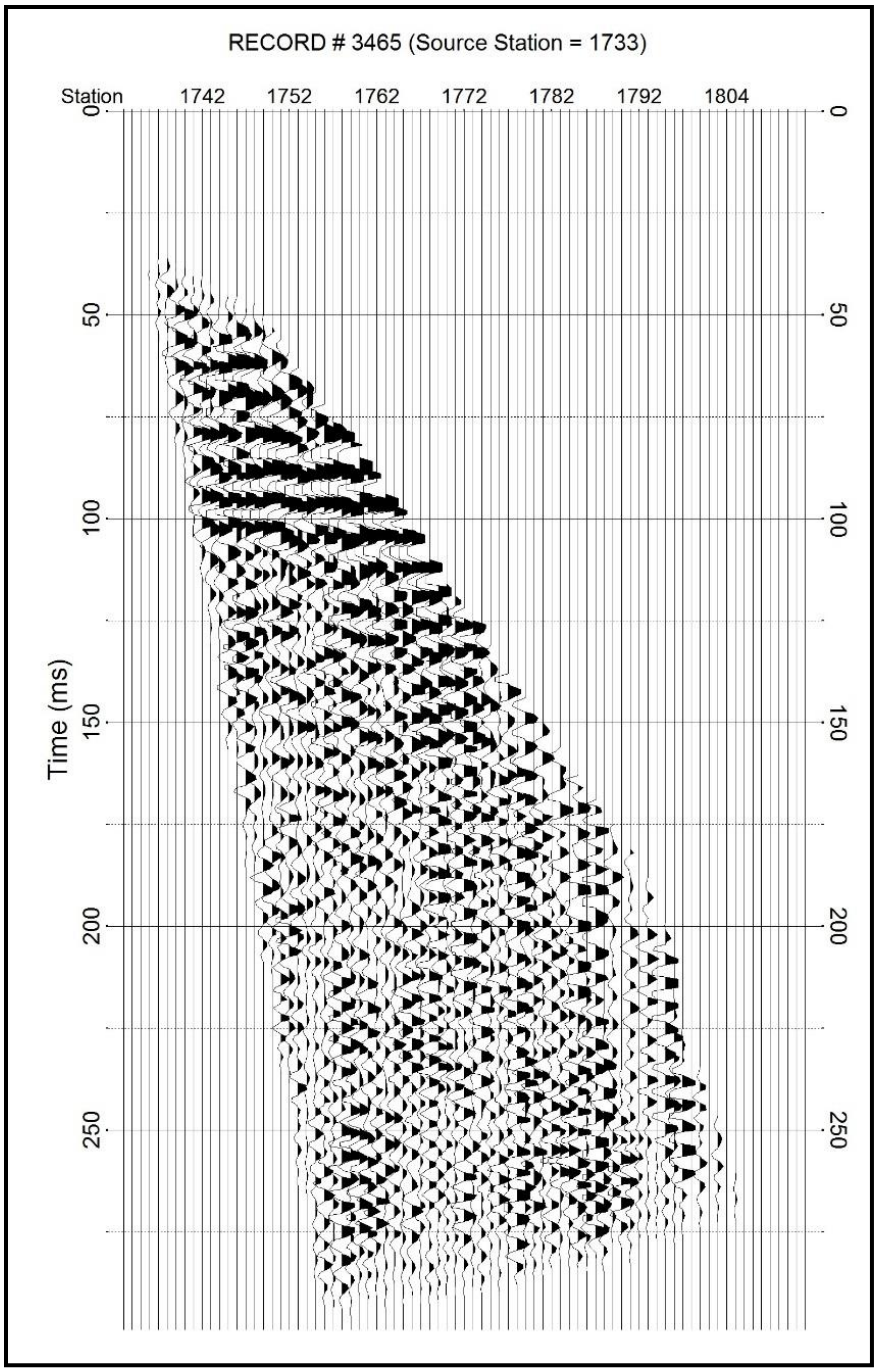

Figure 28: P-wave CMP gather with NMO and static corrections applied.

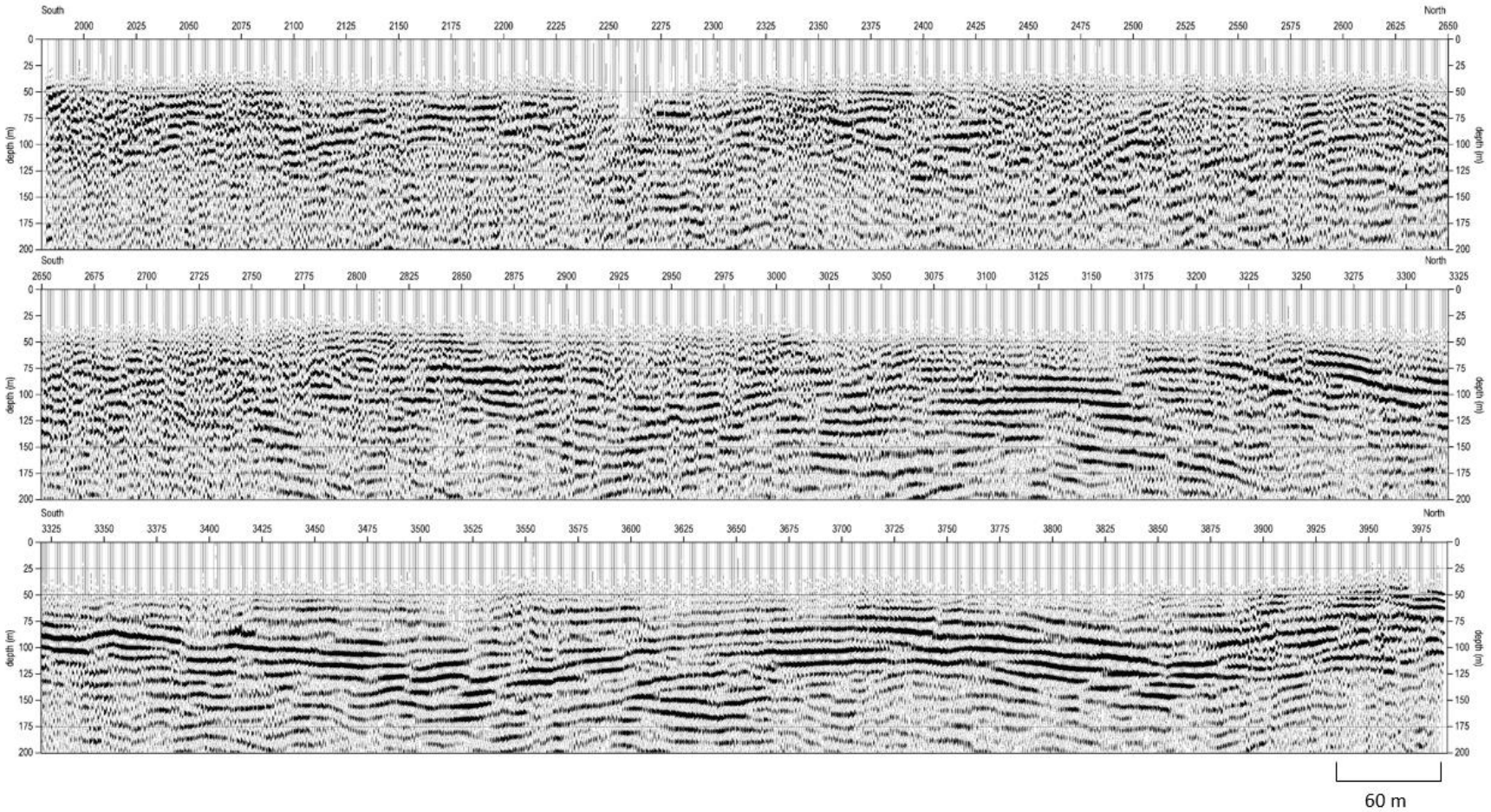

Figure 29: 2-D profile of the fully processed P-wave uninterpreted CMP stacked section. The beginning of the survey starts from the south at CMP ~ 1982 (top image) and ends at CMP ~ 3980 to the north (bottom).

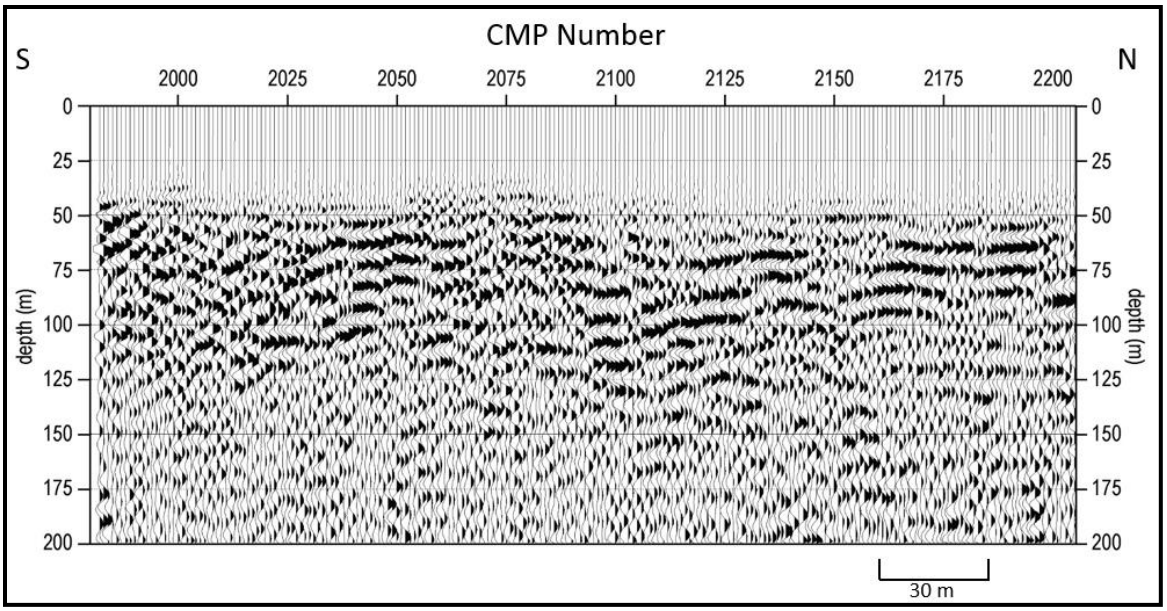

Figure 30a: Zoomed in portion of the southernmost section (~CMPs 1980-2200) of the P-wave stacked section.

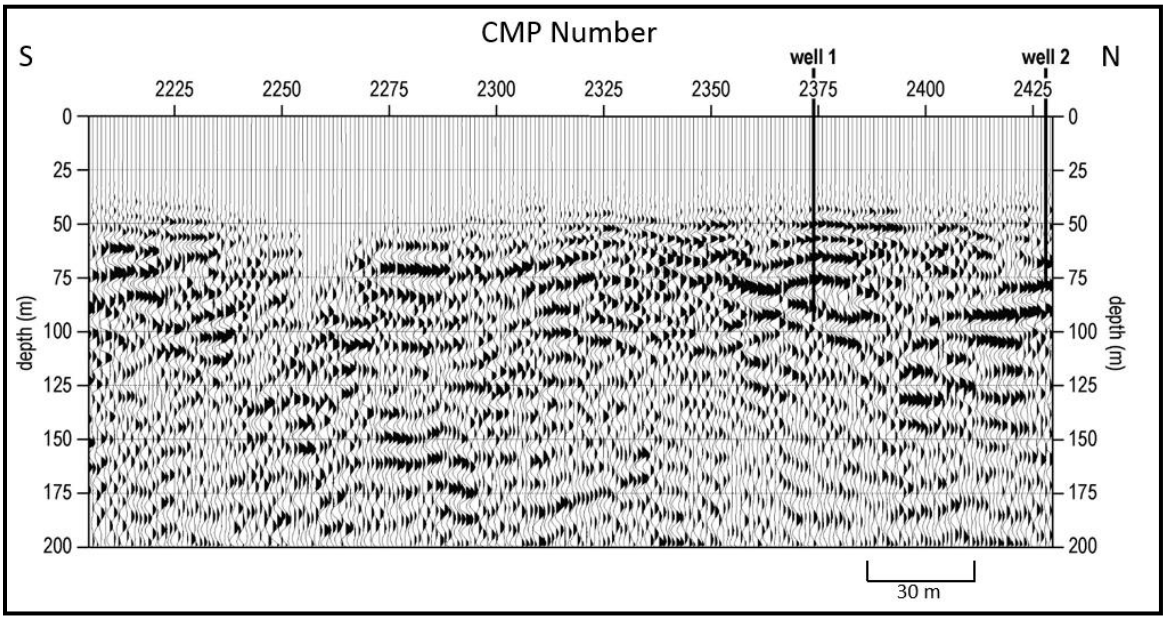

Figure 30b: Zoomed in portion of the ~CMPs 2200 – 2200 of the P-wave stacked section. Wells 1 and 2 are identified at their respected CMP station location.

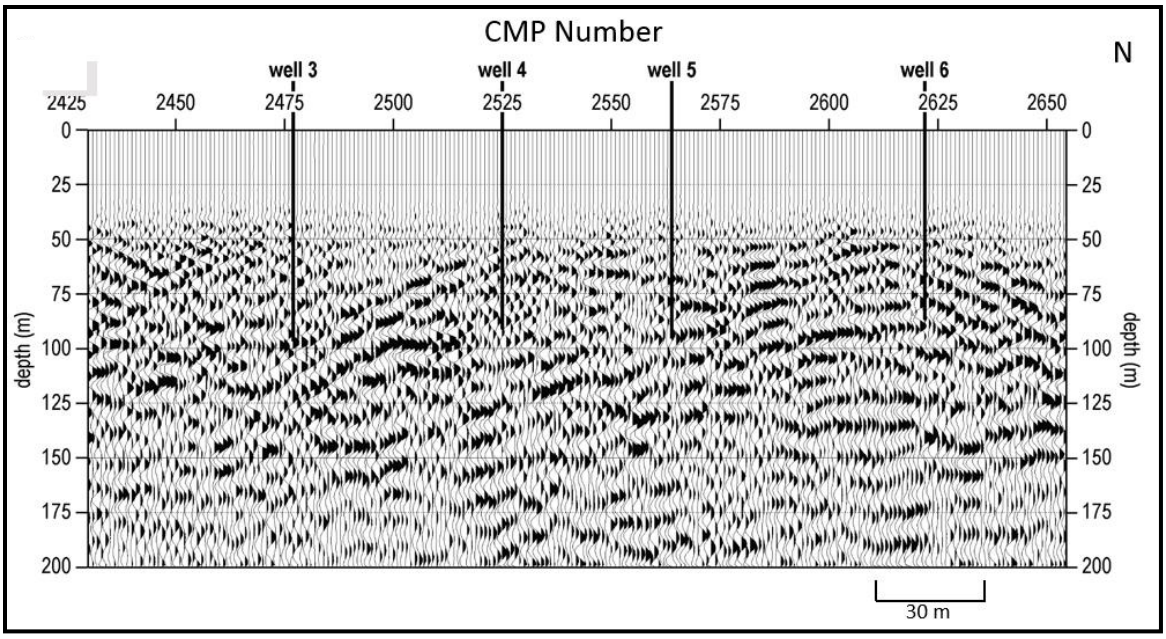

Figure 30c: Zoomed in portion of the ~CMPs 2425 – 2650 of the P-wave stacked section. Wells 3 – 6 are identified at their respected CMP station location.

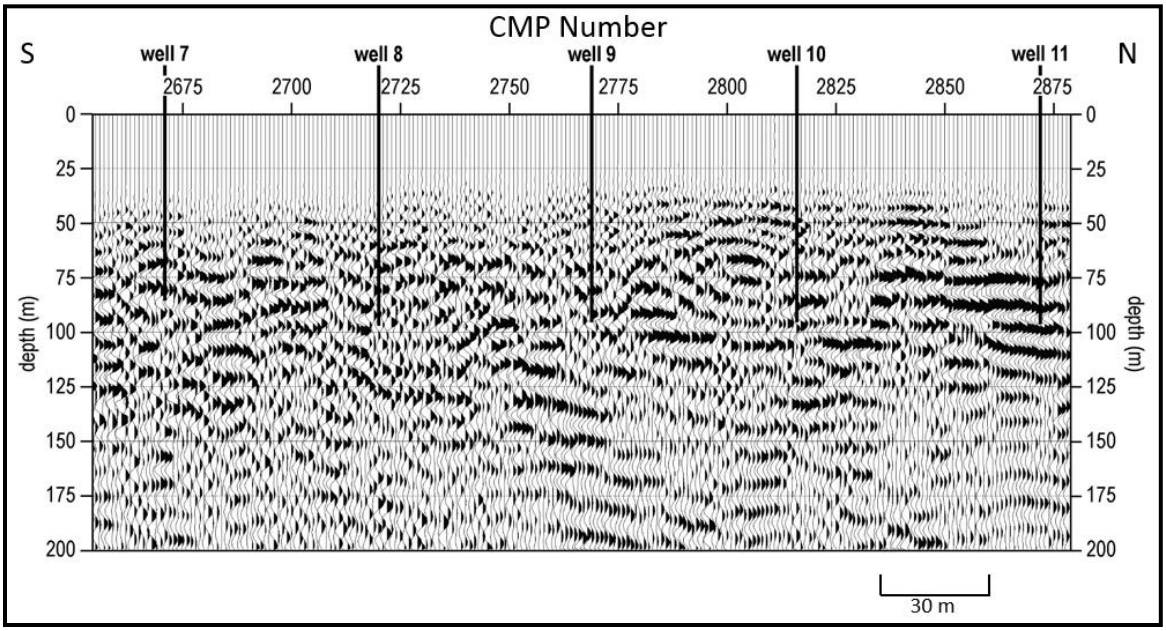

Figure 30d: Zoomed in portion of the ~CMPs 2650 – 2875 of the P-wave stacked section. Wells 7 – 11 are identified at their respected CMP station location.

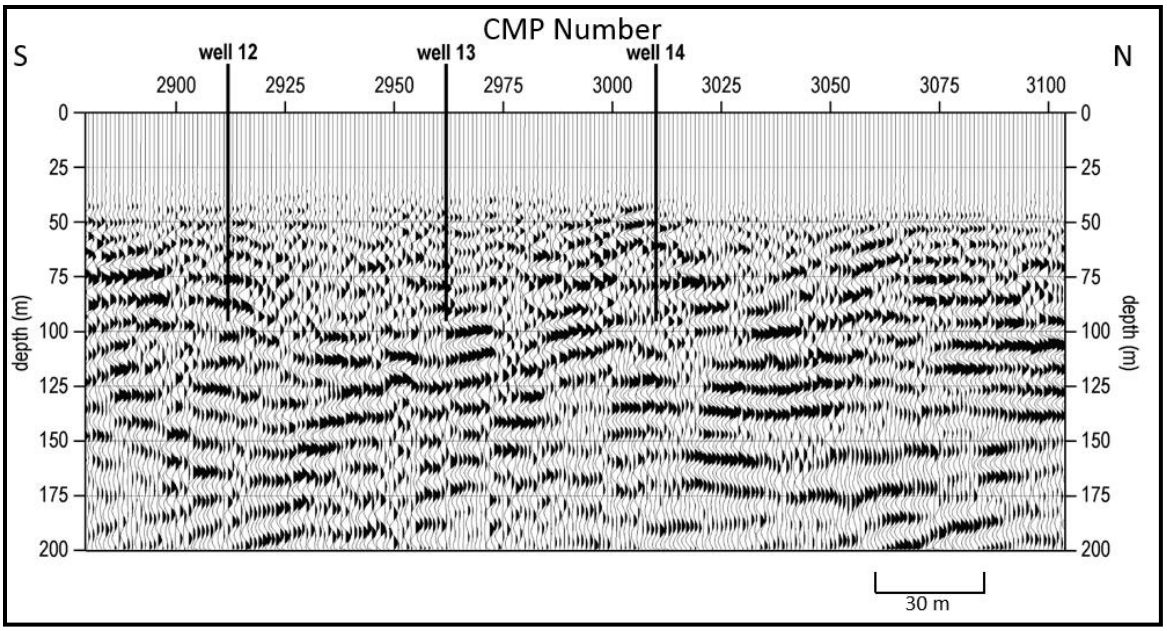

Figure 30e: Zoomed in portion of the ~CMPs 2875 – 3100 of the P-wave stacked section. Wells 12 – 14 are identified at their respected CMP station location.

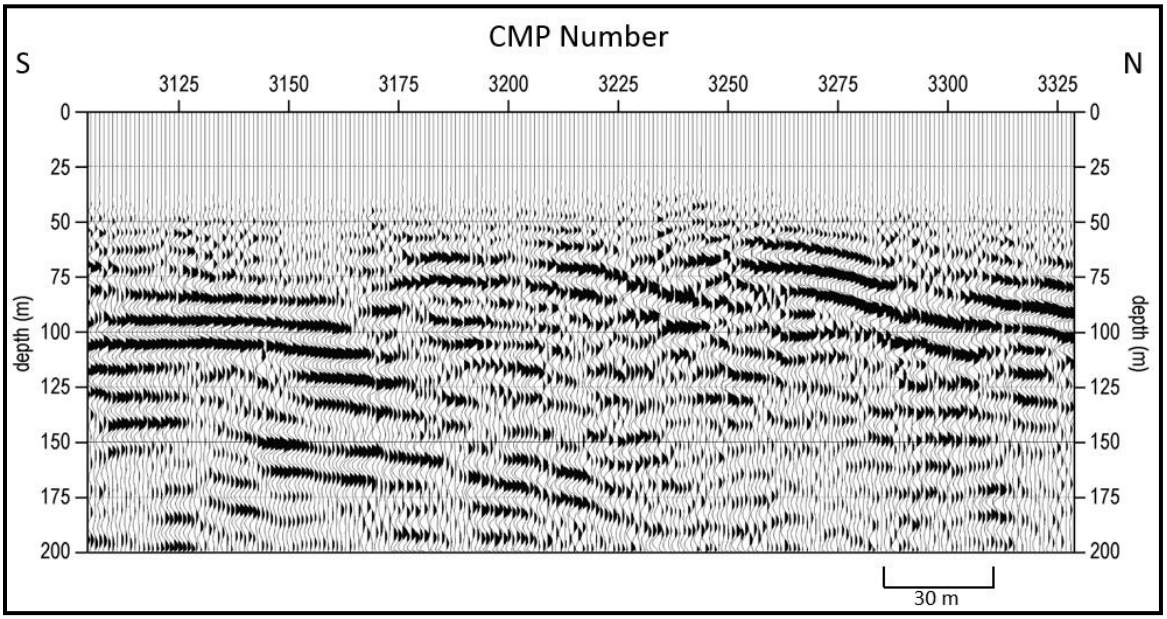

Figure 30f: Zoomed in portion of the ~CMPs 3100 – 3325 of the P-wave stacked section. Reflection amplitude has increased moving north into the vicinity of the Miami Trough.

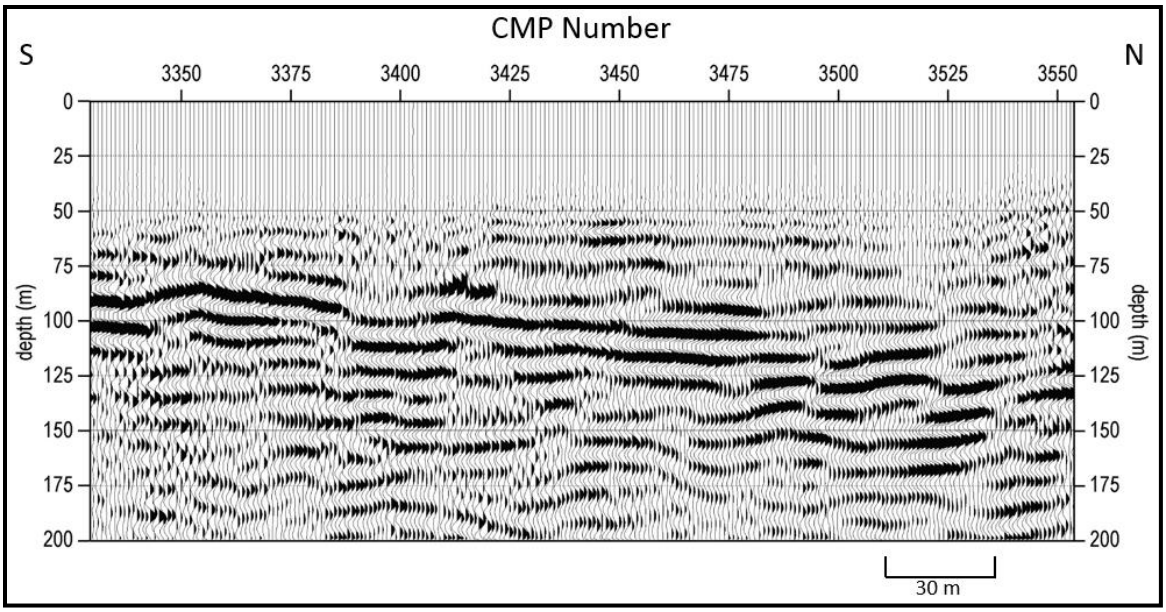

Figure 30g: Zoomed in portion of the ~CMPs 3325 – 3550 of the P-wave stacked section.

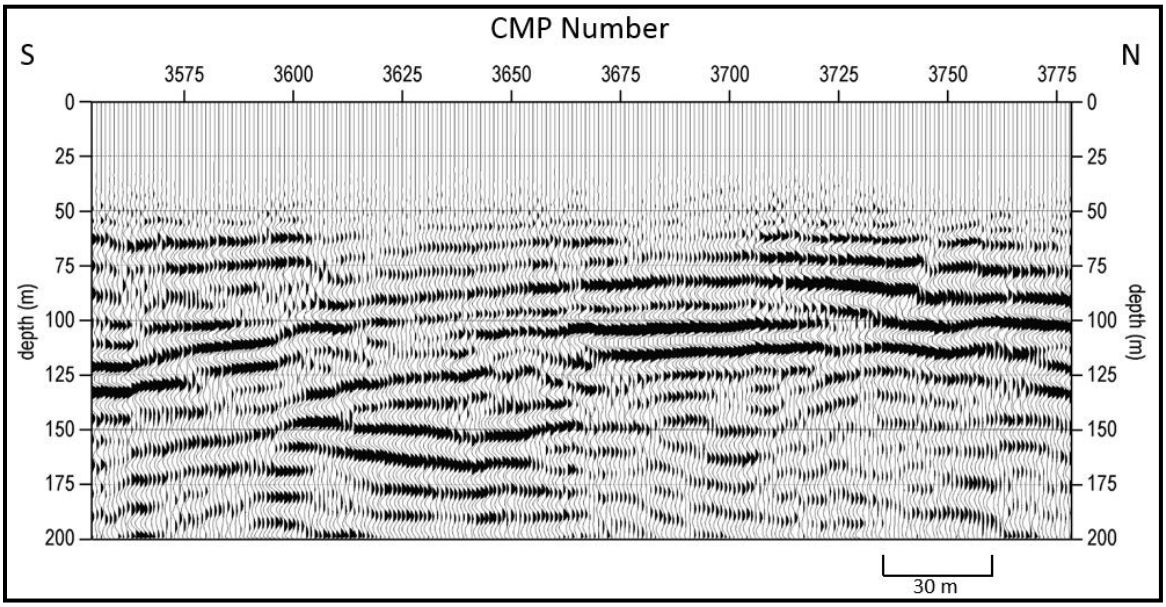

Figure 30h: Zoomed in portion of the ~CMPs 3550 – 3775 of the P-wave stacked section.

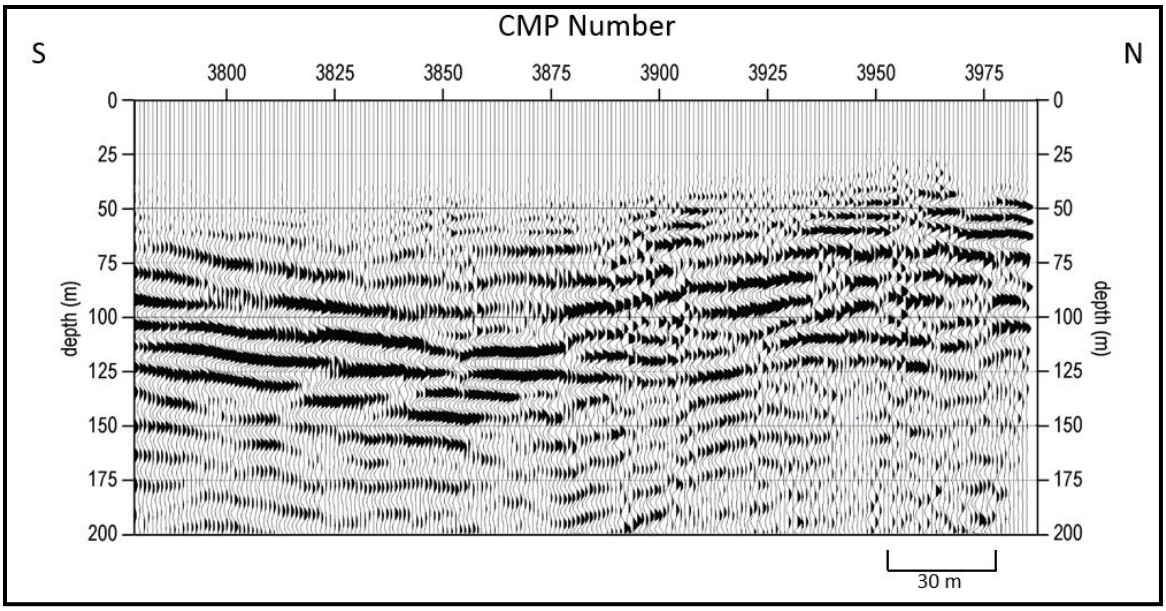

Figure 30i: Zoomed in portion of the northernmost portion ~CMPs 3775 – 3980 of the P-wave stacked section.

S-Wave Data Processing

Although the S-wave processing flow was similar to the P-wave, they were not identical (Figures 20 and 21). Overall these S-wave reflection data lacked laterally consistent reflections and were plagued by lower S/N than the P-wave data. Pre-processing steps were consistent with the P-wave data set and included: VSW, cross correlation using a synthetic sweep matching the vibroseis drive signal, assigning geometry, trace editing, and then vertically stacking all three shot records. As with the P-wave data these steps helped reduce coherent noise caused by traffic, construction, field crew, wind, etc. (Figure 31).

Spectral balancing was applied across the sweep frequency range (15-150 Hz). A bandpass and low cut filter were also used. A high cut filter was applied next to help further decrease the overwhelming spectrally unique noise in the data (Figure 32). First arrival and cone mutes were applied to remove unwanted source energy (Figure 33). The cone mute was used primarily to remove air wave, but also to remove surface wave energy that could not be attenuated through filtering, and that would result in unwanted energy in the final stacked section (Figure34).

Velocity analysis was the most challenging part of this processing flow due to the presence of higher mode surface waves that plagued the data set. Therefore, caution was taken to ensure first arrival and surface wave energy were interpreted correctly and not mistaken as reflection events. Velocity analysis was approached very systematically, using constant velocity panels combined with automatic surface consistent statics, to generate representative stacked sections. The final velocity function was formulated using groupings of 25 CMPs within the upper 440 ms. Stacking velocities ranged from approximately 1,000 m/s to 1,700 m/s. This range is reasonable for the lithology in this vicinity and within expectation, considering the P-wave velocity function (Figure 37). NMO corrected shot gathers and CMP gather stacked sections

(Figure 38) were evaluated to establish quality and cross checked to confirm the reflections on the stacked records were in fact reflections, and not coherent noise stacking coherently on CMP stack images. A 25% NMO stretch mute was assigned to the NMO correction. A maximum shift window of 3 ms for automatic surface consistent statics was used to allow trace by trace arrival times to shift to their zero-offset time. Finally, an F-K migration filter was used in route to generating a final depth converted stacked section (Figures 37 and 38).

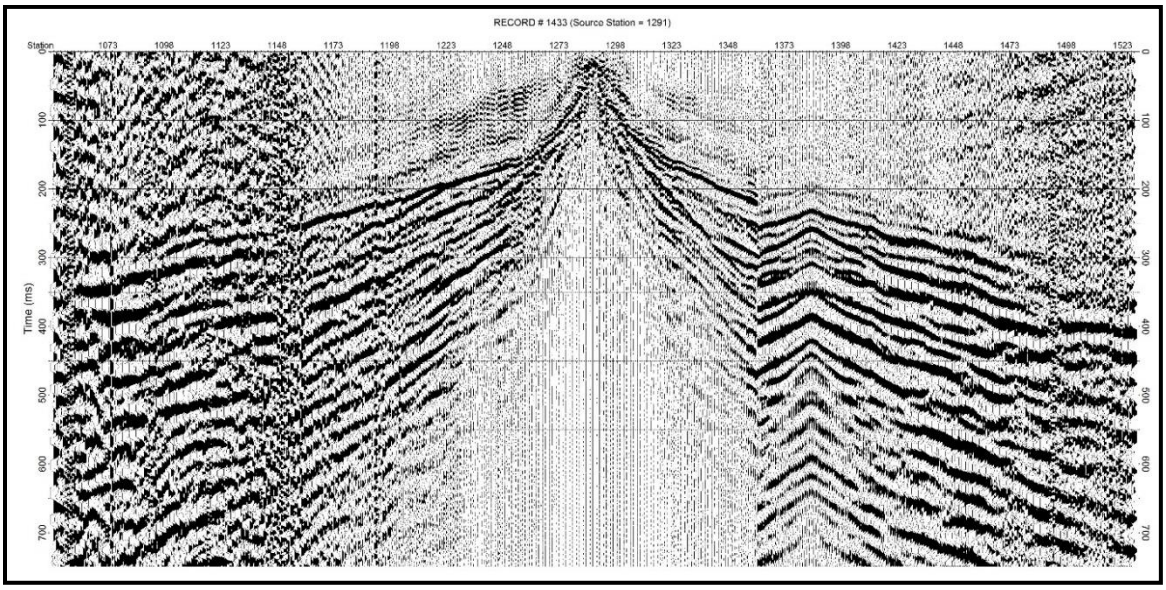

Figure 31: Representative S-wave shot record that has been vertically stacked with pre-correlation vibroseis whitening applied.

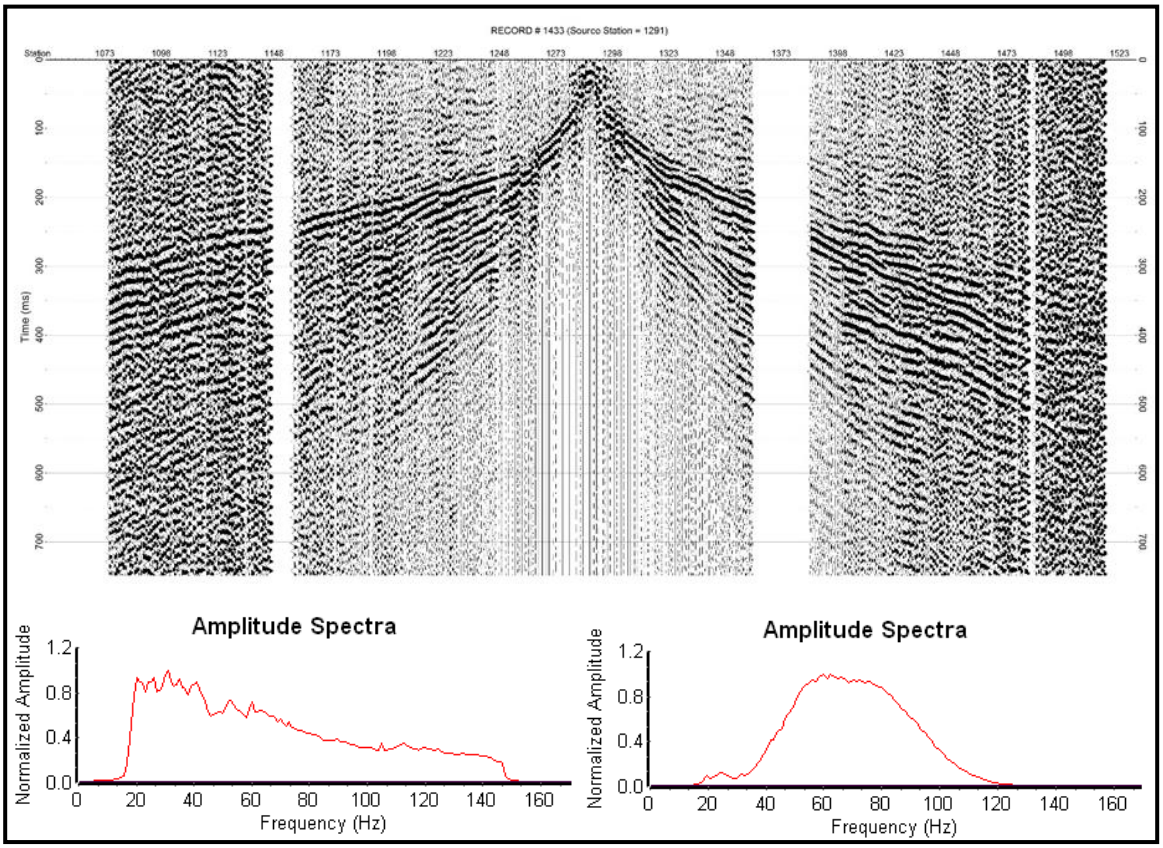

Figure 32: (Top**)** Representative S-wave shot record with trace edits, frequency filtering, and spectral balancing applied. (Bottom left) Amplitude spectrum before spectral balancing and frequency filtering. (Bottom right) Amplitude after spectral balancing and frequency filtering.

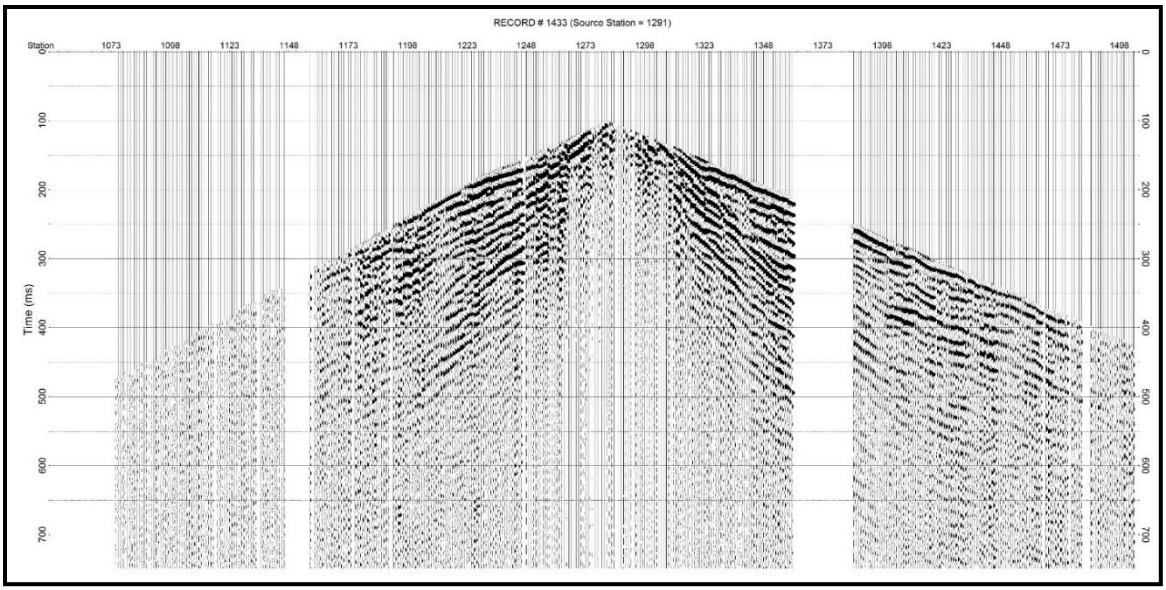

Figure 33: Representative S-wave shot record with first arrival muting applied.

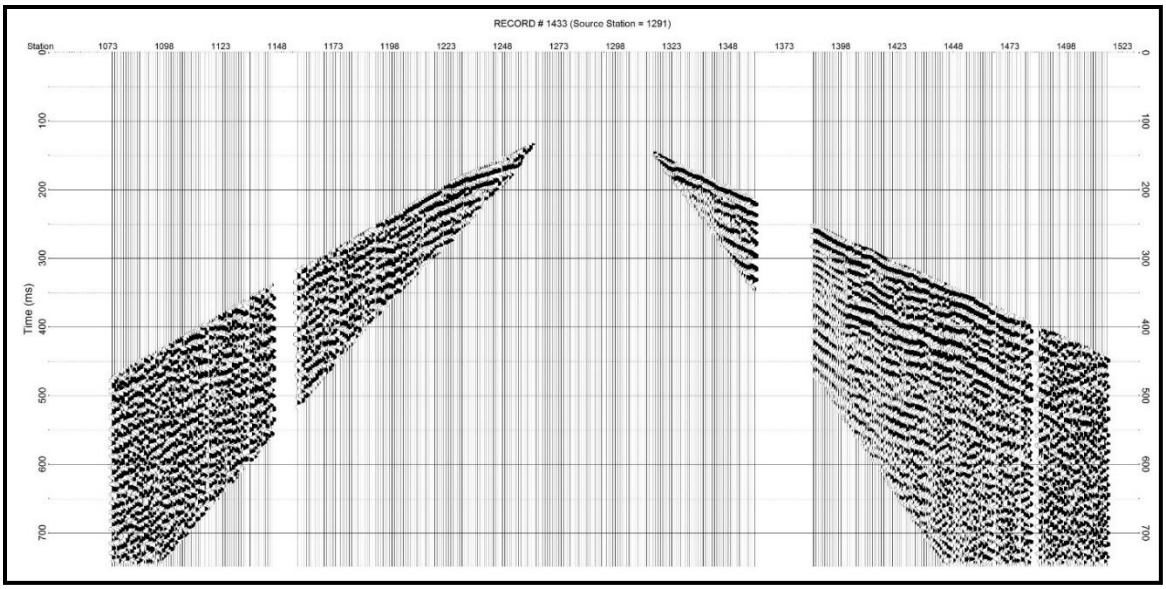

Figure 34: Representative S-wave shot record with first arrival muting and surgical cone muting applied.

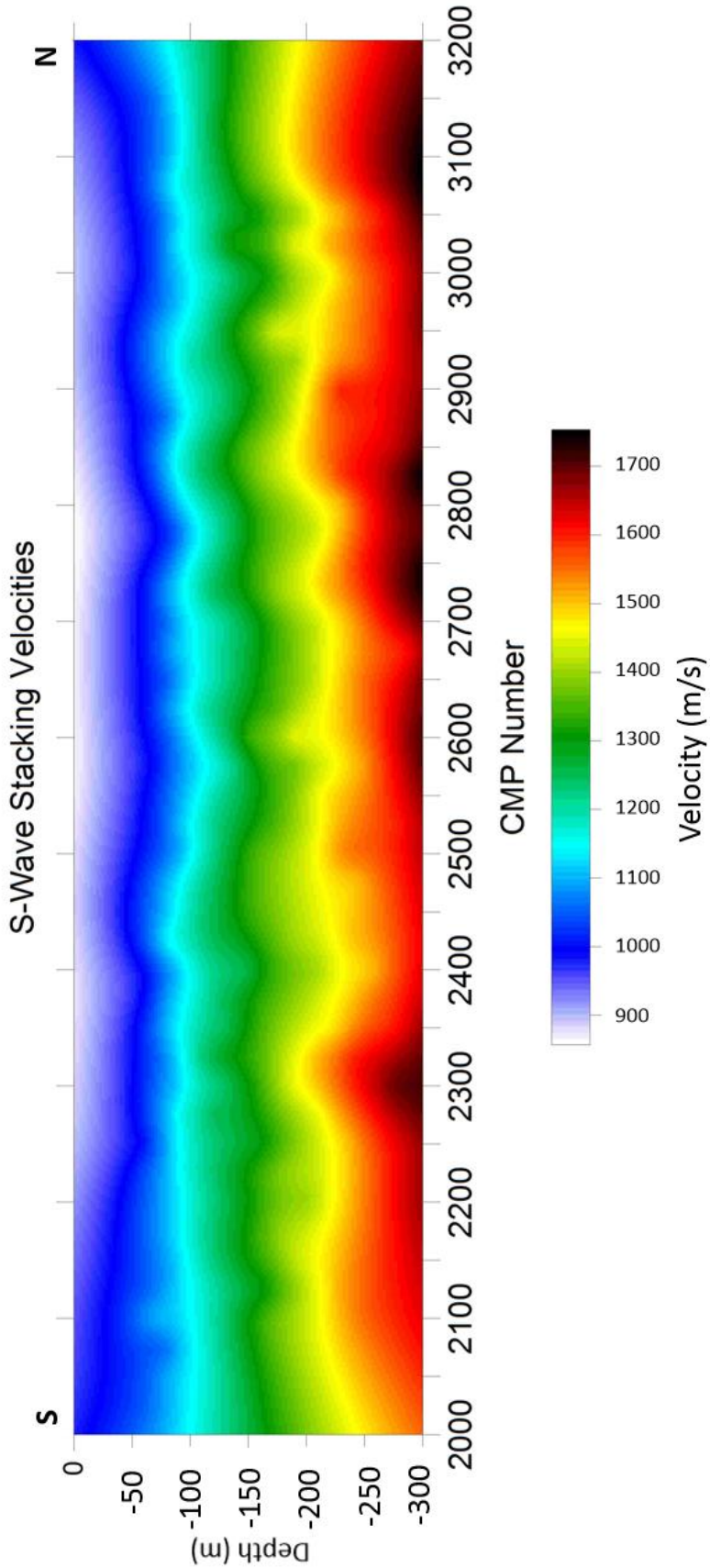

Figure 35: Plotted stacking velocities of the entire S-wave line used for NMO corrections.

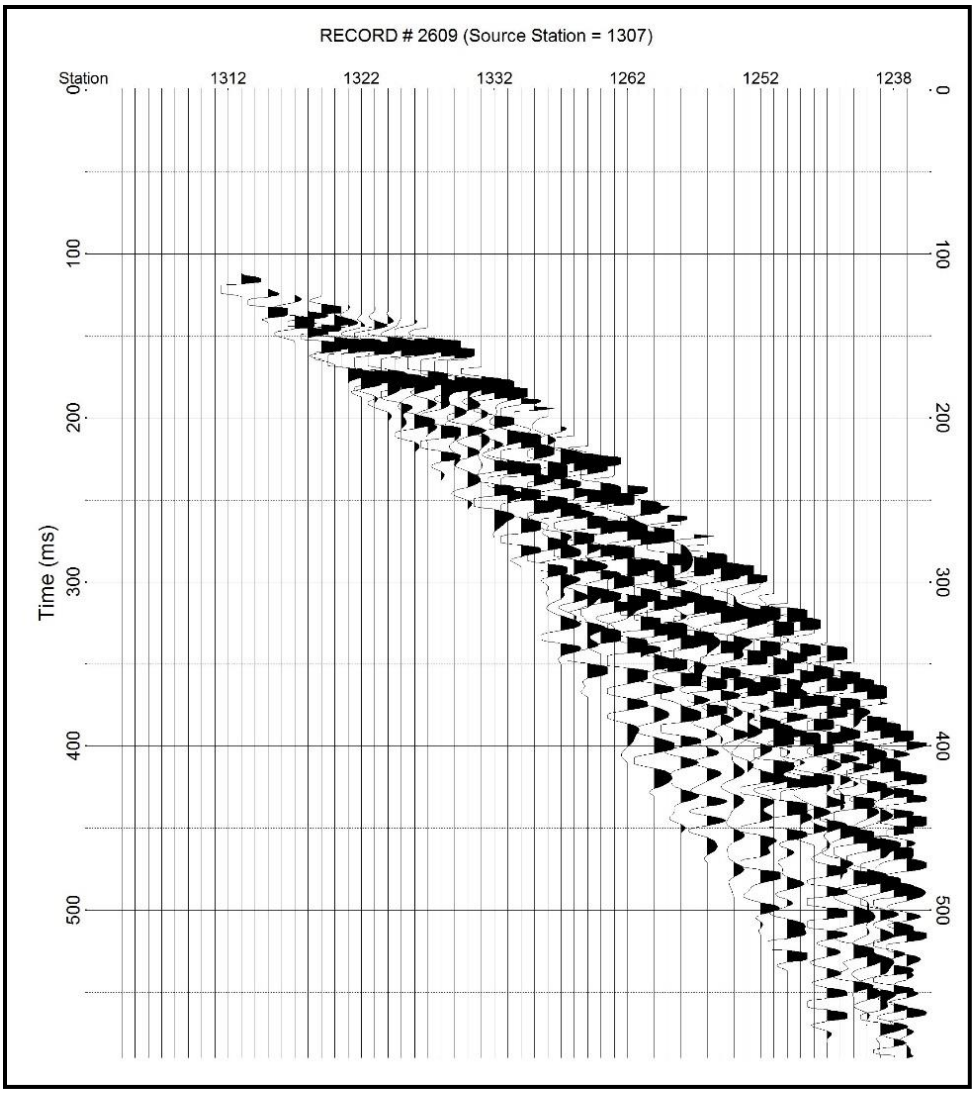

Figure 36: S-wave CMP gather with NMO and static corrections applied.

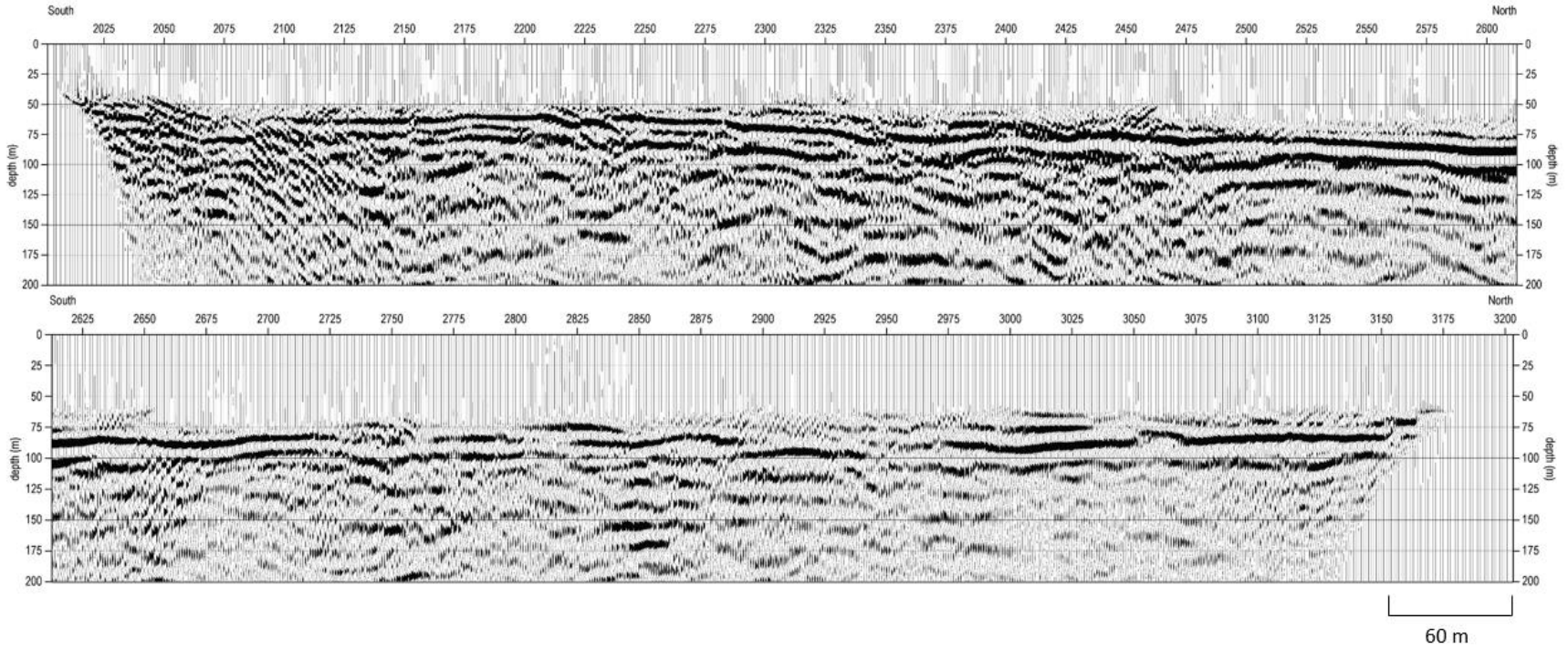

Figure 37: 2-D profile of the fully processed S-wave uninterpreted CMP stacked section. The beginning of the survey starts from the south at CMP ~ 2025 (top image) and ends at CMP ~ 3175 to the north (bottom).

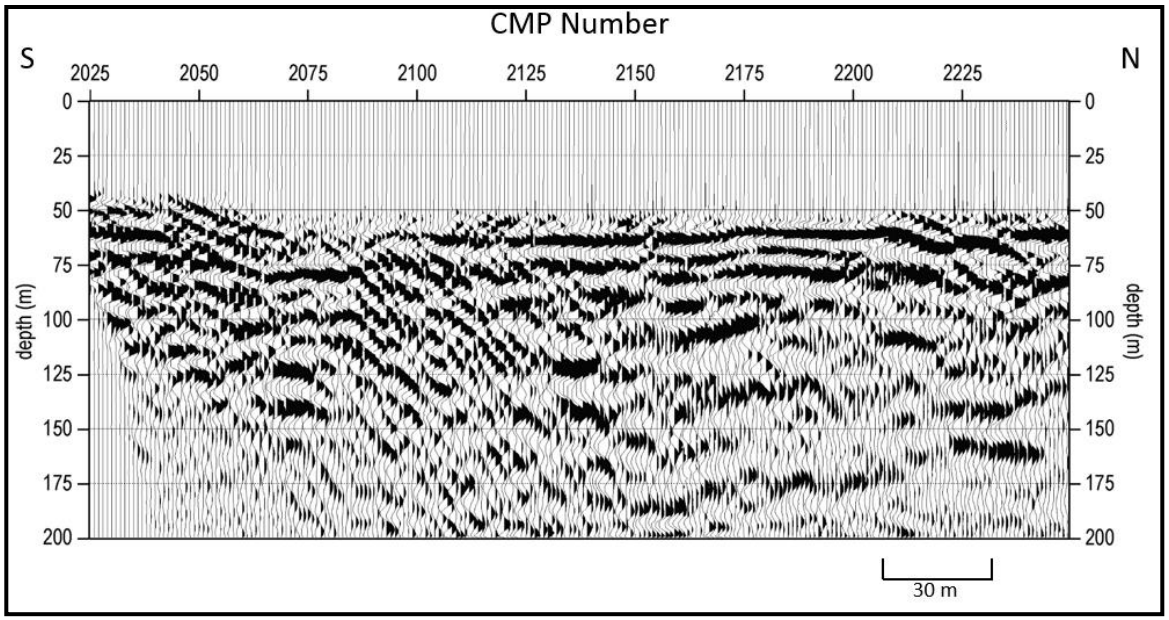

Figure 38a: Zoomed in portion of the southernmost section (~CMPs 2025 – 2250) of the S-wave stacked section

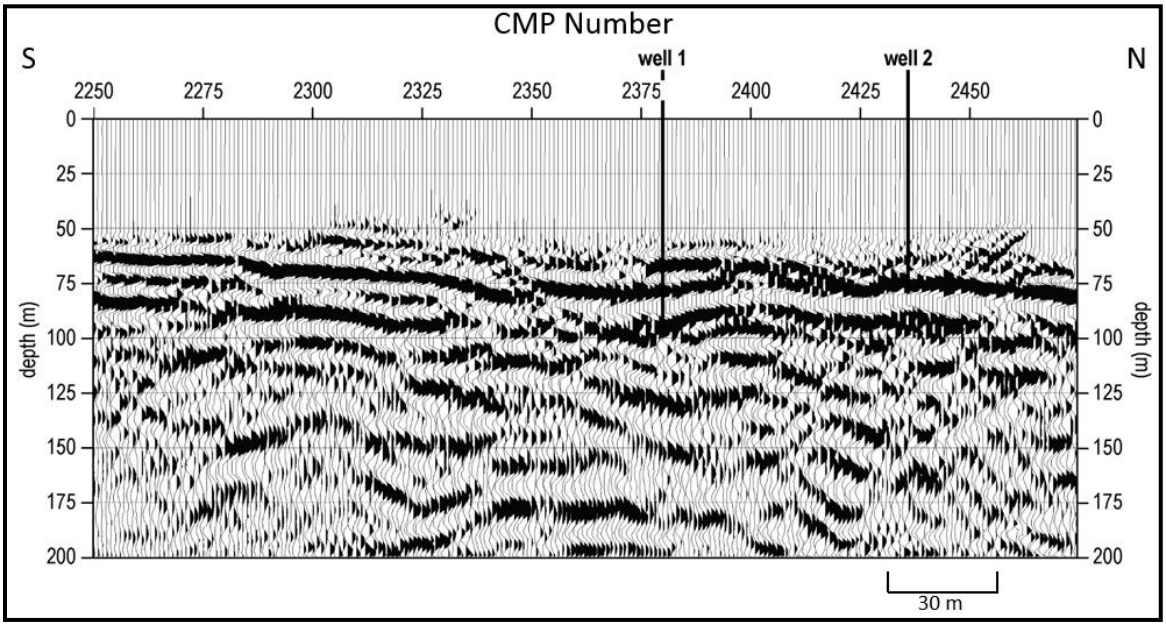

Figure 38b: Zoomed in portion of the ~CMPs 2250 – 2475 of the S-wave stacked section. Wells 1 and 2 are identified at their respected CMP station location.

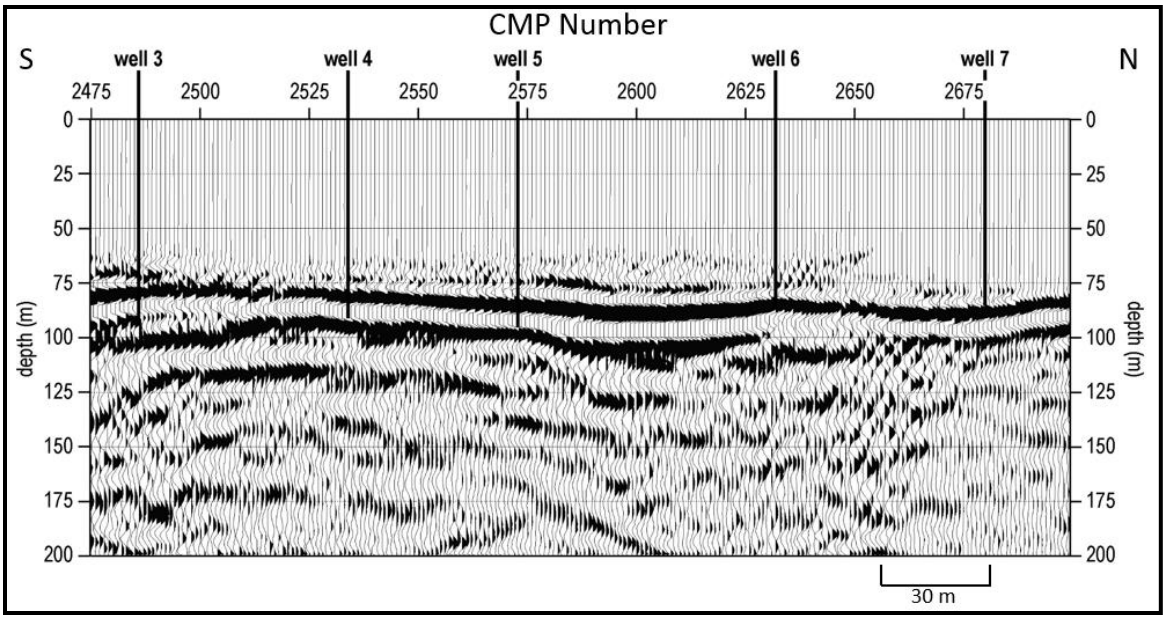

Figure 38c: Zoomed in portion of the ~CMPs 2475 – 2700 of the S-wave stacked section. Wells 3 – 7 are identified at their respected CMP station location.

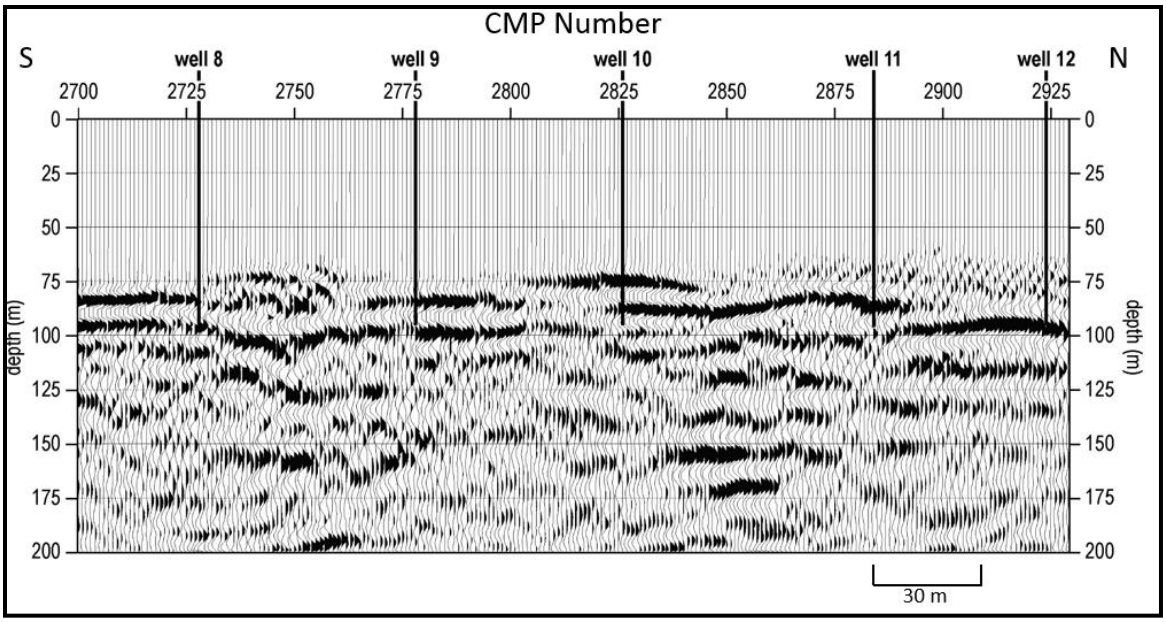

Figure 38d: Zoomed in portion of the ~CMPs 2700 – 2925 of the S-wave stacked section. Wells 8 – 12 are identified at their respected CMP station location.

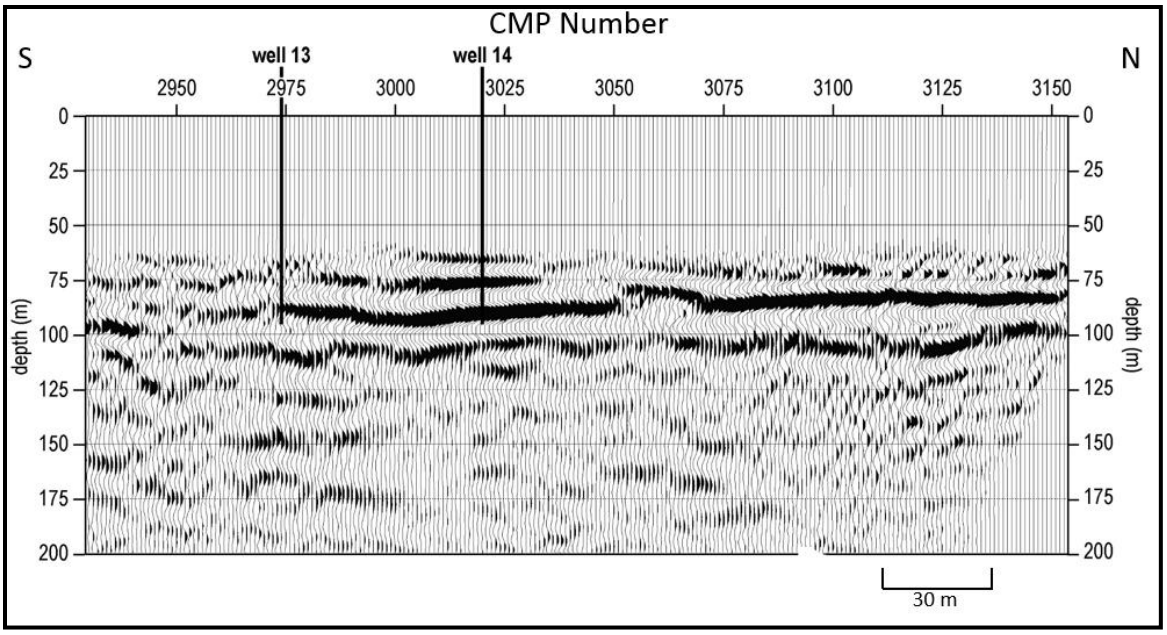

Figure 38e: Zoomed in portion of northernmost portion (~CMPs 2700 – 2925) of the S-wave stacked section. Wells 813 and 14 are identified at their respected CMP station locations.

Data Resolution & Fold

Vertical and horizontal resolutions were calculated using the 1/4 wavelength Rayleigh criteria (Widess, 1973). The dominant frequency for the P-wave section in the upper 125 ms was 140 Hz. In the upper 200 ms of the S-wave section 40 Hz was the dominate frequency. Using these dominate frequencies from both data sets along with interval velocities of the equivalent horizons in each data set wavelength was calculated. The vertical resolution for the P-wave section is ~ 3 – 6 m and for the S-wave section it is ~ 6 – 14 m. Although ¼ wavelength is the acceptable threshold to estimate vertical resolution, it can be overestimated as a result of noise present in the data (Yilmaz, 1987). Therefore, ½ wavelength may be a more reasonable threshold for these data due to their high level of noise contamination. A practical resolution for these data using the ½ wavelength criteria are ~ 6 – 12 m for the P-wave and ~ 12 – 28 m for the S-wave.

The horizontal resolution of this data is based off Rayleigh's standard in measuring the minimum distance between two separate distinguishable objects and is calculated by the Fresnel zone radius:

$$r = \sqrt{\frac{VZ}{2f}}$$

where r is the (horizontal resolution), f is the dominate frequency, V is the velocity of the reflection, and Z is the depth in time of the reflection (Ebrom et al., 1996). The calculated Fresnel zone radius, horizontal resolution, for the Mississippian aged limestone was ~ 25 m for the P-wave data and ~ 31 m for the S-wave data. Collapsing the Fresnel zone radius through migration to the approximate dominate wavelength can improve horizontal resolution, but this is not possible with this data since only a migration filter was used due to frequency loss during migration (Stolt and Benson, 1986).

Data fold varied across both of these fixed-rolling spreads. Data fold defines the number of source to receiver traces that image a subsurface point. Maximum fold of these data would be 226 for the P-wave and 126 for the S-wave based simply on acquisition parameters. Fold will vary with travel-times on near-surface shallow reflection surveys (Liberty and Knoll, 1998). This is due to selected sample removal during processing. Processing steps such as first arrival and surgical muting, as well as NMO corrections will reduce maximum fold. Therefore, the actual fold ranged of these data from ~ 10 – 50 for the P-wave and ~5 – 25 for the S-wave in their respective target time windows (30 – 150 ms, P-wave; 100 – 200 ms, S-wave. Fold increased with depth for both datasets.

Survey	**Vertical Resolution (¼ wavelength)**	**Vertical Resolution (½ wavelength)**	**Horizontal Resolution (Fresnel zone radius)**	**Actual Fold**
P-wave	~ 3 – 6 m	~ 6 – 12 m	~ 25 m	~ 10 – 50
S-wave	~ 6 – 14 m	~ 12 – 28 m	~ 31 m	~5 – 25

Table 5: P-wave vs. S-wave data fold and resolution comparison.

Results and Interpretation

V_P/V_S Ratio

Contrasting the velocity estimates of both P- and S-wave data sets gives additional insight into the subsurface lithology and rock properties using the Vp/Vs ratio (Haines and Ellefsen, 2010; Tatham and Stewart, 1993). Vp/Vs ratio for this study was calculated using interval velocities which were derived from NMO velocities for P- and S-wave data sets using Dix's equation (Figure 39). In general, the same geologic horizons (reflectors) imaged in the P- and S-wave data must be used in the calculations to ensure the Vp/Vs ratio is not mixing reflectors and making the ratio meaningless (Van Dok and Kristiansen, 2003).

Calculating this velocity ratio allowed for an improved understanding of the character of the mine overburden. Vp/Vs ratio analysis results in the upper ~90 m BGS (the mine overburden) varied slightly with no indication of any major anomalous zones of increased or decreased velocity ratio. More specifically, the upper 80 m, where the mine roof resides (per drilling report), do not appear to be experiencing any areas increased stress (Figure 40). The average Vp/Vs ratio of the mine overburden is ~1.8, which falls within an expected Vp/Vs ratio range for limestone (~1.7- ~1.9) (Mavko, 2005; Castagna et. al, 1993). The Vp/Vs ratio ranges in the overburden from ~1.6 to ~1.9. These values are well within an error range of velocity picking. A higher uncertainty in Vp/Vs ratio appeared beneath the mine at a depth of between 85 and 125 m BGS. The higher uncertainty is due to fewer velocity data points available beneath the mine creating a broader range of the Vp/Vs ratio. The limestone overburden is the most spatially picked unit in both data sets. Fortunately, the Vp/Vs ratio calculation remains within the range considered average across the mine. The consistent Vp/Vs ratio values along the entire imaged

profile support the suggestion that lateral changes observed in the ratio of seismic velocities are representative of these rocks in this area.

This Vp/Vs ratio analysis lays the groundwork for time-lapse studies with these data representing a baseline. The Vp/Vs ratio values calculated across this entire profile fall within a range considered normal or expected base on published values for these types of lithology. Not knowing how the rock properties might have changed since the mine was opened, it is not possible to rely on these values as the native values of this limestone. Changes of Vp/Vs ratio due to an increased or decreased Vp or Vs, in future surveys compared to this baseline data set could imply changes in rock properties associated with changes in the stress field over the mine void (Table 3). At the time of these surveys there was no evidence to suggest the stress field has changed within the mine overburden.

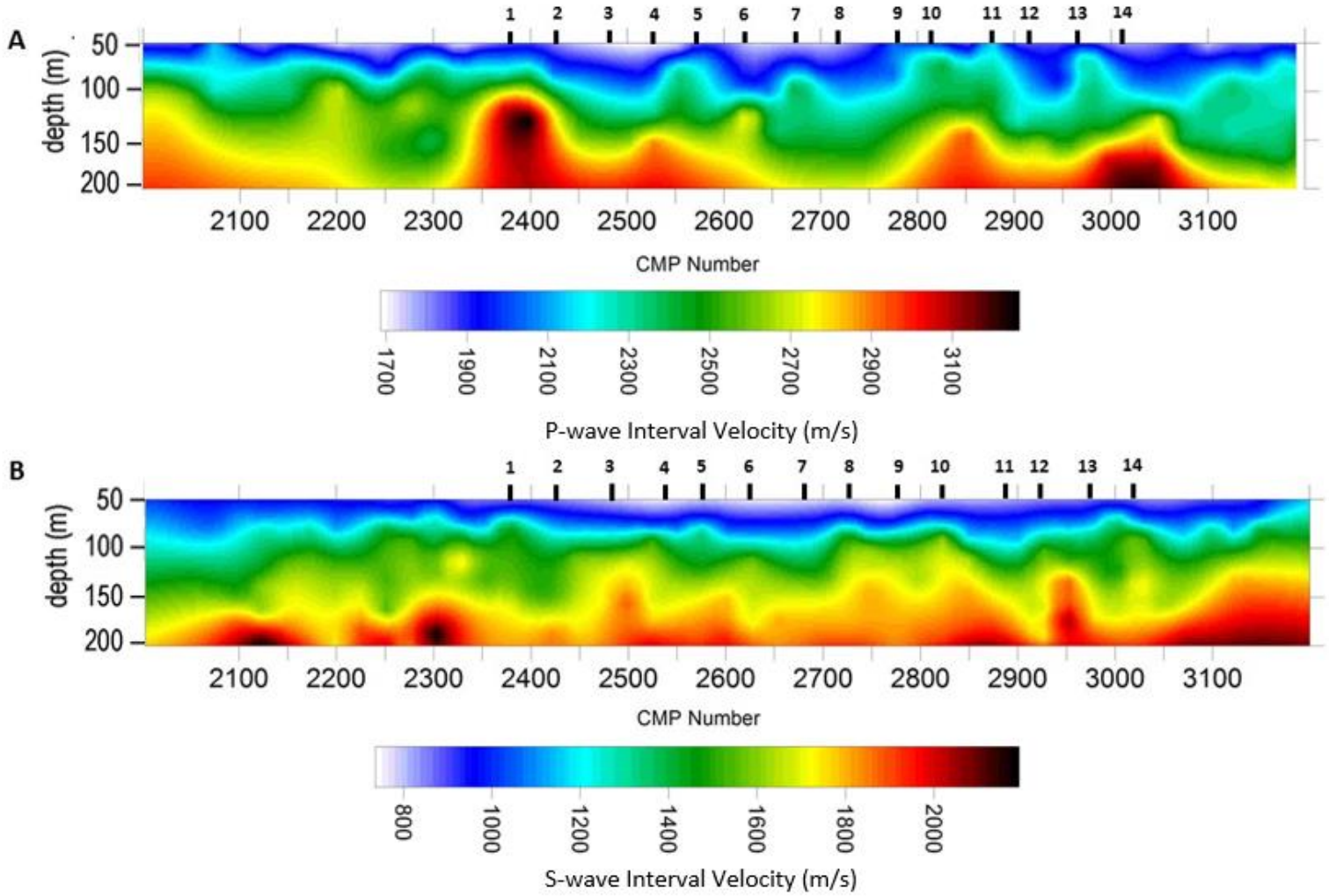

Figure 39: Plotted interval velocities of P-wave (top) and S-wave (bottom) used for calculation of the Vp/Vs. Wells 1-14 are identified at their respective CMP stations.

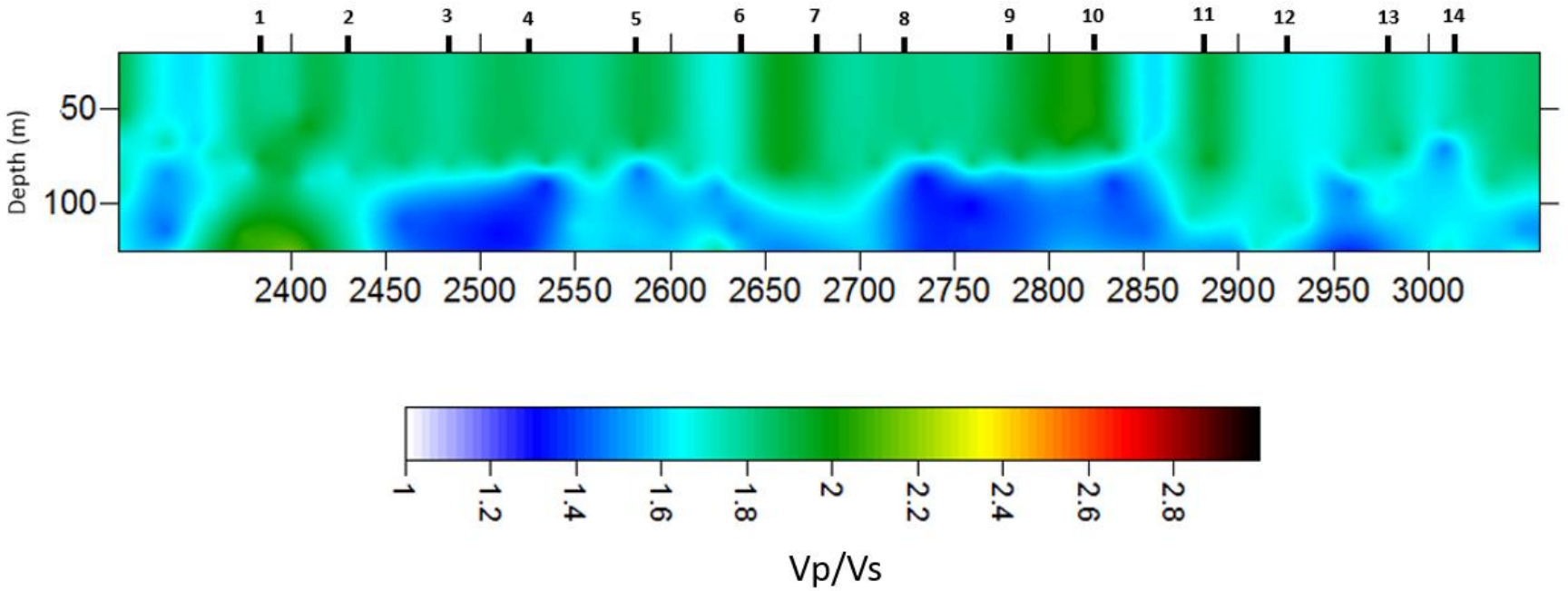

Figure 40: Plotted Vp/Vs. Well locations are identified at the top. Notice the slight variability of change across the section. The varying Vp/Vs in the upper ~ 75m is due to slight changes in lateral velocities of the P- and S-wave data. The minimal variation (1.6 – 1.9) does not fall within a threshold of concern. Due to the complexities in picking velocities during data processing these values are within a range of picking velocity error and not related to extreme changes in lithology.

Well Correlation

Fourteen wells were drilled by the KDOT for a previous lithology and cross-hole seismic survey. The lithology logs from those wells were used to correlate to seismic reflections to mine location and geologic units in the subsurface. From ground surface to approximately 6 m depth lies silty clay. The silty clay overlies shale units which range in thickness from ~22 to ~34 m. Boone Fm limestone underlies these shale units, where the shale-limestone contact ranges from ~ 28 m to ~ 40 m BGS (Figures 12, 46-59). Both the silt-shale and shale-limestone contacts were too shallow for either seismic data set to image (KDOT, 2002). Limestones within the Boone are the primary reflections on CMP stacks. If the mine void was present at a well the depths of the mine roof and mine floor were given on the lithology logs. The mine void ranges in vertical thickness from ~ 6 m to ~ 28 m, which is within the range of the seismic vertical resolution. A detailed analysis of each well (KDOT, 2002) and its correlation to the upper 200 m of the seismic data is given in the Appendix (Figures 46 – 59).

P-Wave Interpretation

The Miami trough (CMPs 3200 - 3975) is interpreted at the northern end of the section possessing the highest S/N and coherent reflection (Figures 41 – 42 and 45). The axis of the Miami Trough is located approximately 90 m BGS in this area (McKnight and Fischer, 1970). A southern dipping normal fault interpreted at CMP 3175 bounds the southern flank of the trough. This fault likely played a role restricting mineral rich fluids from significant migration of the ore mineralization zone further north and into the trough. The interpreted green horizon is a limestone within the Mississippian Boone Fm that is bound on top and bottom by other varying limestone units. The shale units identified in drilling reports that overlie the limestone were too shallow to be imaged due to acquisition and processing parameters. This limestone contact can

be tracked across the section from the northern end of interpretable reflections (CMP 3980), southward across the fault plane (CMPs 3170-3175). Interpreting seismic events becomes difficult near CMP 3100 where lateral continuity of the reflections diminishes and S/N decreases. Coherent reflections between CMPs 2830 – 2900 at approximately 76 m BGS terminate to the south in the vicinity of the northern most mine void identified in well data.

No clear, continuous reflection(s) appear to be originating from the mine or within the mine overburden in the P-wave data. The CMP stacked section lack any continuous reflections from approximately CMP 2800 southward. No continuous reflections were identified in the location where the well data identified a mine void. This supports the idea that the absence of laterally continuous reflections is indicative of the presence of the mine; approximately CMPs 2370 – 2755. The mine location is marked on the seismic section using the location of the mine identified in the well data (highlighted blue area Figures 41 and 42).

Diffractions (highlighted in red CMPs 2275 – 2670) are evident throughout the interpreted mine area in the stacked section (Figures 41, 42b-42d, & 45). An interpreted pillar, corroborated by well data, is shown highlighted in orange (Figures 41, 42c, & 45) and is seen as an area of coherent reflections at approximately CMPs 2555 – 2585. Disturbed reflections with a diffraction event south of Well No. 1 could be evidence that the mine extends further south than previously inferred from well data. It is unknown if the mine extends further south beneath U.S. Highway 69, or if the disrupted nature of the data on southern extent of the line is an artifact of out of the plane reflectors, as a result of off line mine meanders and/or associated geological structures in the subsurface.

A Boone Fm limestone that is interpreted the full length of the line was utilized as a geological marker bed, and is within the mine overburden (Figured 41, 42, & 45). The limestone

can be traced from the north end of the line south to the area the reflections from that interface deteriorate in the mine vicinity (~ CMP 2800). Based on well data alone it is difficult to confirm the lateral extent of this reflector through the mine area and across the southern portion of the line. The well data confirms that the unit overlying the mine is a limestone. The green marker horizon is tracked from the wells, north where reflections become continuous. North of the mine where reflections are continuous the green horizon is interpreted along a reflection as a Boone Fm. limestone.

Overall the data lacks uniformity in reflections. The nature of the disturbed subsurface is interpreted to be the driving force in the chaotic nature of the reflections on stacked sections. At various stages of processing and interpreting the P-wave stacked section it was interpreted that the noisy shot records, inconsistency in lateral reflections, and diffraction presence were a consequence of the highly altered, fractured, and faulted subsurface geology. The mine workings present at this site in conjunction with the highly-altered overlying roof rock likely contribute to the lack coherent reflections from within the mine overburden. Out of the plane reflections, which are possible considering the known geology, could also contribute noise that impacts the lack of coherency.

The Miami Trough is defined by laterally continuous reflections, which abruptly terminate in proximity of the mine. This further supports the suggestion that the mine overburden lacks layered/continuous reflectors. Seismic data appears limited to a maximum depth of approximately 200 m BGS. Apparent reflection events deeper than 200 m are chaotic and plagued by scatter, making confident interpretation of deeper units difficult. The stacked section allowed both the Miami Trough and the mined zones to be interpreted with reasonable confidence.

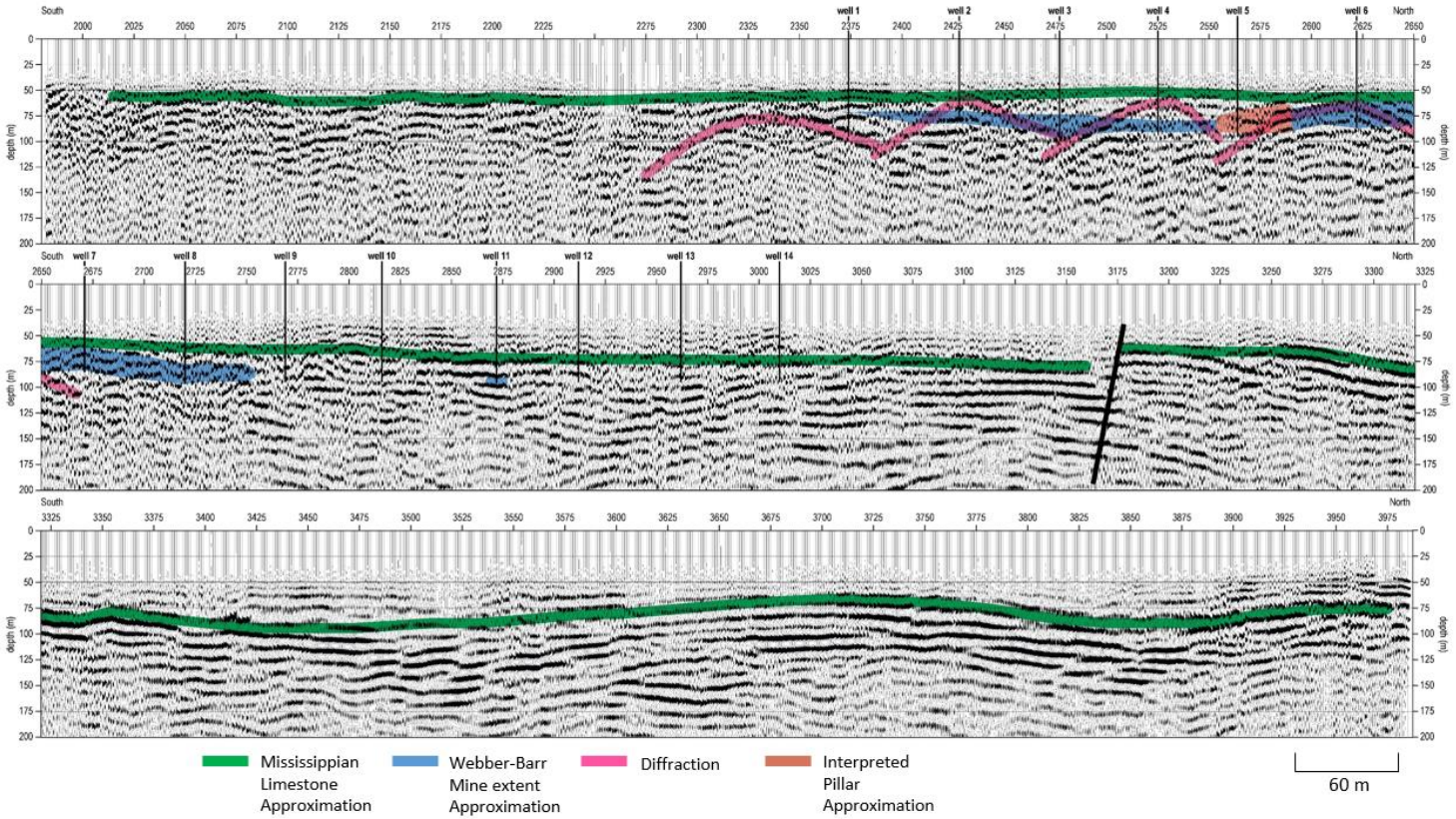

Figure 41: Interpreted P-wave stacked section. The Mississippian Boone Fm limestones (green) have the highest amplitude and best coherency in the vicinity of the Miami trough north of the interpreted fault (CMP 3175) (middle and bottom images) bounding the troughs southern flank. The Boone Fm is tracked across the fault plane (middle) and correlated with well data through the southern portion of the section (top). The mine location (blue) is interpreted with the aid of well data (marked at their CMP locations). Diffractions (pink) over the mine are present due to source scatter from bed terminations associated with the mine geometry (pillars and edges) and structural alterations in the subsurface. Reflections lack lateral consistency in the mine area because of the altered subsurface.

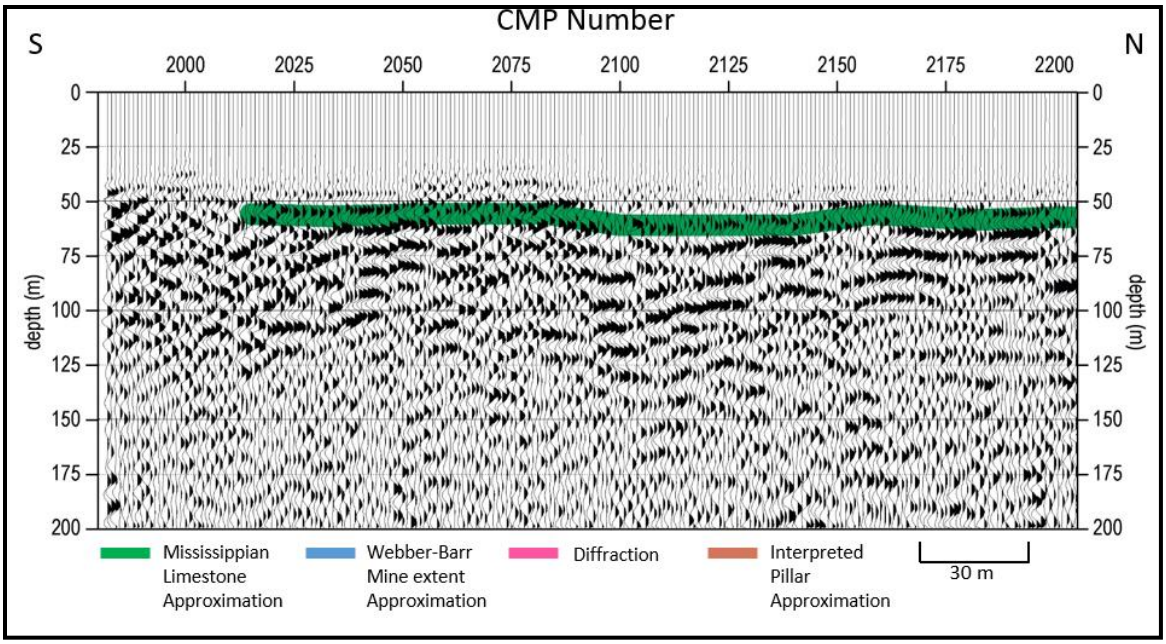

Figure 42a: CMPs 1982 – 2200 of the interpreted P-wave stacked section. This is the southern extent of the survey and the green is identified as Mississippian limestone.

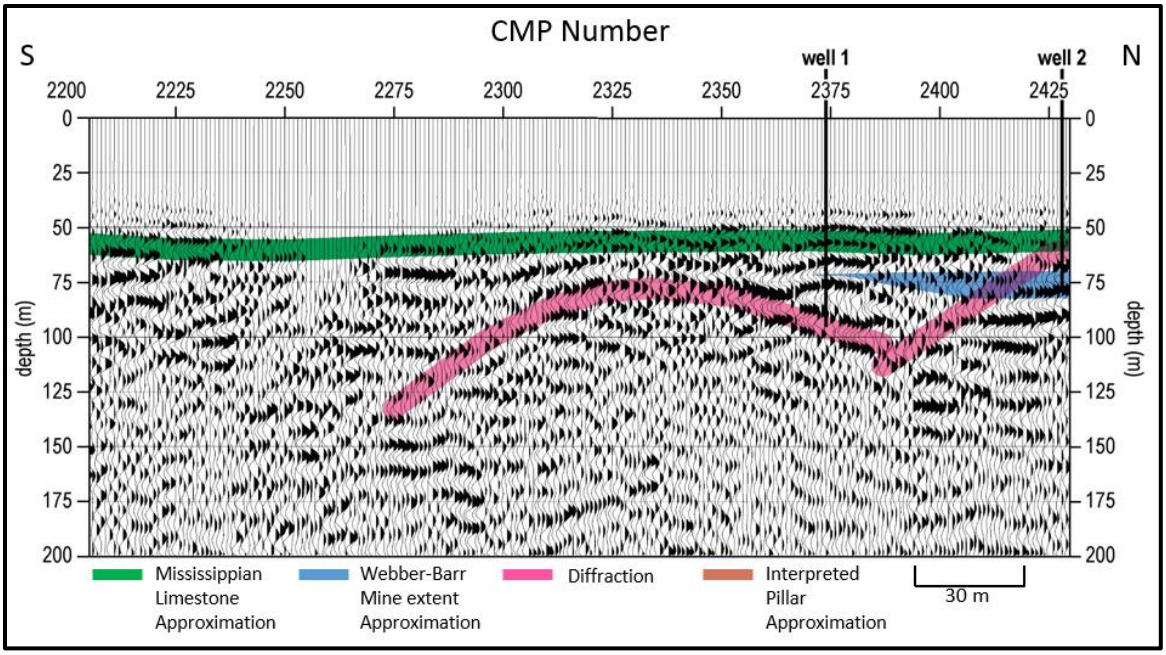

Figure 42b: CMPs 2200 – 2425 of the interpreted P-wave stacked section. The green is identified as Mississippian limestone. Notice the diffractions (pink) near the edge of the mine (blue). These diffractions are a result of bed terminations and edges within the subsurface, which here are related to the mine geometry and fractures and faults in the rock units.

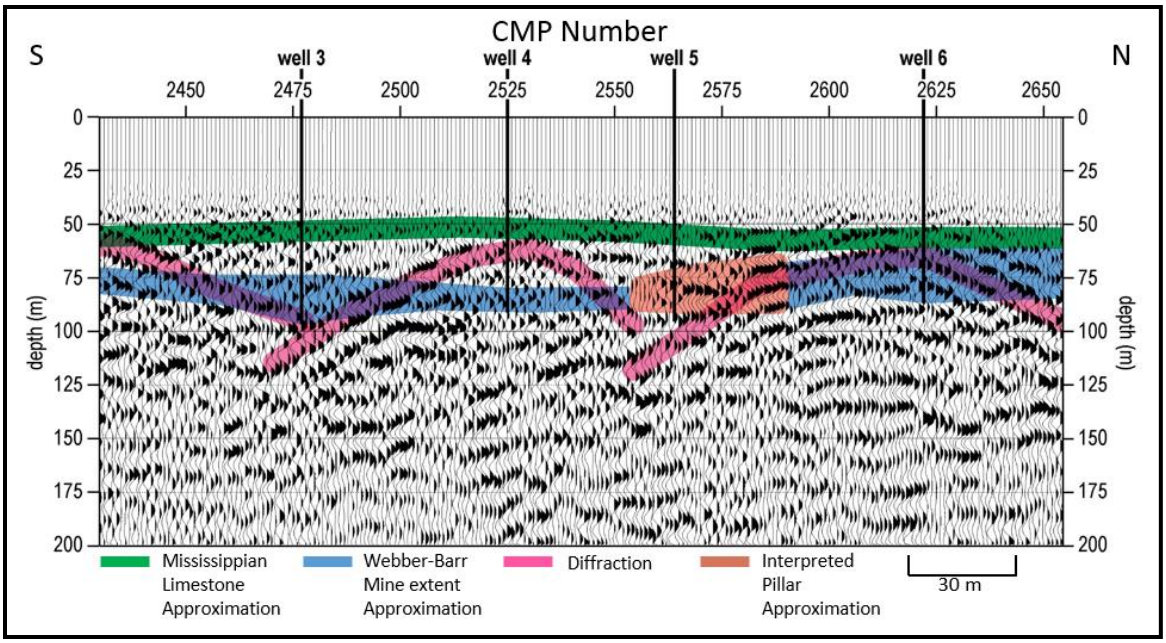

Figure 42c: CMPs 2425 – 2650 of the interpreted P-wave stacked section. Diffractions (pink) are present in the mine vicinity (blue). The geologic log for well 5 indicated no mine presence at its location, and has been interpreted as a pillar (orange)

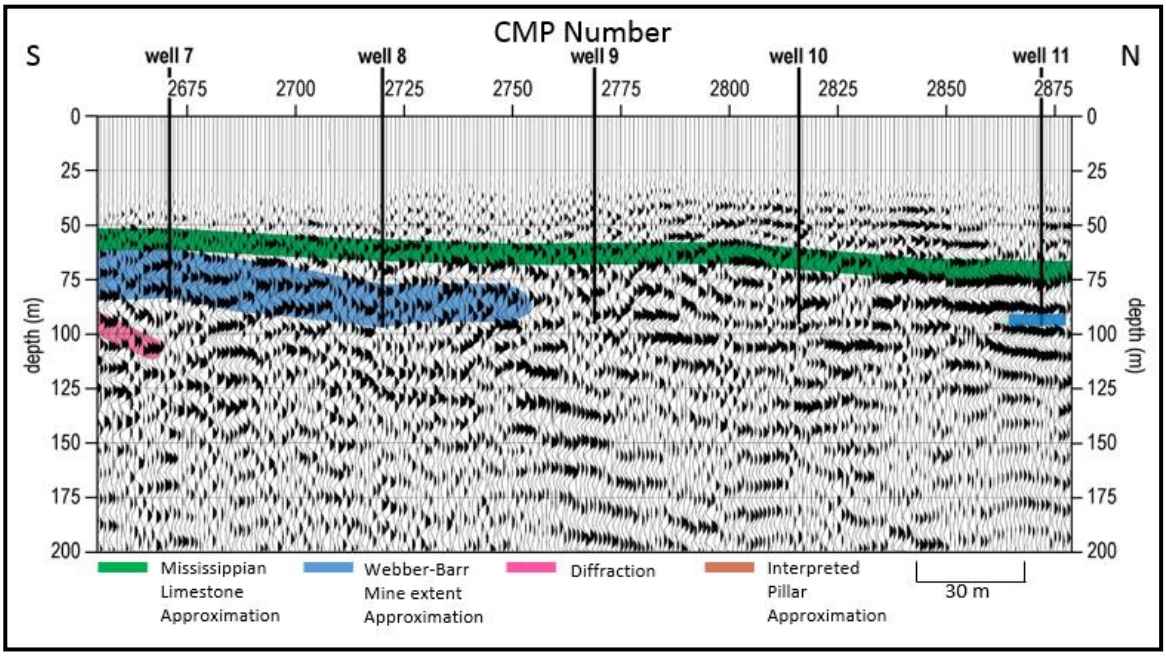

Figure 42d: CMPs 2650 – 2875 of the interpreted P-wave stacked section. Notice the change in lateral continuity in the reflections (green) moving away from the mine (blue) to the north. This is due to moving into less disturbed lithology and more competent rock off the mine. Well data indicates a small 7 m thick void (blue) at well 11, but no void is present in wells 10 or 12 beside it. This is likely a room of the Webber-Barr mines northwestern most extent.

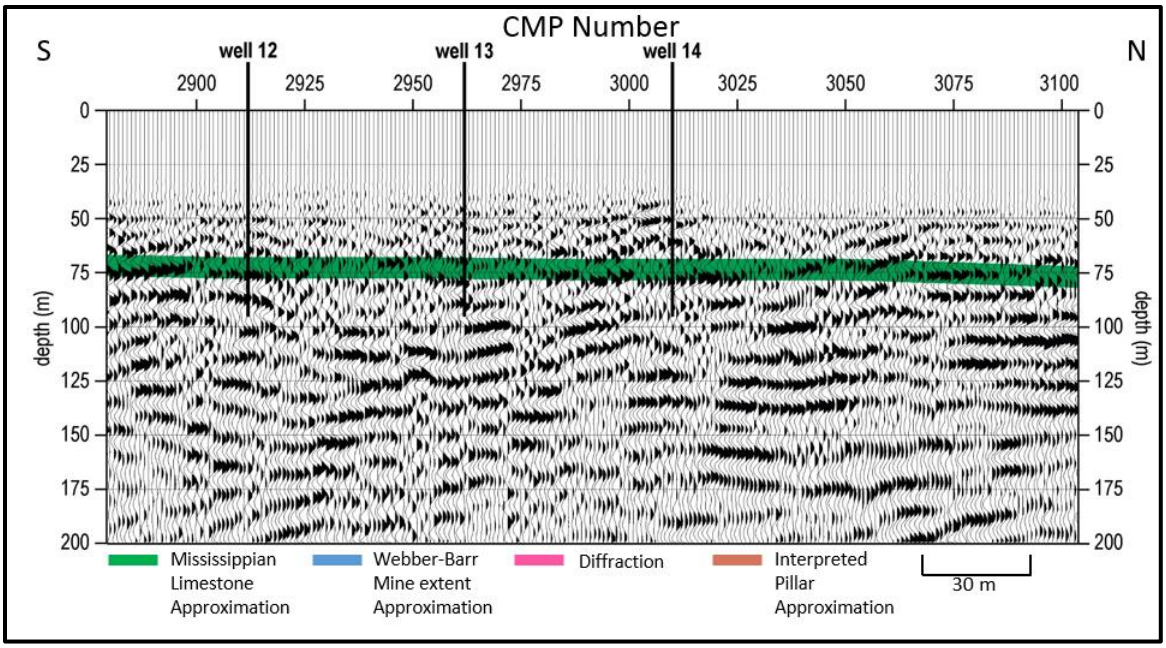

Figure 42e: CMPs 2875 – 3100 of the interpreted P-wave stacked section. Mississippian limestone is present, verified by wells 11-14, and continue to trend north with minimal to no dip towards the Miami Trough.

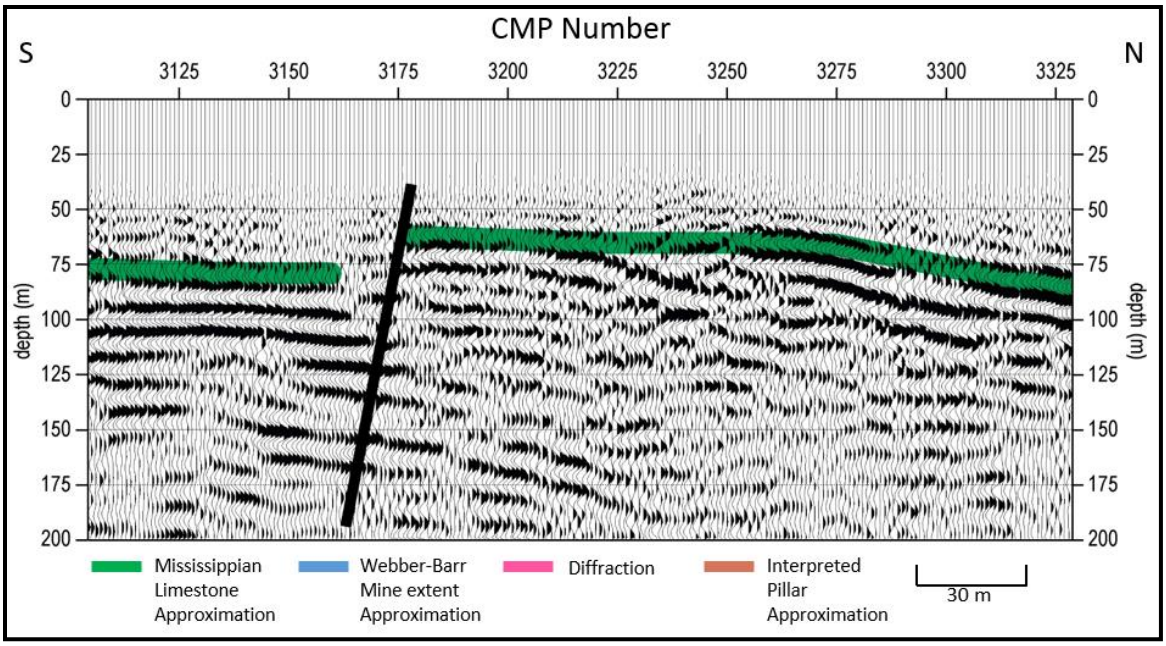

Figure 42f: CMPs 3100 – 3325 of the interpreted P-wave stacked section. A normal fault (black) is present at ~ CMP 3175. The limestone here is interpreted across the fault successfully by characteristics of the reflections present. This fault bounds the Miami trough to the south and likely what is causing the tightly spaced contours observed in Figure 4.

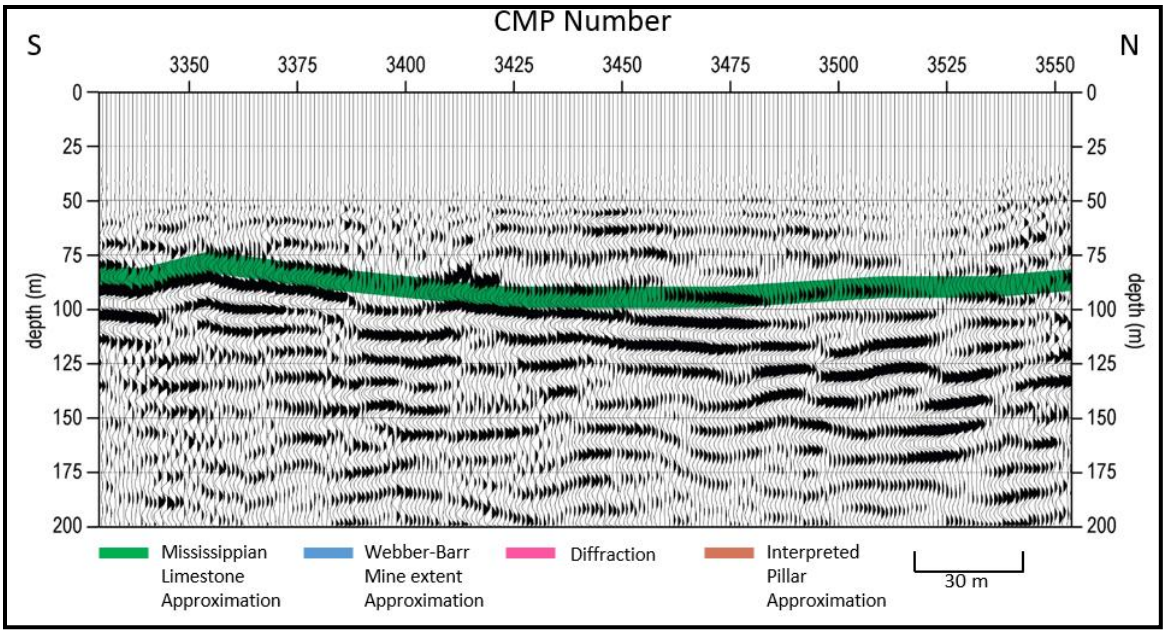

Figure 42g: CMPs 3325 – 3550 of the interpreted P-wave stacked section. The limestone (green) is now in the Miami trough, and is evident by the change in flat lying structure south of the fault in Figure 42f.

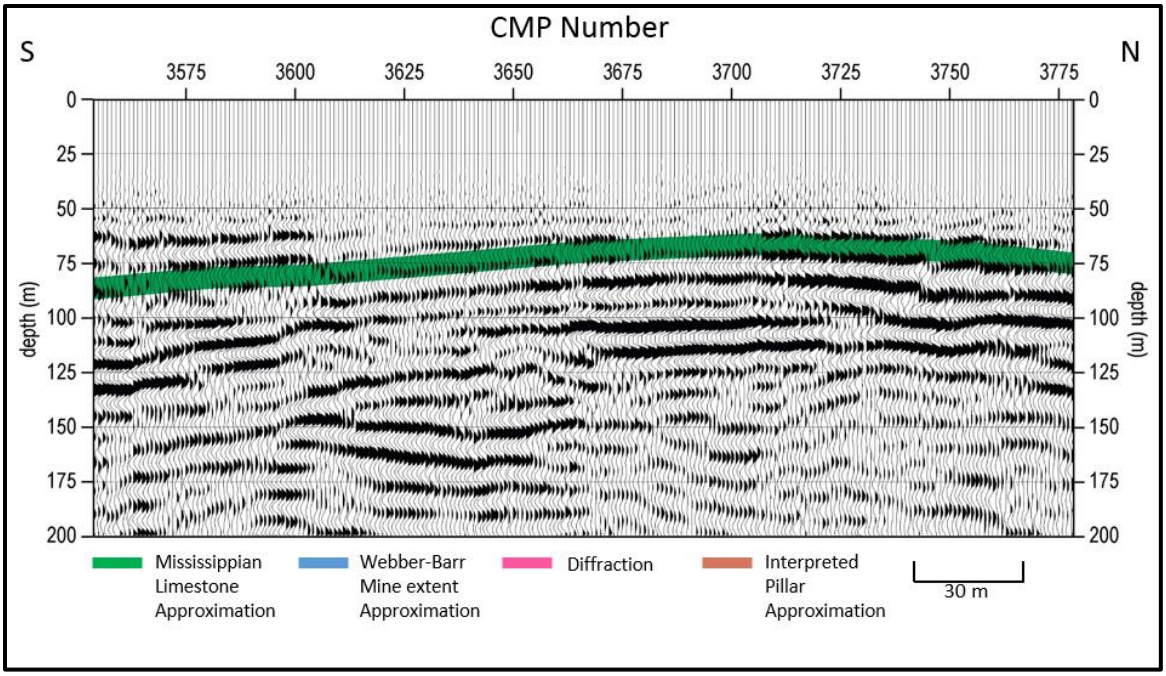

Figure 42h: CMPs 3350 – 3775 of the interpreted P-wave stacked section continuing through the Miami Trough.

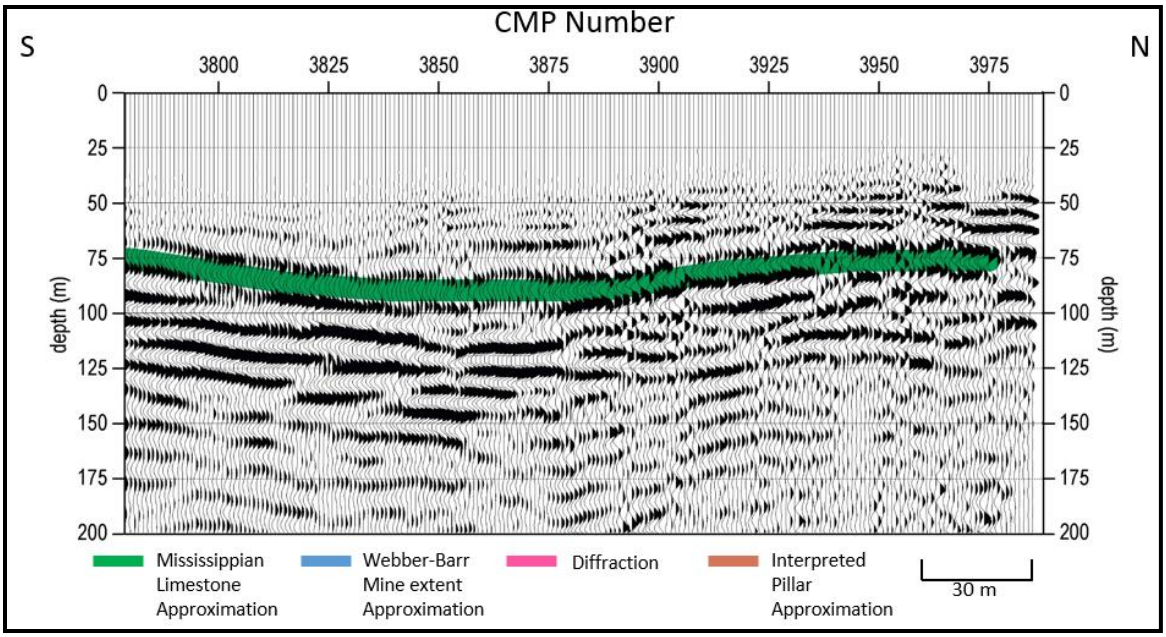

Figure 42i: The northern extent of the P-wave data CMPs 3350 – 3775 showing interpreted Mississippian limestone on the north end of the Miami Trough.

S-Wave Reflection Interpretation

A high amplitude reflection present in the vicinity of the mine at ~ 80 m BGS on the S-wave section is interpreted as the contact between the of limestone overburden and water filled void (Figures 43 - 45 in blue). The interpreted mine location on the stacked section correlates with the well data and spans from CMP 2350 to 2750 (Table 1). A pillar is interpreted from the seismic data at approximately CMPs 2570 to 2590 and is consistent with the borehole information from Well 5. The actual dimensions of this pillar are unknown, and due to the resolution limits of the seismic data it is not possible to quantify them from CMP stacked sections. Interpreting a pillar present at CMPs 2570 to 2590 is consistent with well data and mine practices of that time.

In general, reflections north (CMPs 2750 to 3175) and south (CMPs 2025 to 2350) of the drill-inferred mine location drop in amplitude and lateral consistency (Figures 43 – 45). Reflections on the south end of the CMP stacked section lack the lateral consistency observed on the north end and suffer from elevated high frequency noise interference and lower amplitudes. The area interpreted in green on the S-wave section correlates to a reflector in the Mississippian Boone Fm and is consistent with the P-wave section (Figure 45). Uniquely locating the roof of the mine is impossible due to velocity picking error and data resolution. Interpretations here are generally consistent with the mine void. High-amplitude reflectors are a result of a large acoustic impedance contrast between the overburden rock and water filled void.

The structurally complex subsurface resulted in an ideal environment for scattering seismic energy. The large percentage of scattering at this site inhibited reflection events from small contrast interference stacking in. As a result, interpretation of interfaces between rock units other than the overburden/mine contact was difficult to do with confidence. Interpretation

of a reflection associated with the mine/overburden with no sign of structural alteration was a key characteristic pulled from this S-wave CMP stacked data set.

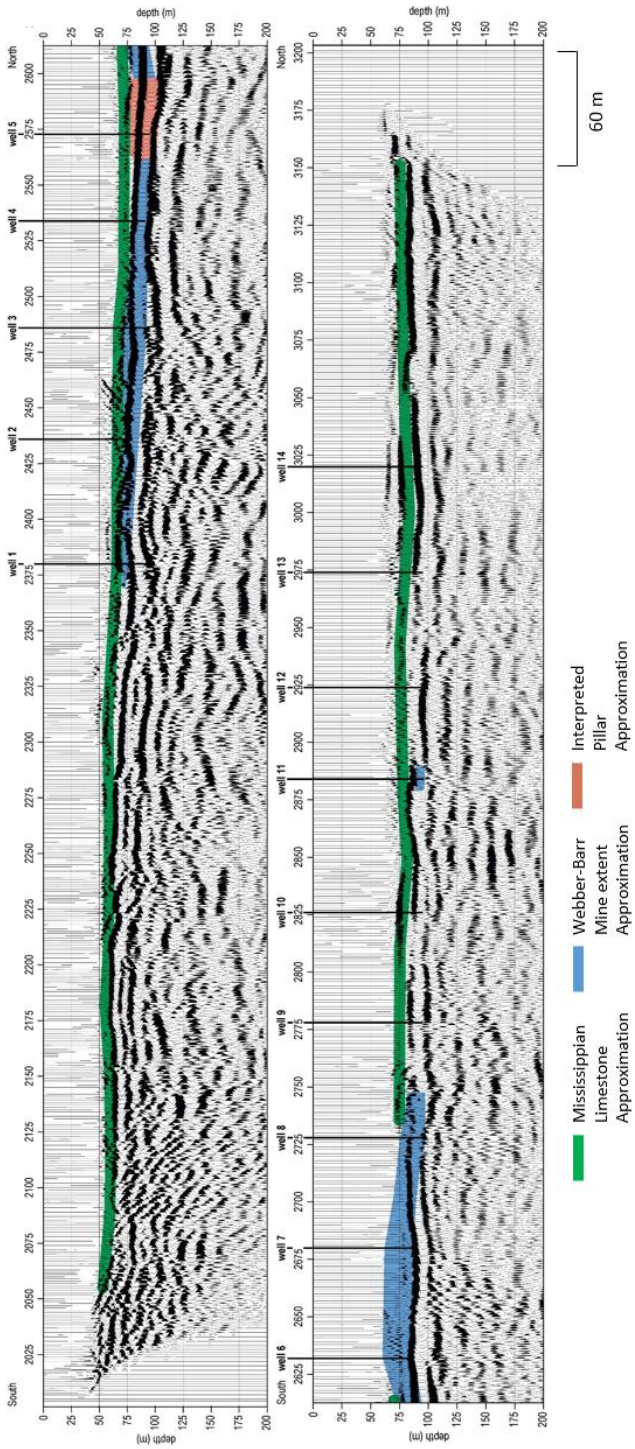

Figure 43: Interpreted S-wave stacked section. The Mississippian limestone (green) and Webber-Barr Mine were correlated from the well data and P-wave data and tracked across this S-wave section from the north (bottom) to the south (top). Wells are identified at their CMP locations, and the interpreted pillar (orange) is shown at Well 5.

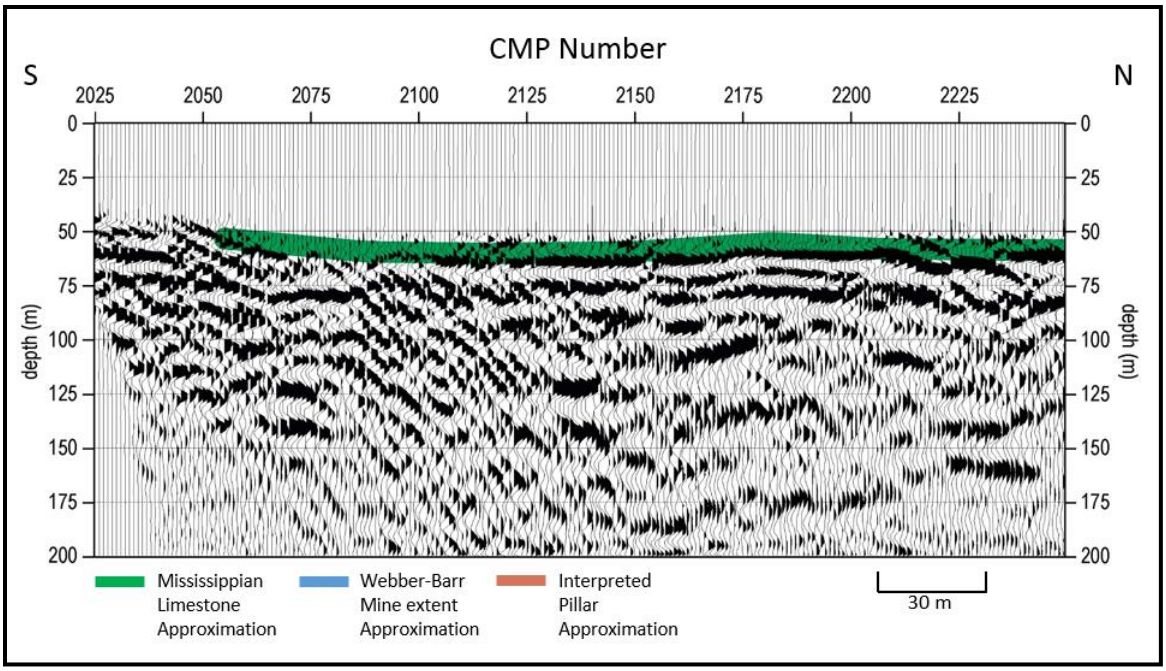

Figure 44a: The southern extent, CMPS 2025 – 2250, of the interpreted S-wave data.

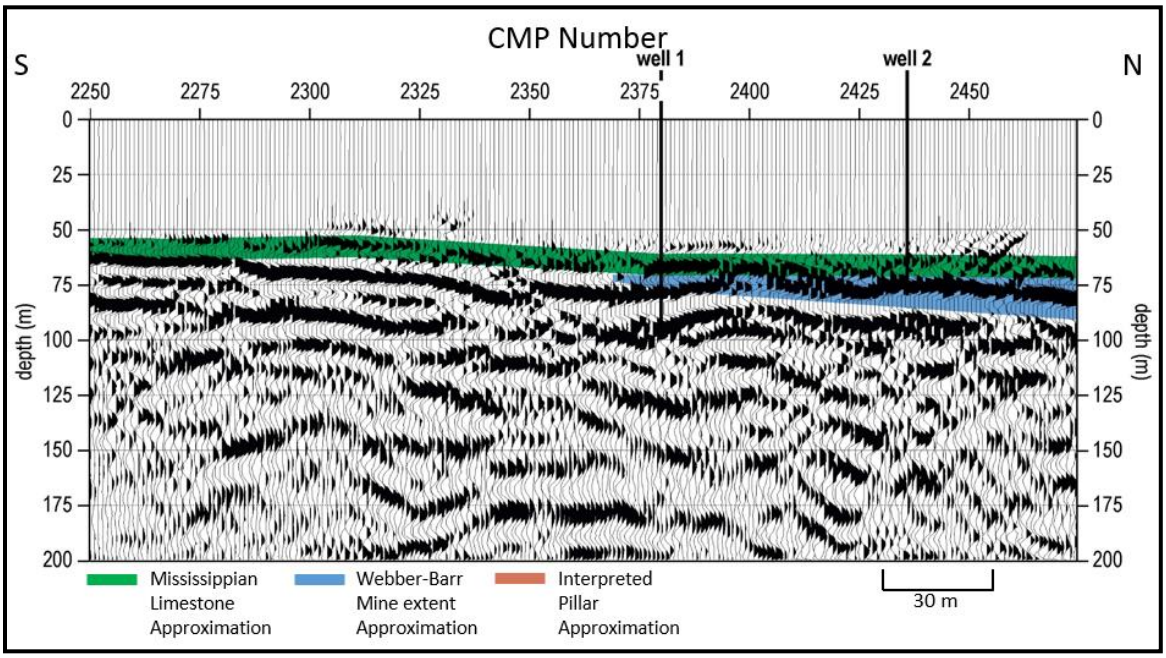

Figure 44b: CMPs 2250 – 2475 of the S-wave showing the southern edge of the Webber-Barr Mine (blue).

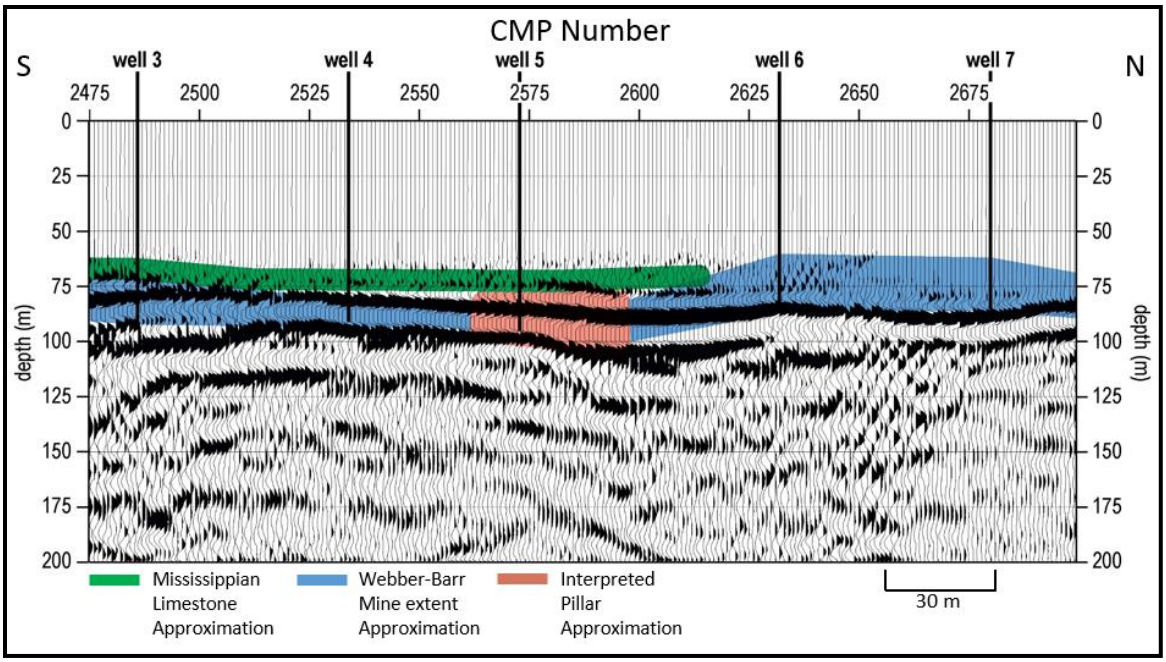

Figure 44c: CMPs 2475 – 2700 of the S-wave showing the Webber-Barr Mine (blue). The well 5 interpreted pillar is shown in orange. The high amplitude reflection is interpreted as a result of the water filled void rock contact. No interpretable events are present beneath this due to water having no shear modulus, the S-wave can not propogate through it. At wells 6 and 7 the high amplitude reflection associated with mine sits deeper than expected. A slight change in picking velocites in data processing could effect this reflection. Even though it appears somewhat deep the reflection is interpreted as a result of water-limestone contact of the mine.

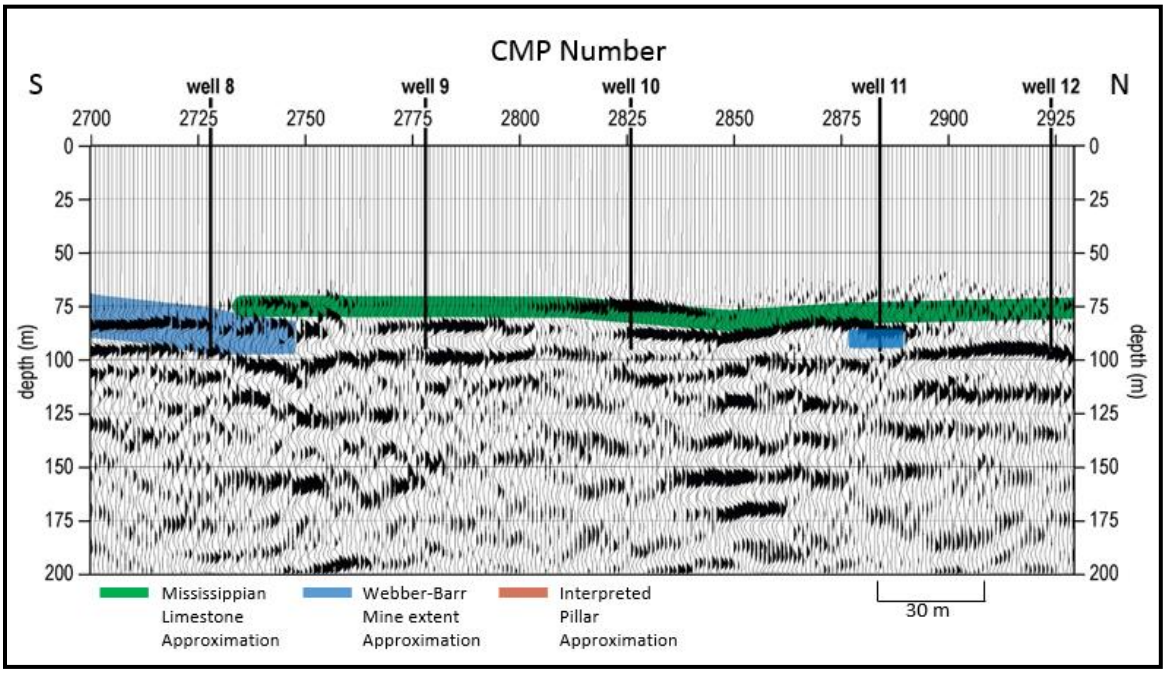

Figure 44d: CMPs 2700 – 2925. The high amplitude reflection decreases in amplitude moving north off the mine between wells 8 – 9 due to no water rock contact. It is expected for the S-wave data to have a high amplitude releflection at a water contact. A small void is present at well 11 and is interpreted as a north western room of the Webber-Barr Mine.

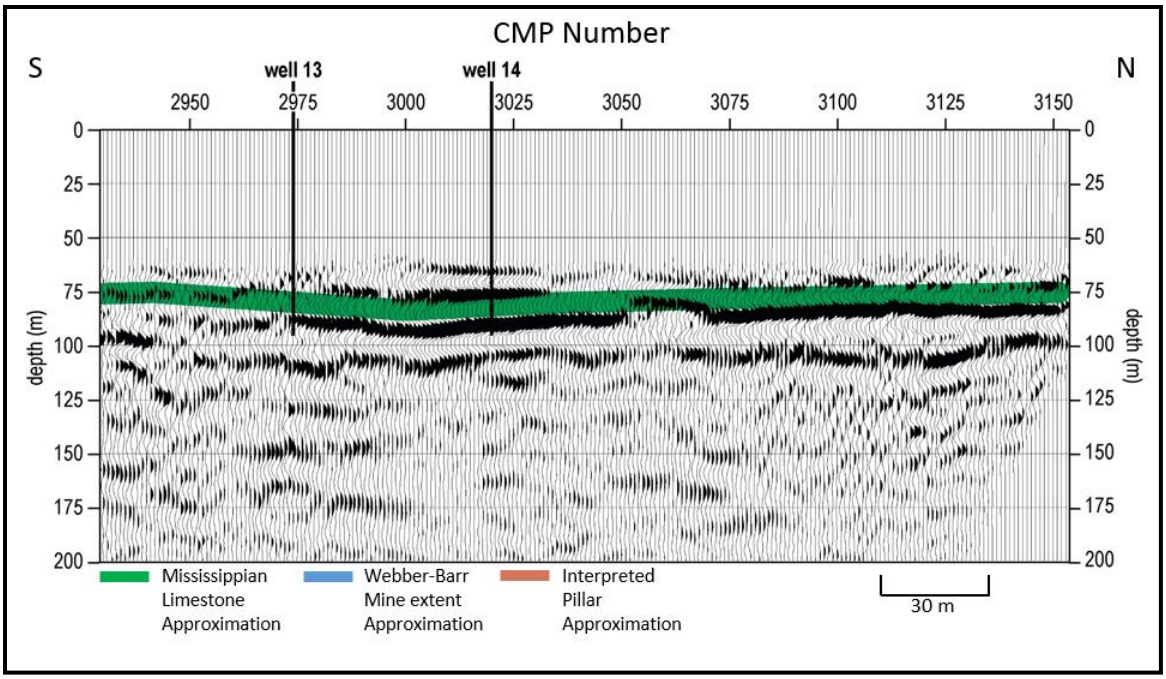

Figure 44e: The northern extent of the S-wave survey, CMPs 2925 – 3150, show laterally consistent reflections with high amplitude that correlate well to the limestone reflections (green) in the P-wave data (Figure 58) at the same depth.

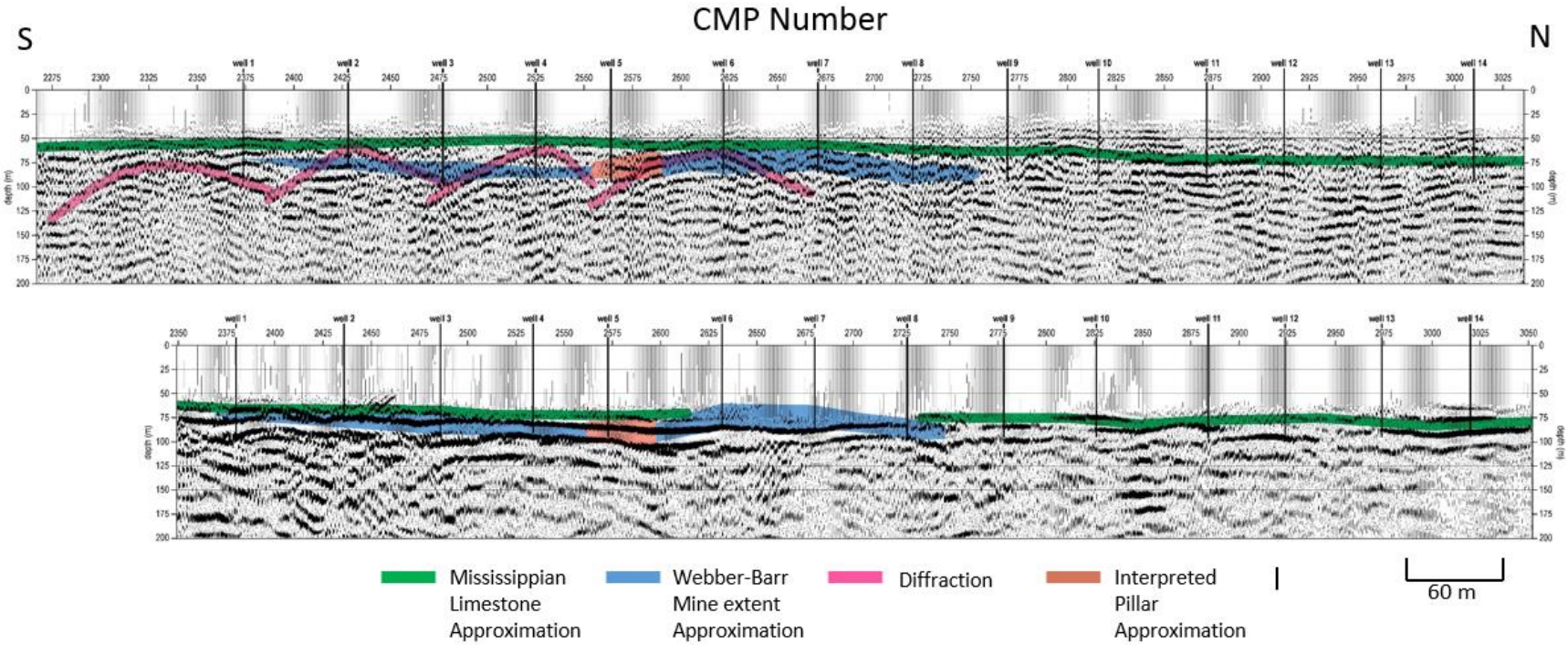

Figure 45: Interpreted S-wave (bottom) stacked section vs interpreted P-wave (top) section of Webber-Barr Mine area. Notice that areas on the P-wave (top) that lack laterally continuous reflections and have diffractions present, match the area on the S-wave (bottom) where a high amplitude reflection is present at the depth of the mine. Combining these data with the well data allowed for verifying these features as indication of mine presence. Also, the data sets show laterally consistent reflections (green) at the same depth, ~ 75 m, at the north end of these profiles which correlate to the Boon Fm limestone.

Discussion

Interpretations of both P- and S-wave reflection data sets are consistent with highly complex subsurface rock units within the mine overburden. A lack of lateral continuity in P-wave reflections across the profile (Figures 41– 42 and 45) is consistent with disturbed near-surface rock layers that are complicated by coherent out of plane energy arrivals. Lack of interpretable reflections from the mine void and the presence of diffractions (CMPs 2325 – 2650) on the P-wave section, could suggest that the overburden is structurally altered (e.g. faults, fractures, etc.).

Differences between the mineralized zones and unmineralized zones vary from south to north on the P-wave section. Tracking laterally continuous reflections of the Boone Fm. limestone from the northern portion of the P-wave section towards the KS/OK border in the south, structurally altered areas above the mine were identified. The coherent rock layers associated with the Miami Trough terminate to the south in the vicinity of where the drilling reports confirmed mine (CMP 2800). This transition is also evident in the S-wave stacked section (Figures 43 – 44) where the character of the reflection changes from a consistent high amplitude reflection to a more chaotic lower amplitude reflector at the north end of the 2-D stacked section (CMP 2775) (Figure 43). A high amplitude reflection in the S-wave data at CMPs 2350 to 2750 is interpreted as the contact of limestone and water filled void based on its wavelet character (Figures 43 - 45). Improved consistency in the reflection wavelet trace-to-trace are observed in the S-wave reflection section in the depth between 60 – 100 m BGS, and at locations consistent with the drill confirmed mine. The characteristics of these S-wave reflections change from consistent high amplitude events over the mine, to lower amplitude less consistent waveforms off the mine. Correlations of well confirmed voids with the S-wave

reflection data support the suggestion that the area of high amplitude reflection is related to the mine.

Overall, the seismic reflection data sets possessed unique characteristics the could be correlated to well confirmed voids and contrast with well confirmed competent material. Nothing in the character of the seismic reflections was an obvious indicator that any major structural alteration of the overburden had occurred that might indicate instability in the roof rock. This seismic study offers a solid baseline for the condition of the subsurface suitable for the future time-lapse surveys. Future changes in the overburden structure interpreted in the S-wave reflection could indicate failure has begun to occur.

In the upper 80 m Vp/Vs ratio values averaged ~ 1.8. No areas showed an increase or decrease in Vp/Vs that appeared anomalous or inconsistent with the rest of the unit. The S-wave and P-wave velocities remained relatively consistent from areas over the mine to areas north and south of the mine. Although the Vp/Vs ratio did vary (~1.6 – ~1.9) in the overburden it is within the error of velocity picking (Figure 40). Overall the Vp/Vs ratio suggests laterally consistent rock velocities, indicating that material properties over the mine are similar to those of the undisturbed geological section away from the mine. The Vp/Vs ratio calculation from these data allow for an additional baseline survey. Currently this relationship provides a reasonable value for limestone (Mavko, 2005) and is consistent with a stable overburden. Any change to the Vp/Vs ratio on future studies will be determined if the source of the change is due to increased or decreased P- or S-wave velocity (Table 3).

Conclusion

There is no way to confirm when or if mine failure will occur along the stretch of U.S. 69, in extreme southern Kansas, based on this study alone. Findings presented here suggest a relatively stable overburden at the time these data were acquired. These data provide an excellent baseline for future seismic surveys at this site where subtle temporal changes can be distinguished from static heterogeneous rock properties or characteristics. There are no clear indications roof rock failure is imminent, but other locations in this area over mined out intervals have experienced catastrophic failure and collapse. This study successfully detected the drill confirmed mine location and estimated the Vp/Vs ratio of the mine overburden. It is also the first known study to characterize a mine overburden using P- and S-wave seismic reflection images and their velocity functions recorded separately and then combined to generate a Vp/Vs ratio map. It is also the first published seismic reflection survey to image the Miami Trough in this part of southeastern Kansas. The Vp/Vs ratio provides an excellent tool for interpreting the strength and stress characteristics of the mine overburden. Interpreted seismic reflection sections indicate a lack of lateral consistency in the seismic response to geologic units over the mine (i.e. overburden). These data resulted in reasonable stacked reflections and calculated velocity variations that correlated to drill confirmed mine locations. The high-resolution seismic reflection sections combined with the Vp/Vs ratio map justifies concern for potential future overburden failure in several places along the seismic profile. Depending on size and location of the roof rock failure, void migration to the ground surface could be rapid or gradual. Sinkhole development along the seismic profile would threaten public safety and transportation.

At the time of this study no obvious signs of imminent failure were observed in the seismic reflection or Vp/Vs ratio data. In this geologic setting and with the known mine

geometry failure is possible due to rapid changes in Vp/Vs ratio that cannot be anticipated from a single seismic data set. Therefore, future monitoring and difference analysis is a must to ensure public safety and prevent transportation interruptions. Principal findings presented here allow for optimum design and comparison of future seismic investigations. A change in subsurface geology, as evidence in the P- and S-wave stacked sections, would indicate further invasive investigations should be considered to determine if failure had occurred and void migration had begun. Increased Vp/Vs ratio, due to decreased Vs interval velocities relative to these baseline observations at the mine location in the future could indicate the overburden is becoming weaker and failure could be imminent. While a decreased Vp/Vs ratio value, due to increased Vs interval velocities, would indicate increased stress and a heightened probability for future failure. Changes in Vp could also indicate pore fluid changes in the mine overburden (Table 4).

Further monitoring of this site incorporating P- and S-wave reflection and surface wave surveys would provide the best noninvasive, complimentary measurements reasonable to appraise site stability. Repeat imaging of the subsurface layers as well as an updated Vp/Vs ratio will allow subtle changes in rock properties to be detected through differencing repeat surveys with this baseline study. Density logs would be valuable complements to these seismic and borehole data allowing stiffness and rigidity estimates. The density values combined with Vs and Vp values from this study would allow quantification of these elastic parameters. These analyses would provide further insight to the integrity of the overlying units as well as the potential risk for failure in this area.

Integration of the methods used in this study offer a new way to appraise mine overburden and potential failure of roof rock. Combining the velocities from different data sets (Vp & Vs) allows accurate estimates of Vp/Vs ratio beyond anything possible with state of the

practice approaches. Vp/Vs ratio can help identify regions of the overburden experiencing increased stress or partial failure. These characteristics cannot be inferred from structural interpretation of the seismic alone. If the methods used here are repeated at this site with the intent of performing time-lapse monitoring and prove effective they could be evaluated at other sites. Changes in the velocity ratio calculated from seismic reflection analysis could detect changes in the subsurface beyond what is resolvable/interpretable on the seismic. This elevated fidelity could be a key component in mapping temporal changes to the subsurface.

References

Bailey. B.l., 2014 High-resolution shear-wave reflection profiling to image offset in unconsolidated near-surface sediments: M.S. Thesis, Lawrence, Kansas: University of Kansas.

Bastin, E. S., 1939, Contributions to a knowledge of the lead and zinc deposits of the Mississippi Valley region: Geol. Soc. America, Special Paper 24, p. 1-156.

Beck, B.F., A.J. Pettit, and J.G. Herring, eds., 1999, Hydrogeology and engineering geology of sink-holes and Karst-1999: A.A. Balkema.

Black, R. A., Steeples, D., and, Miller, R. D., 1994, Migration of shallow reflection data. Geophysics, 59, no. 3,402-410.

Bradford, J.H., Liberty, L.M., Lyle, M.W., Clement, W.P. and Hess, S., 2006, Imaging complex structure in shallow seismic-reflection data using prestack depth migration. Geophysics, 71(6), pp.B175-B181.

Brittle, K. F., L.R. Lines, and A.K. Dey, 2001, Vibroseis Deconvolution: a synthetic comparison of cross correlation and frequency-domain sweep Deconvolution: Geophysical Prospecting, v 49, p 675-686.

Brady, L.L., McCauley, J.R., Knoche, L., Buchanan, R., 1989, Duied to Mined-land Problems and Reclamation in Southeast Kansas. KGS Open File Report v 89 n 19

Castagna, J. P., M. L. Batzle, and T. K. Kan, 1993, Rock Physics–The link between rock properties and AVO response, from: Offset-dependant reflectivity–theory and practice of AVO analysis, published by the Society of Exploration Geophysicists, edited by Castagna." *J, and Backus, M*.

Coruh, C., and J.K. Costain, 1983, Noise attenuation by Vibroseis whitening (VSW) processing: Geophysics, v 48, no 5, p 543-554.

Davies, W.E., 1951, Mechanics of cavern breakdown: National Speleological Society, v 13, p 6-43.

Doll, W.E., and C. Coruh, 1995, Spectral Whitening of impulsive and swept-source shallow seismic data. [Exp. Abs.] SOC. Explor. Geophys., p. 398-401.

Domenico, S.N., 1974, Effect of water saturation on seismic reflectivity of sand reservoirs encased in shale: Geophysics, v. 39 n. 6, pp.759-769.

Dressel, W.M., McFarland, M.C. and Brown, J.C., 1986, Post-mining hazards of the Kansas-Missouri-Oklahoma Tri-State zinc-lead mining district. *Guidebook to the Geology and Environmental Concerns in the Tri-State Lead-Zinc District, Missouri, Kansas and Oklahoma. Association of Missouri Geologists, 33 rd Annual Field Trip*, p.47-54.

Ebrom, D.A., S.A. Markley, and J.A. McDonald, 1996, Horizontal resolution before migration for broadband data [exp. abs.]: Society of Exploration Geophysics, p. 1430-1433.

Fowler, G. M., and Lyden, J. P., 1932, The ore deposits of the Tri-State district: Am. Inst. Mining Metall. Engineers Trans., v. 102, p. 206-251.

Gaiser, J.E., 1996, Multicomponent VP/VS correlation analysis. *Geophysics*, v *61 no* 4, p.1137-1149.

Hagni, R.D., 1986, A summary of the geology of the ore deposits of the Tri-State district, Missouri, Kansas, and Oklahoma, in *Guidebook to the Geology and environmental concerns in the Tri-State lead-zinc district, Missouri, Kansas, and Oklahoma*: Association of Missouri Geologists, 33rd annual field trip, September 26-27, 1986, p. 30-46.

Hambleton, W.W., J.P. Lyden, and D.C. Brockie, 1959, Geophysical investigations in the Tri-State zinc and lead mining district, *in* W.W. Hambleton, ed., Symposium on geophysics

in Kansas: Kansas Geological Survey Bulletin 137, p. 357-375. Available online at http://www.kgs.ku.edu/Publications/Bulletins/137/Hambleton/index.html

Ivanov, J., Miller, R. and Xia, J., 1998 High frequency random noise attenuation on shallow seismic reflection data by migration filtering: In SEG Technical Program Expanded Abstracts 1998 p. 870-873

Judy, B.E., 2015, High resolution seismic reflection to characterize small scale mechanisms of large scale natural dissolution in the Hutchinson Salt Member: M.S. Thesis, Lawrence, Kansas: University of Kansas.

Kansas Department of Health and Environment (KDHE), 2016, Treece Voluntary Relocation Program. http://www.kdheks.gov/treece/.

Kansas Department of Transportation (KDOT), 2009, Borehole report, US-69 Tomography, Project #K-6799-04, Sounding #6.

Klemperer, S.L., 1987, Seismic noise-reduction techniques for use with vertical stacking: An empirical comparison: Geophysics, v 52, no 3, p 332-334.

Knapp, R.W., D.W. Steeples, and R.D. Miller, 1989, Seismic-reflection surveys at sinkholes in central Kansas: Kansas Geological Survey, Bulletin 226.

Kinsler, L. E., A.R. Frey, A.b. Coppens, and J.V. Sanders, 1982, *Fundamentals of Acoustics (3rd ed.),* New York: John Willey and Sons Inc., 480 pp.

Lambrecht, J.L., 2006, Time-lapse high resolution seismic imaging of a catastrophic salt-dissolution sinkhole in Central Kansas: Kansas Geological Survey Open-File Report No. 2006-23.

Lambrecht, J.L., R.D. Miller, T.R. Rademacker, 2004, Advantages and disadvantage of pre-correlation, pre-vertical stack processing

Lee, M. W., 2003, Velocity ratio and its application to predicting velocities. US Department of the Interior, US Geological Survey.

Lee, S., Shaw, J., Ho, R. and Steeb, D., 1999, Deepwater reservoir prediction using seismic and geomechanical methods: The Leading Edge, v 18 no 6, p. 726-728.

Liberty, L.M., and M. Knoll, 1998, Time-varying fold in stacked seismic reflection data: A new quality procedure for shallow high-resolution applications: Proceedings of the Symposium on the Application of Geophysics to Engineering and Environmental Problems (SAGEEP98), p 745-751.

Lillie, R.J., 1999, Whole earth geophysics. *An Introductory Textbook for Geologists*.

Lines, L., Zou, Y., Zhang, A., Hall, K., Embleton, J., Palmiere, B., Reine, C., Bessette, P., Cary, P. and Secord, D., 2005, Vp/Vs characterization of a heavy-oil reservoir. The Leading Edge, v 24 no 11, p.1134-1136.

Luza, K.V., 1986, Stability problems associated with abandoned underground mines in the Picher Field, Northeastern Oklahoma. *Oklahoma Geological Survey Circular 88.*

Maleki, H., Jung, Y. and Hollberg, K., 1993, December. Case study of monitoring changes in roof stability. In *International journal of rock mechanics and mining sciences & geomechanics abstracts* (Vol. 30, No. 7, pp. 1395-1401). Pergamon.

Mavko, G., 2005, Conceptual overview of rock and fluid factors that impact seismic velocity and impedance. *Retrieved*, *11*(11), 2012.

McCauley, J.R., L.L. Brady, and F.W. Wilson, 1983, Study of stability problems and hazard evaluation of the Kansas portion of the Tri-State mining area (Contract 10100131 report): U.S. Bureau of Mines Open-file Report 75-83, 193 p. (Also Kansas Geological Survey Open-file Report 83-2.)

McFarland, M. C., and J.C. Brown. 1983, Study of Stability Problems and Hazard Evaluation of the Missouri Portion of the Tri-State Mining Area (Contract 10100132 report): U. S. Bureau 790 of Mines Open-file report 97-83, p. 141

McKnight, E.T., and R.P. Fischer, 1970, Geology and ore deposits of the Picher Field, Oklahoma and Kansas: Geological Survey Professional Paper 588, U.S. Government Printing Office, http://pubs.usgs.gov/pp/0588/report.pdf.

Merriam, D. F., 1963, The Geologic History of Kansas: Kansas Geological Survey, Bulletin 162.

Miller, R.D., D.W. Steeples, R. Hill, and B. Gaddis, 1990, Identifying intra-alluvial and bedrock structures shallower than 30 meters using seismic-reflection techniques: Soc. Explor. Geophys., *Investigations in Geophysics no. 5,* Volume on Environmental Geophysics, S. Ward, ed., p. 89-97.

Miller, R.D., and D.W. Steeples, 1991, Detecting voids in a 0.6-m coal seam, 7 m deep, using seismic reflection: *Geoexploration*, Elsevier Science Publishers B.V., Amsterdam, The Netherlands, v. 28, p. 109-119.

Miller, R. D., 1992, Normal moveout stretch mute on shallow-reflection data: Geophysics, v 57, no 11, p 1502-1507.

Miller, R.D., A.C. Villella, and J. Xia, 1997, Shallow high-resolution seismic reflection to delineate upper 400 m around a collapse feature in Central Kansas: Environmental Geosciences, v. 4, no. 3, p 119-126.

Miller, R.D., and R. Henthorne, 2004, High-resolution seismic reflection to identify areas with subsidence potential beneath U.S. 50 Highway in eastern Reno County, Kansas: Proceedings of the 55th Highway Geology Symposium, September 8-10, Kansas City, Missouri, p. 29-48.

Miller, R.D., Steeples, D.W., Rademacker, T.R. and Lambrecht, J.L., 2006, Seismic reflection characteristics of subsidence affecting transportation: *Goephysical Solutions for Environment and Engineering----Proceedings of the 2nd International Conference on Environmental and Engineering Geophysics (Volume 1).*

Miller, R. D., 2007, High-resolution seismic investigation of subsidence from dissolution: PhD. Dissertation, University of Leoben.

Miller, R.D. and Steeples, D. W. 2008, High-resolution Seismic-reflection Imaging of I-70 Sinkholes, Russell County, Kansas. Kansas Geological Survey Open-file Report 2008-18.

Miller, R.D., Ivanov, J., Peterie, S.L., Buchanan, R., Hinman, P., Billinger, K., 2015, Seismic Characterization of Abandoned Mine Overburden Along U.S. 69 Highway North of the Kansas/Oklahoma State Line. Kansas Geological Survey: Proposal to the Kansas Department of Transportation, p. 1-25.

Miller, R.D., Fontana, J.M., Morton, S.L.C., Peterie, S.L., Feigenbaum, D.Z., Ivanov, J, Bennett, B., Wedel, B., Anderson, J., Stevens, T., and Banks, A., 2017, Seismic Characterization of Mine Overburden Along U.S. 69 Highway North of the Kansas/ Oklahoma State Line. Kansas Geological Survey: Report to Kansas Department of Transportation. p. 26-35.

Myers, P. B., Miller, R. D., and Steeples, D. W., 1987, Shallow seismic-reflection profile of the Meers fault, Comanche County, Oklahoma: Geophys. Res. Lett., 14? no. 7, 749-752

Nairn, R.W., Calvey, M.J. and Landers, T.L., 2005, Current and planned remediation demonstration projects of the Oklahoma Plan for Tar Creek. In *Proceedings of the 2005 National Meeting. Breckinridge (CO): American Society of Mining and Reclamation*, p. 770-790.

Ostrander, W., 1984, Plane-wave reflection coefficients for gas sands at nonnormal angles of incidence. *Geophysics*, v *49* no.10, p.1637-1648.

Pasquet, S., Bodet, L., Dhemaied, A., Mouhri, A., Vitale, Q., Rejiba, F., Flipo, N. and Guérin, R., 2015, Detecting different water table levels in a shallow aquifer with combined P-, surface and SH-wave surveys: Insights from V P/V S or Poisson's ratios. *Journal of Applied Geophysics*, *113*, p.38-50.

Pfeiffer, J., Spott, T., Hild, J., and Hanna, K., 2009, Seismic Tomography Ground Imaging of Old Mine Workings Along US Highway 69, Cherokee County, Kansas. Pfeiffer Incorporated, Blackhawk Division, Project Number 5139. Report to the Kansas Department of Transportation, pg. 19.

Pullan, S.E., and J.A. Hunter, 1990, Delineation of buried bedrock valleys using the optimum-offset shallow seismic reflection technique; in Stan Ward, ed., *Volume 3: Geotechnical*: Society of Exploration Geophysicists, Investigations in Geophysics No. 5, p. 89-97.

Rice, D., 2009, Applicability of 2-D time-lapse high resolution seismic reflection approach to image natural salt-dissolution and subsidence in central Kansas and improved post-processed vibroseis data characteristics: M.S. Thesis, Lawrence, Kansas: University of Kansas.

Ristow, D., and, Jurczyk, D., 1975, Vibroseis Deconvolution. Geophysical Prospecting, 23, no. 2, p. 363-379.

Rojas, E., 2008, Vp-Vs ratio sensitivity to pressure, fluid, and lithology changes in tight gas sandstones: *First Break*, v *26* no 3.

Schepers, R., 1975, A seismic reflection method for solving engineering problems: *Journal of Geophysics*, v. 41, p. 367-384.

Seevers, W.J., 1975, Description of the surficial rocks in Cherokee County, southeastern Kansas: Kansas Geological Survey Geology Series No. 1.

Sherriff, R.E., 2002, Encyclopedic Dictionary of Applied Geophysics, 4th ed.: Oklahoma Society of Exploration Geophysicists, Tulsa, p 429.

Sheriff, R. E., and, Geldart, L. P. 1995, Exploration Seismology: Cambridge University Press.

Sofianos, A.I., 1996, Analysis and design of an underground hard rock voussoir beam roof: *International Journal of Rock Mechanics, Mining Science, Geomechanics Abstracts*, V. 33, p. 153-166.

Steeples, D.W., R.W. Knapp, and C.D. McElwee, 1986, Seismic reflection investigations of sinkholes beneath interstate highway 80 in Kansas: *Geophysics*, v. 51, p. 295-301.

Steeples, D. W., and R.D. Miller, 1998, Avoiding pitfalls in shallow seismic surveys. Geophysics, p 1213-1224.

Stolt, R.H., and A.F. Benson, 1986, *Seismic Migration*: Geophysical Press.

Tatham, R. H., and, Stewart, R. R., 1993, Present status and future directions of shear-wave seismology in exploration. CREWES Research Report, 5.

Van Dok, R. and Kristiansen, P., 2003, Event registration and Vp/Vs correlation analysis in 4C processing. In *SEG Technical Program Expanded Abstracts 2003:* (pp. 785-788). Society of Exploration Geophysicists.

Weidman, S., 1932, The Miami-Picher Zinc-Lead District, Oklahoma: Oklahoma Geological Survey Bulletin No. 56, http://www.ogs.ou.edu/pubsscanned/BULLETINS/Bulletin56mm.pdf.

Westman, E.C., Luxbacher, K.D. and Swanson, P.L., 2008, January. Local earthquake tomography for imaging mining-induced changes within the overburden above a longwall

mine. In *The 42nd US Rock Mechanics Symposium (USRMS)*. American Rock Mechanics Association.

Widess, M.B., 1973, How thin is a thin bed?: *Geophysics*, v. 38, p. 1176-1180.

Williams, W.T., and W.F. Fredericksen, 1985, Mine subsidence report; Mine subsidence 1.1 miles north of the Oklahoma line on US 69, Cherokee County: Kansas Department of Transportation report, December 1985.

Wichita Eagle, 2009, Town Over Mines Could Dry Up Soon. Photograph. http://www.kansas.com/latest-news/article1010282.html

Yilmaz, Ö., 1987, *Seismic Data Processing*: Tulsa, Society of Exploration Geophysicists.

Yilmaz, Ö., 2001, Seismic Data Analysis: Society of Exploration Geophysics, 2nd Edition.

Appendix

Well 1

Two small voids present were encountered in Well 1. The first at a depth of 70 m and the second at a depth of 74 m. Overlying the shallower void is 42 m of cherty limestone that is described as gray, hard, black and firm, and with coal seams present. This water filled void is only 10.33 m thick. Between these two voids are multiple individual limestone units described as brecciated and soft. The deeper void is 1 meter thick and overlies layers of limestone which are described as plattey with small voids and soft. The well total depth (TD) was ~ 95m. Multiple reflections in the P-wave dataset are interpreted at Well #1 from ~ 45 m depth to ~ 75 m. Data resolution limits negate any possibility of imaging the voids. The reflections on the CMP stacks in this area are result of layered varying limestone units. The S-wave data set possesses reflection events coincident with this well location, but they lack lateral consistency compared to those in the P-wave. The high amplitude reflection at ~ 75 m closely correlates to the contact between the thick cherty limestone layer and the layered limestone with interbedded voids (Figure 46).

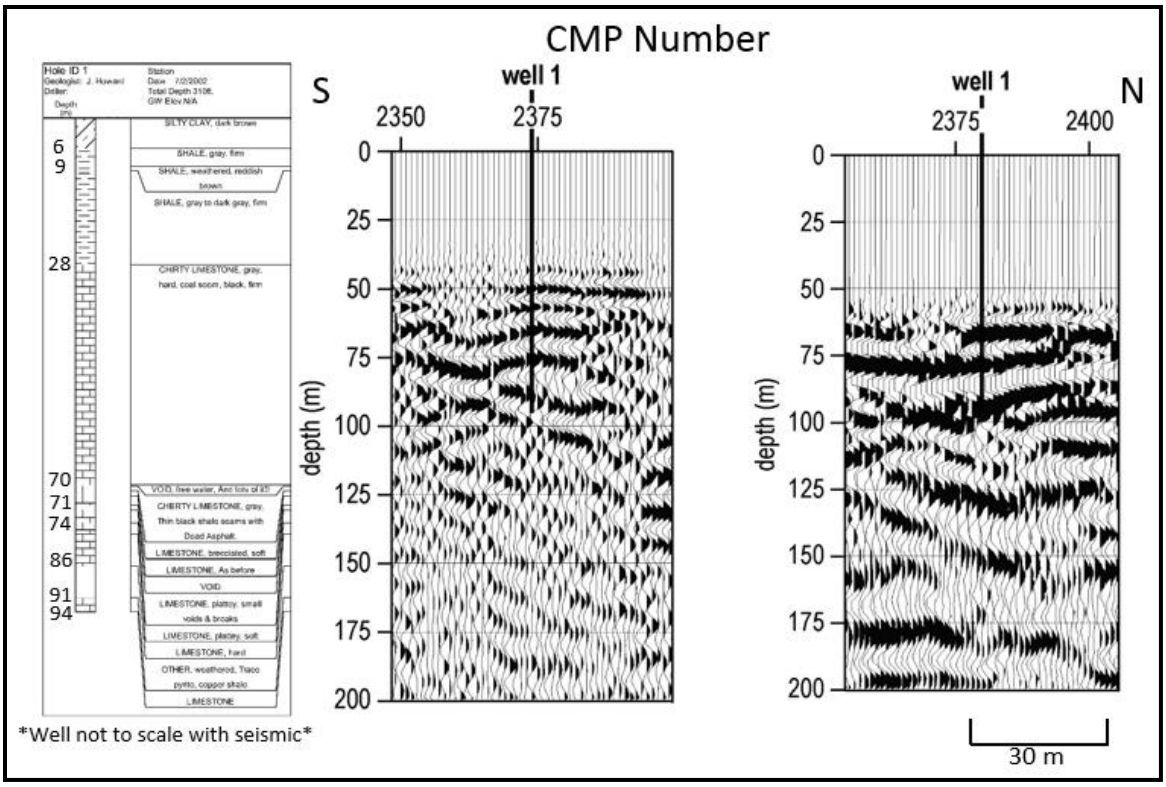

Figure 46: Correlation of Well 1 (left) vs P-wave (middle) and S-wave (right) seismic.

Well 2

Well 2 encountered a 40-m thick hard gray limestone overlying a water filled void. The void roof is at a depth of 70 m. The well TD was 79 m, and no void floor was encountered, therefore at Well 2, it can be assumed that the mine void is at least 9 m thick. There are two P-wave reflection events estimated to be from reflectors between 75 and 100 m depths. A diffraction event is centered near Well 2. Diffractions are generally indicative of a fault, fracture, or bed termination. The S-wave data has a high amplitude reflection at ~ 75 m, which is interpreted to be from within the mine overburden (Figure 47).

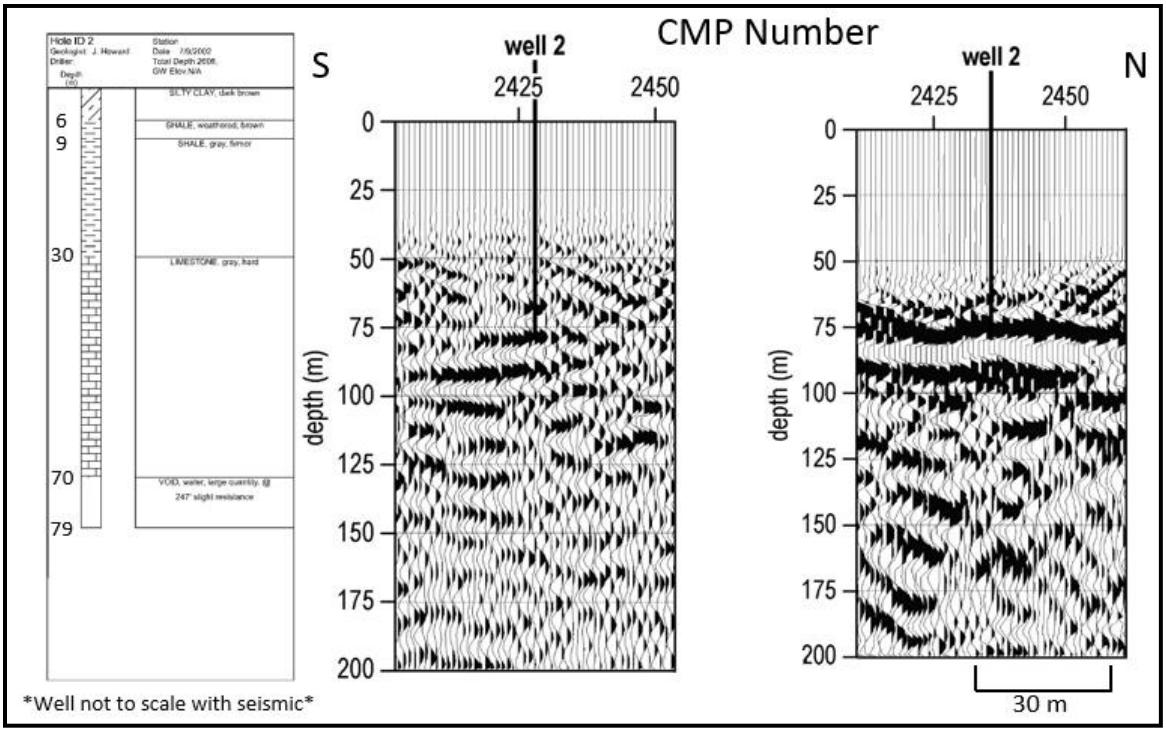

Figure 47: Correlation of Well 2 (left) vs P-wave (middle) and S-wave (right) seismic.

Well 3

The mine roof was encountered in Well 3 at 73 m. The mine, was drill confirmed to be ~ 21 m in height and overlain by 40 m of a hard light gray limestone. The well TD was the mine floor at ~ 94 m BGS. No coherent or interpretable reflections are interpretable at Well 3 on the P-wave data, while the high amplitude reflection evident on the S-wave data continues from Well 2 to this Well at velocity estimated depth of 75 m. This reflection in the S-wave continues at a depth reasonable to be the contact between the mine void and overburden (Figure 48).

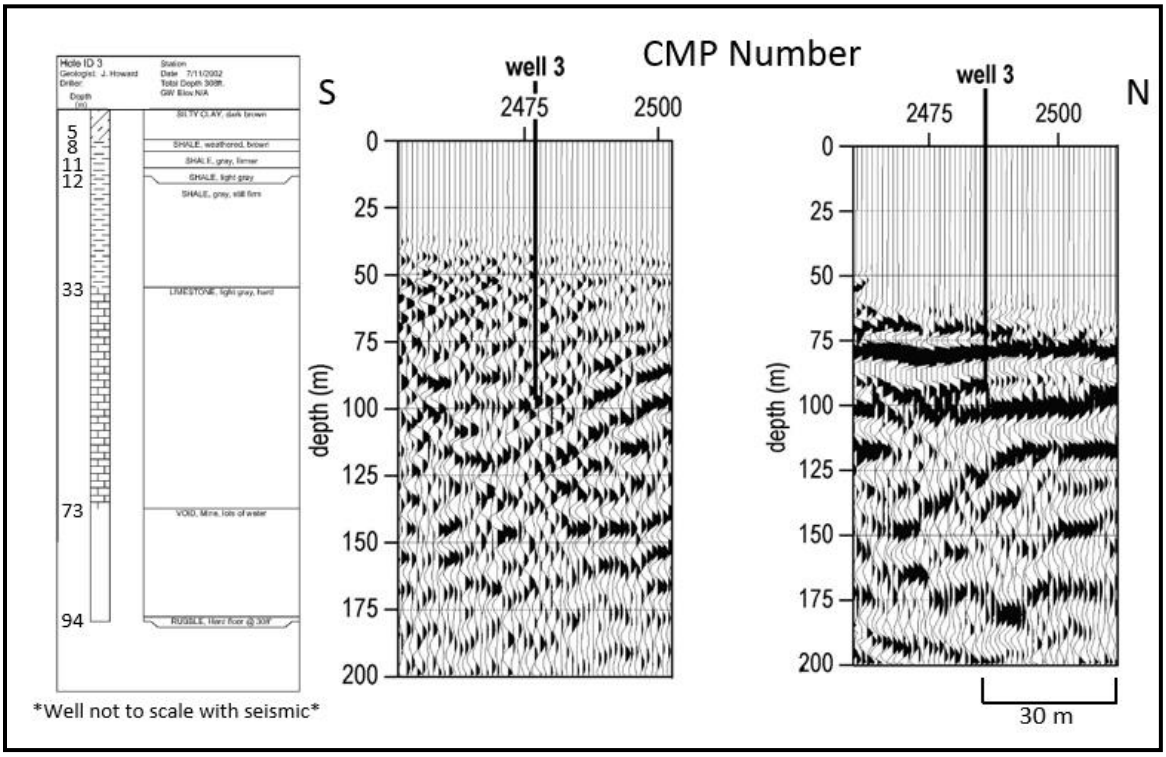

Figure 48: Correlation of Well 3 (left) vs P-wave (middle) and S-wave (right) seismic.

Well 4

A 7-m thick void was encountered in Well 4 from ~ 83 m to ~ 90 m BGS. The Well was drilled to a TD of 91 m. The mine roof is overlain by 3 m of cherty limestone and 4 m of limestone that is described as porous and water filled. A stiff gray limestone overlies the cherty limestone. As observed at Well 3, no coherent or interpretable reflections are evident in the P-wave stacked section. Although no reflections are interpretable, a diffraction event can be observed centered at this Well. The high amplitude laterally continuous reflection evident at other Wells intersected by the S-wave data can be observed at this well at a depth of ~ 80 m. This reflection is from a depth consistent with the mine as indicated on the geologic log (Figure 49).

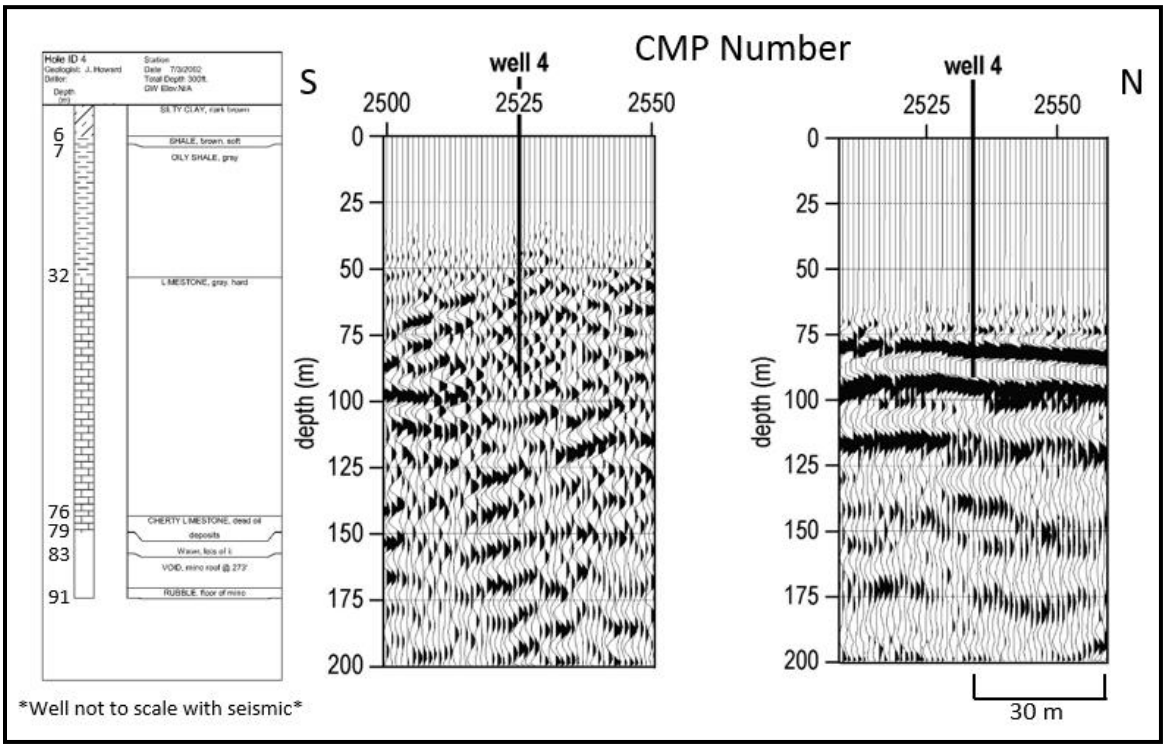

Figure 49: Correlation of Well 4 (left) vs P-wave (middle) and S-wave (right) seismic.

Well 5

Drilling at the Well 5 location did not encounter a void at the reported mine depth. The borehole was drilled to a total depth of ~ 94 m and encountered a cherty limestone from 76 m depth to the bottom of the hole. The cherty limestone is overlain by a 44-m thick light gray hard limestone. A pillar could be located at the location of this well resulting in no mine being encountered. On the P-wave data north of Well 5 (CMP 2575) are reflections that are present which are ~ 6 – 8 CMP wide. These reflections could be a result of narrow band wavelets from the pillar. The S-wave data here shows very similar characteristics to the well locations north and south of this well, therefore a pillar or change in mine geometry is not evident on the S-wave data, possibly due to the horizontal resolution of the data not being able to image the pillar (Figure 50).

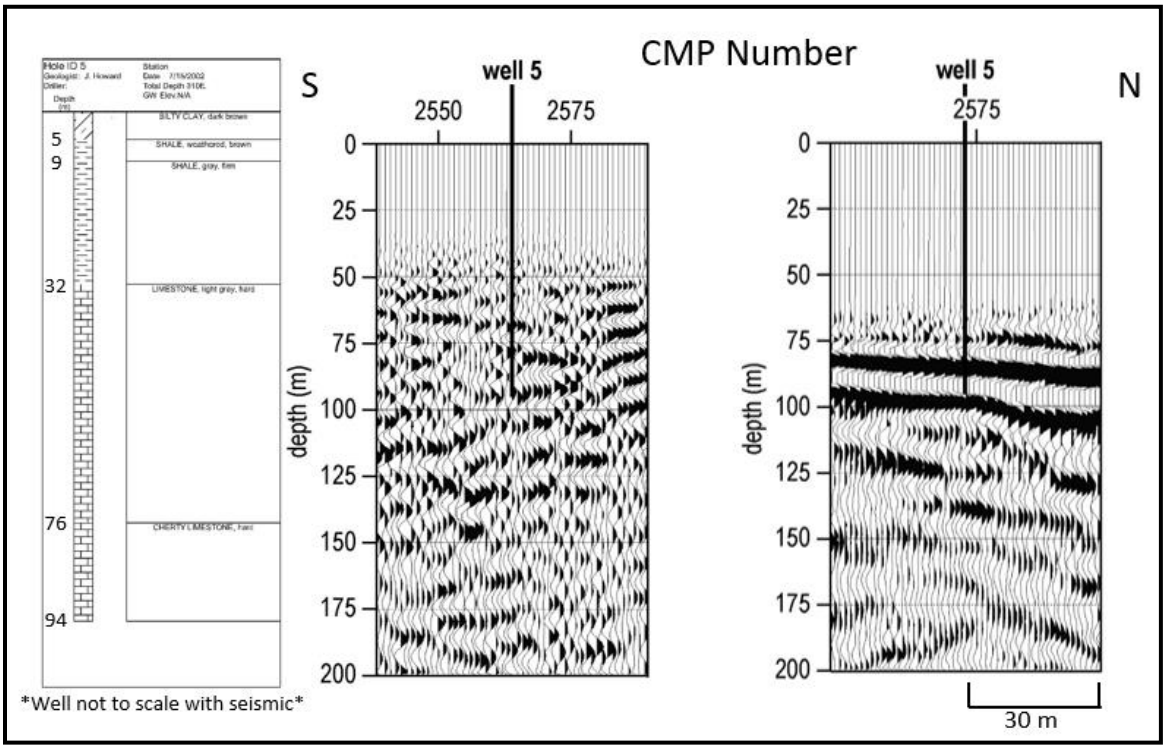

Figure 50: Correlation of Well 5 (left) vs P-wave (middle) and S-wave (right) seismic.

Well 6

The largest vertical extent of the mine void was encountered at boring 6 where the mine roof was penetrated at a depth of ~ 58 m BGS and the floor was tagged 28 m below the top of the void. The water filled mine void is overlain by a 26-m thick light gray, hard limestone. Well 6 was drilled to a total depth of 87 m. No reflections appear on the P-wave data, but a diffraction can be observed that is centered at this well location. This could be generated by the bed terminations associated with the interpreted pillar south of Well 6, alternatively the diffractions could be from fractures in the overburden rock. A high amplitude reflection in the S-wave stacked section is deeper than expected ~ 80 m, but is within the time to depth estimate of the void. (Figure 51).

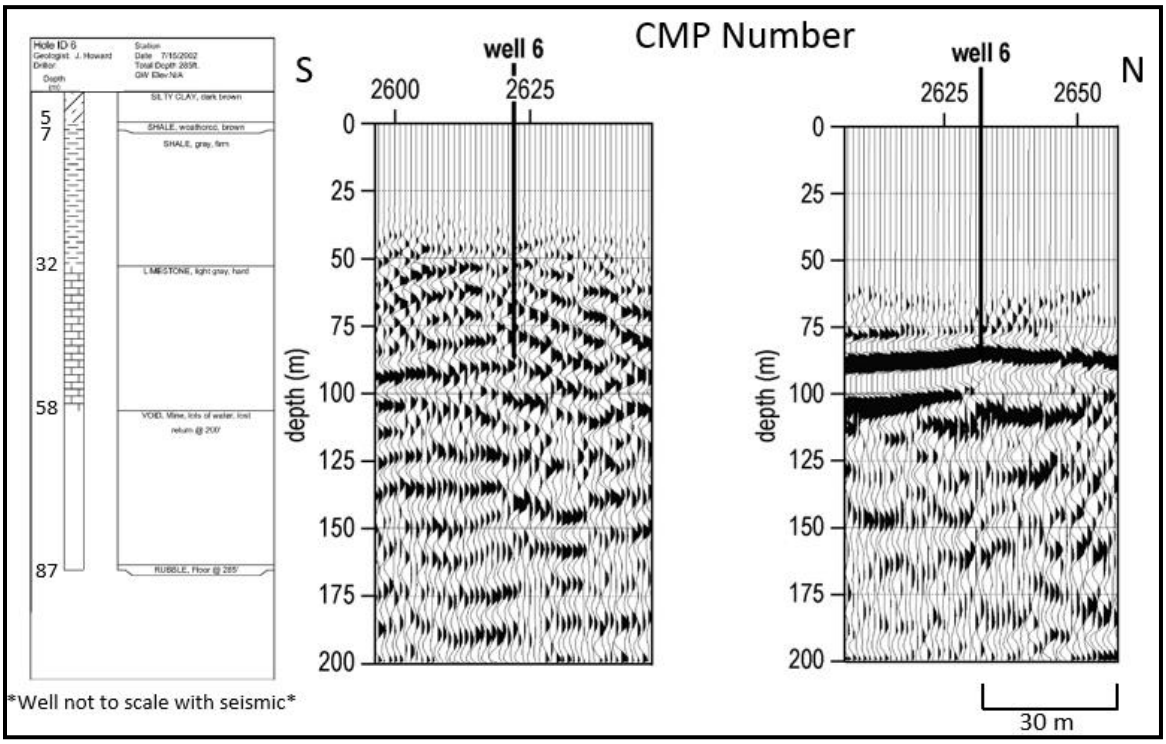

Figure 51: Correlation of Well 6 (left) vs P-wave (middle) and S-wave (right) seismic.

Well 7

The Mine roof is an overlying cherty limestone, at a depth of 60 m. The mine void is 24 m thick and water filled at Well 7. Overlying the cherty limestone is 26 m of hard gray limestone with traces of weathered copper shale. Well 7 was drilled to a total depth of 86 m. The P-wave stacked section lacks laterally continuous events in this well's vicinity that can be interpreted as reflection. Similarly, to Well 6, there is a high amplitude reflection in the S-wave data, but it is deeper (80 m) than expected when compared to the geological log (60 m). Although it does fall with the depth of the mine (60 m – 85 m), the reflection is interpreted as coming from within the mine overburden, but should not be iterated as the interpretation of the exact location of the mine roof (Figure 52).

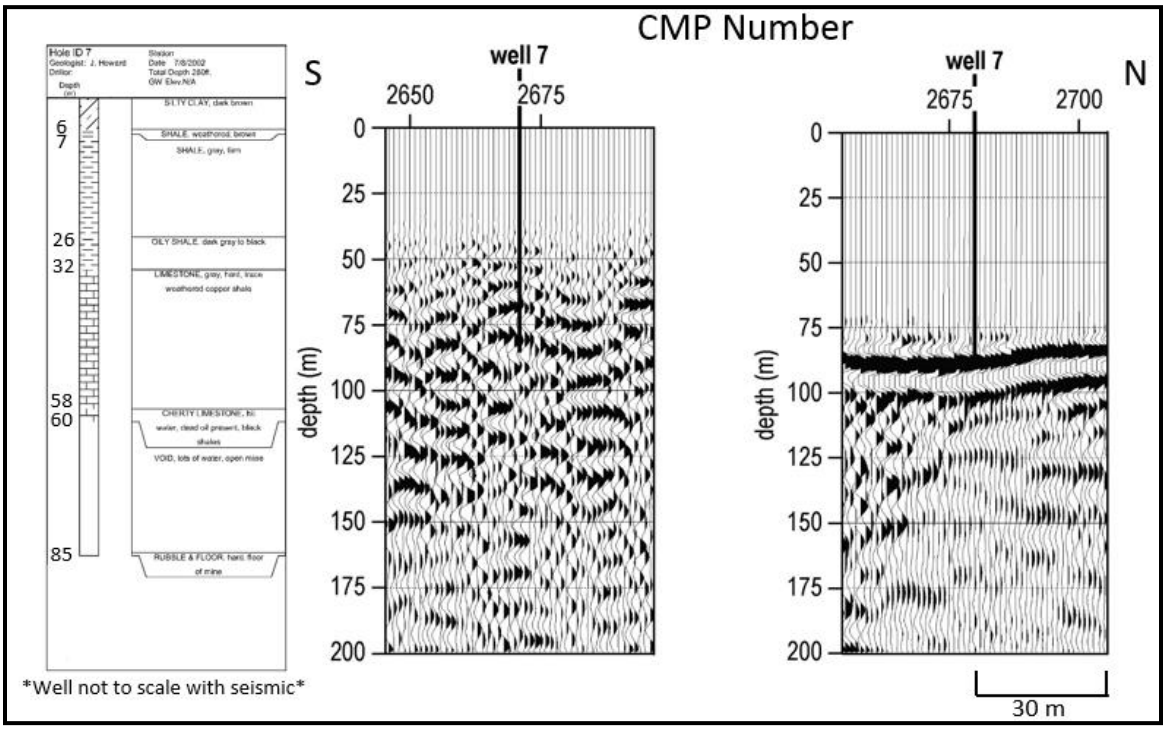

Figure 52: Correlation of Well 7 (left) vs P-wave (middle) and S-wave (right) seismic.

Well 8

A 42-m thick light gray hard limestone overlays 2 m thick brecciated and cherty limestone containing water at a depth of 74 m. Underlying the cherty limestone is a water filled void, which is ~ 20 m thick at this location. The mine roof is interpreted at a depth of 76 m and the well was drilled to a total depth of 97 m. No interpretable reflection events are present in the P-wave stacked data. The high amplitude, laterally continuous reflection in the S-wave data appears to decrease in coherency and amplitude near Well 8. The S-wave reflection (80m depth) calculate to be at a depth reasonably consistent with that of the mine roof (76 m depth). The decreased amplitude north of Well 8 could be related to edge of the mine located at some point between Well 8 and 9. Lower amplitude reflections north and south of the mine are expected because of a smaller acoustic impedance contrast between native rock layers, compared to rock/void contact over the water filled mine. The S-wave would not propagate at the rock water contact because the shear modulus of water = 0 (Figure 53).

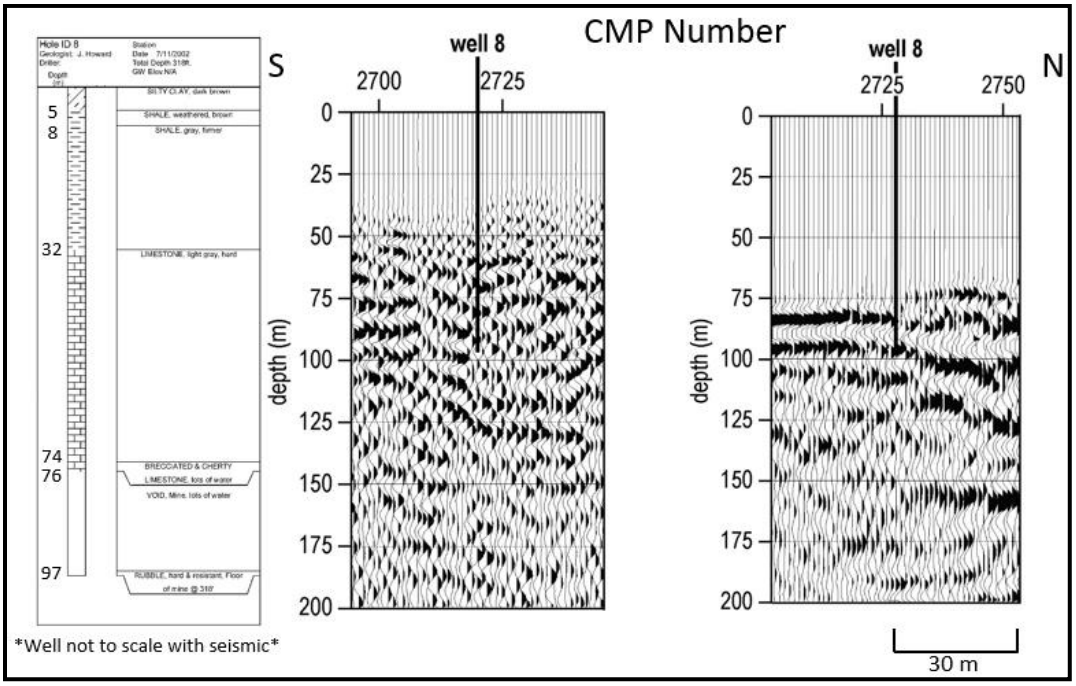

Figure 53: Correlation of Well 8 (left) vs P-wave (middle) and S-wave (right) seismic.

Well 9

No void was encountered during the drilling of Well 9. A hard light gray limestone was the predominant unit in this geologic log throughout the 94-m boring. Water was encountered in this unit were at 58 m depth and continued to the bottom of the well. Still no reflections are present in the stacked section at Well 9 location on the P-wave. Lack of coherent reflection arrivals from 58 m to 94 m in the saturated interval is likely do to the edge effects of the mine. Considering the mine geometry, fracture sets, and bed irregularity the signal is being masked by noise and unwanted energy (i.e. out of the plane reflections) as a result of these components. A reflection in the S-wave data is present at a similar depth (~ 85 m) to the previous wells but has a lower amplitude and less laterally consistency than previous wells (Figure 54).

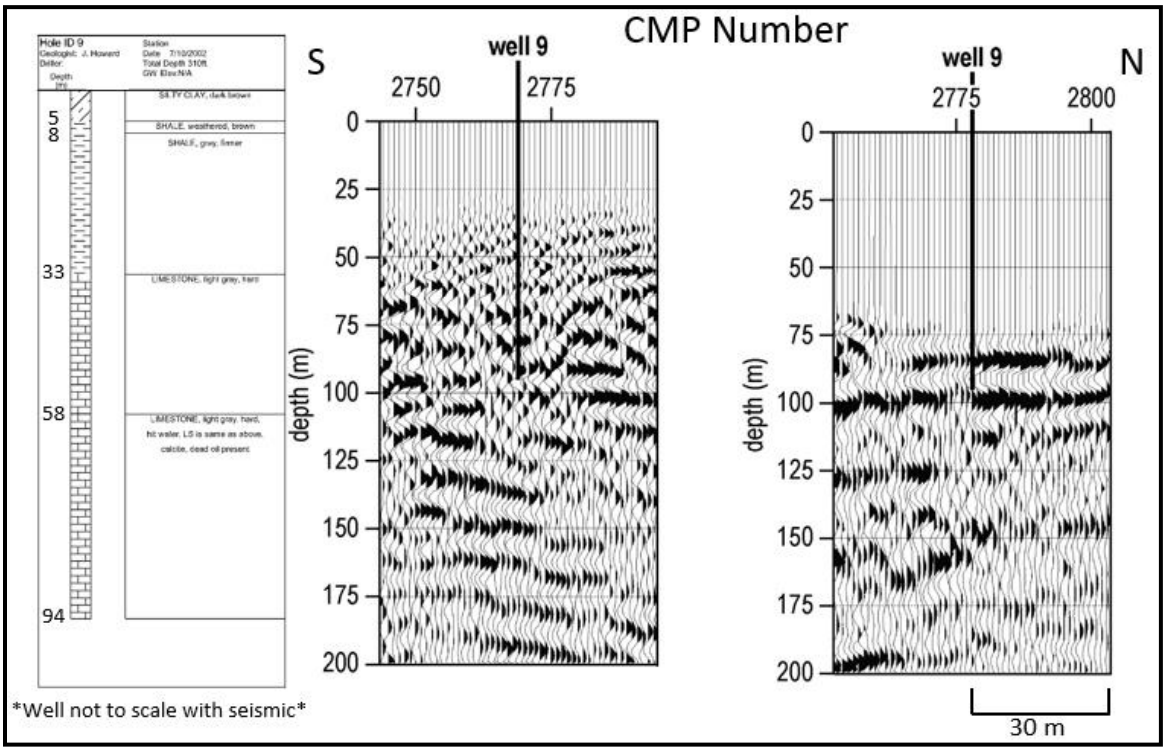

Figure 54: Correlation of Well 9 (left) vs P-wave (middle) and S-wave (right) seismic.

Well 10

No void was encountered drilling Well 10. Total depth of well 10 was 94 m. Water was encountered at Well 10 at 65 m in a cherty limestone interval that continued to the bottom of the hole. The cherty limestone interval is overlain by a 32-m thick hard gray limestone. Coherency of reflections in the P-wave data has increased from Well 9 to 10. Shallow seismic events (~ 45 m depth) associated with varying limestone units are more prominent in the data. Also, more evident are reflections from limestone units stacking in from 45 - 100 m deeper Boone Fm units and possible the Chattanooga Shale. The S-wave reflection data lacks lateral consistency and experience a drop in amplitude from Well 8 to this point (Figure 55).

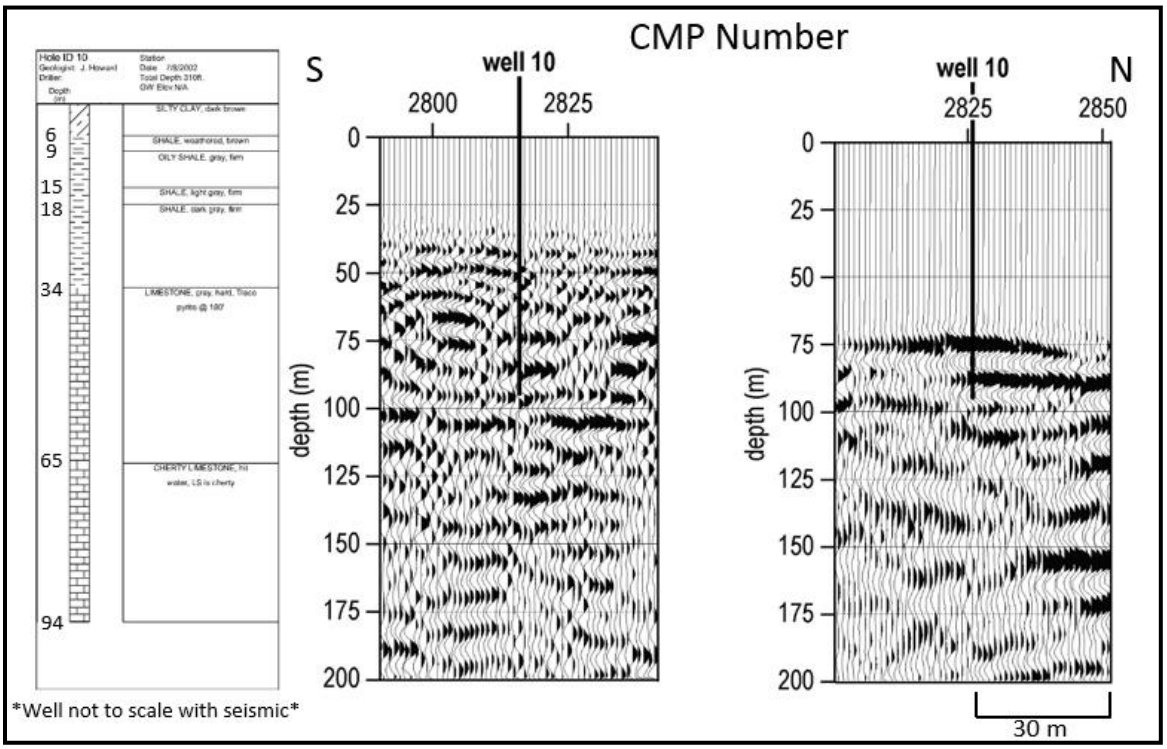

Figure 55: Correlation of Well 10 (left) vs P-wave (middle) and S-wave (right) seismic.

Well 11

An approximately 8 m thick void was encountered when drilling Well 11 at the base of the well, which was drilled to the mine floor at a depth of 96 m. It is overlain by 56 m of light gray hard limestone. In the vicinity of this well, the P-wave data possesses its greatest consistency in lateral reflections, from south to north. Multiple reflection events from ~ 40 m to ~ 120 m BGS are associated with the limestone unit. The S-wave data lacks sufficient consistency across the profile to provide a meaningful interpretation (Figure 56).

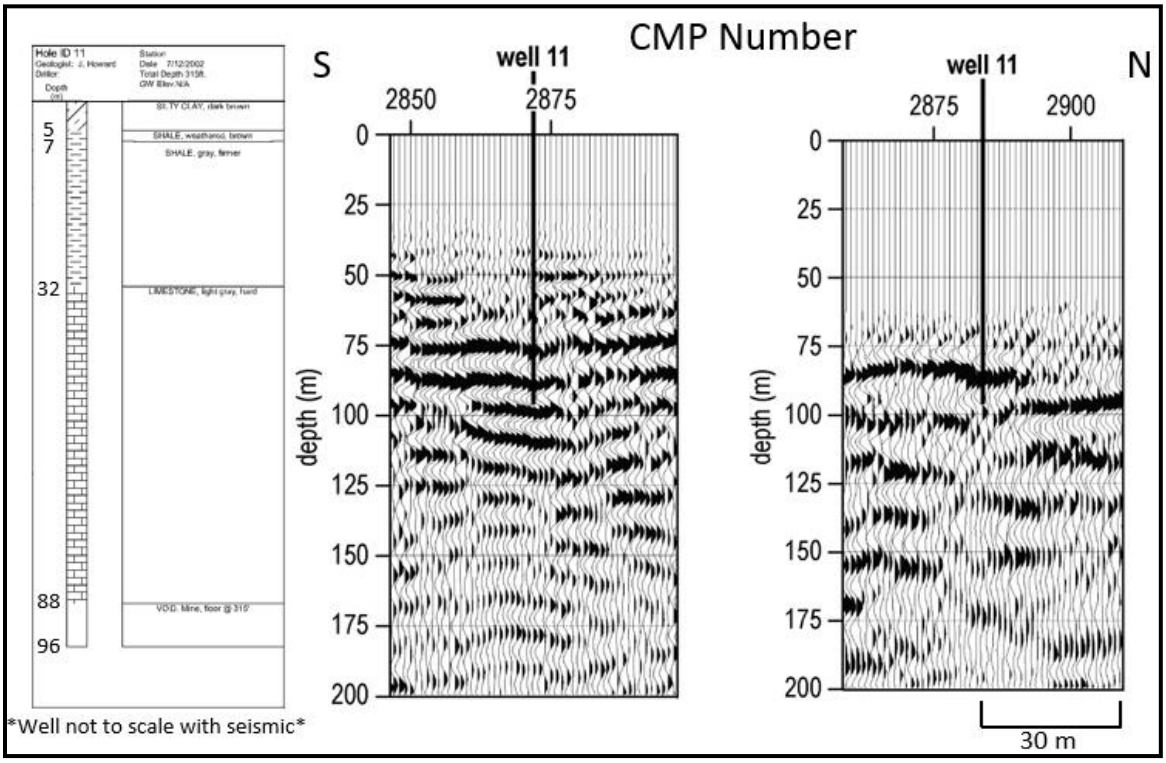

Figure 56: Correlation of Well 11 (left) vs P-wave (middle) and S-wave (right) seismic.

Well 12

No void was encountered during the drilling of Well 12. A light gray, hard water saturated limestone was encountered at 40 m BGS and extends to the bottom of Well 12, which TD was 94 m. Reflections in proximity to the location of Well 12 lack lateral consistency compared to the previous stacked section (Well 11). There are some narrow bandwidth effects for 75 – 85 m BGS in the P-wave. Similar to the previous stacked section at Well 11 the S-wave lacks data coherency. An event is present at ~ 90 m but it terminates north and south of the well (Figure 57).

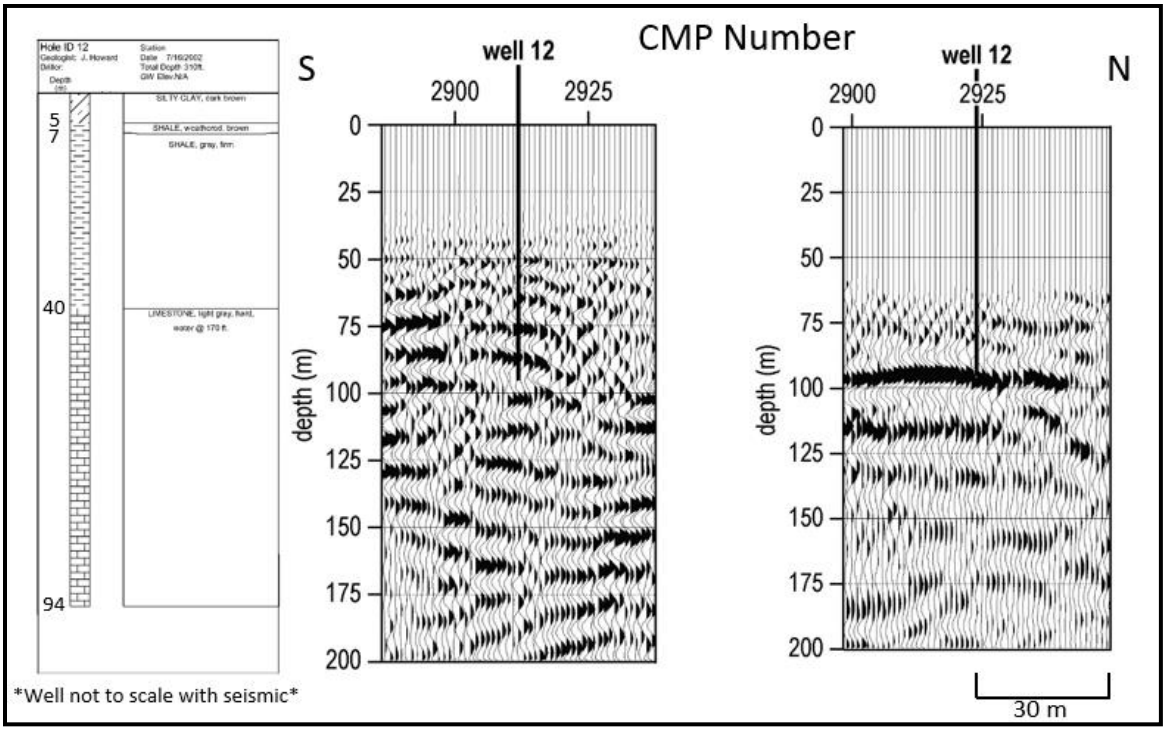

Figure 57: Correlation of Well 12 (left) vs P-wave (middle) and S-wave (right) seismic.

Well 13

A cherty limestone was encountered at a depth of 52 m and was present to the bottom of the well, which was drilled to 94 m. Minimal coherent events can be observed, in the upper 100 m of the P-wave data. A continuous event at ~ 90 m depth is present in the S-wave as a result of more competent rock north of the mine. Events in P- and S-wave stacked sections can be correlated to the limestone units present in the well data. Both data sets are increasing in consistency moving from the mine are north into more competent rock (Figure 58).

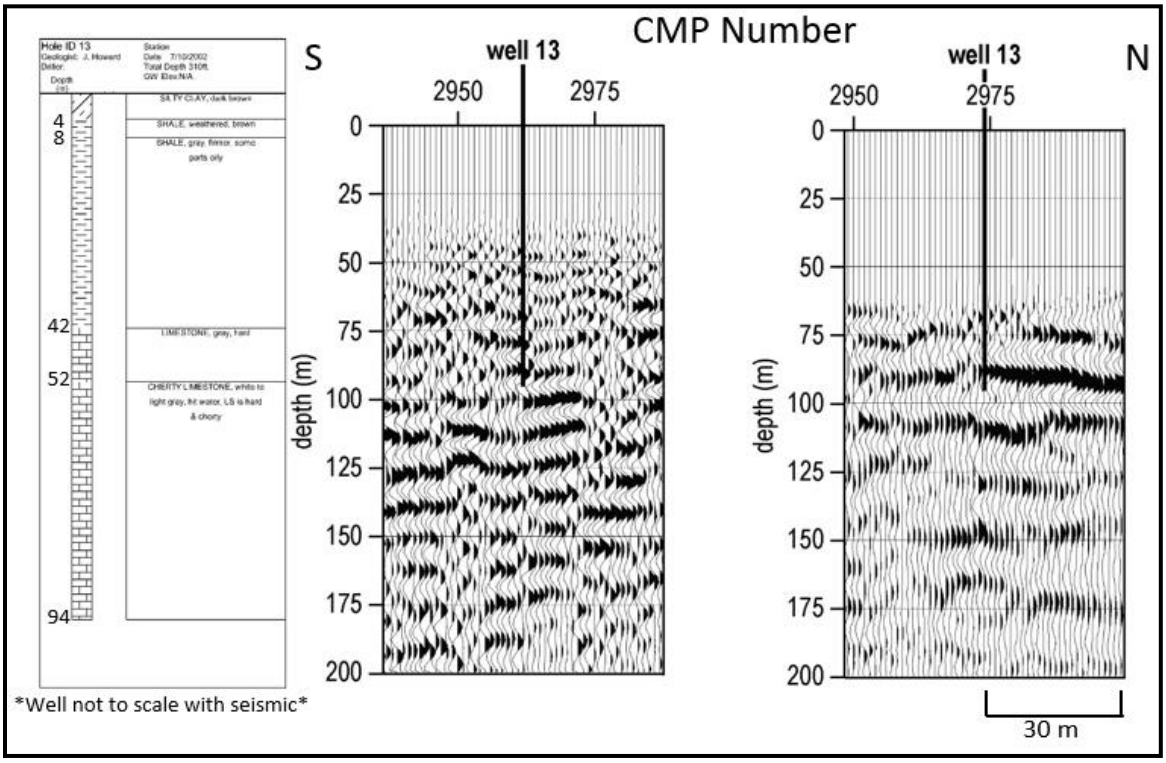

Figure 58: Correlation of Well 13 (left) vs P-wave (middle) and S-wave (right) seismic.

Well 14

Three voids were encountered in Well 14 that were less than 2 m thick. These voids were between 0.5 and 2 m and were separated by cherty and hard limestone layers. The small voids observed in this well are not related to the mine works. These small voids are likely the result of dissolution of the limestone unit along faults or fractures. Water was present in the limestone units in many of the other wells, so dissolution of some of these units is expected. No coherent reflection events within the upper 100 m stacked in on the seismic section in proximity to Well 14 on P-wave data. This could be due to the structurally disturbed nature of the subsurface here which has led to the intrusion of water allowing for dissolution of these limestone units (McKnight and Fischer, 1970). The S-wave data possesses two high amplitude reflections that extended north to the end of the survey. These shear wave reflections align well with the coherent P-wave reflections north of Well 14, and are likely associated with the varying limestone units within the Boone Fm. The comparative increase in reflections suggests more competent rock is present from the mine, north to the vicinity of the Miami trough (Figure 59).

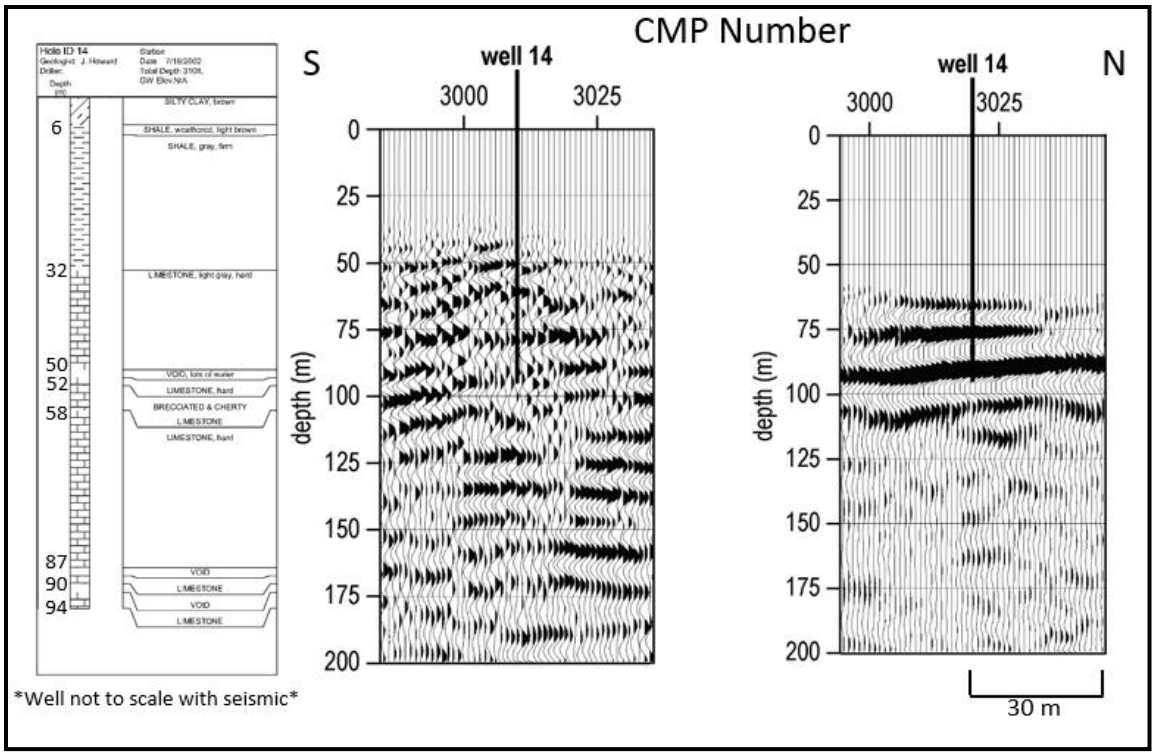

Figure 59: Correlation of Well 14 (left) vs P-wave (middle) and S-wave (right) seismic.

Well Summary

Seismic data interpretations were drastically improved and refined through incorporation of these well data. Understanding and extrapolating the mine's location between drill confirmed encounters using the seismic data was a crucial component in this study. It also improved the understanding of the subsurface geology as inferred from the reflection character. Key to confident interpretations of these data was the lateral consistency of the limestone – shale contact. With minimal to no dip as correlated across all 14 Wells, flat lying reflections were expected and confirmed as real on the CMP stacked sections. The lack of signal in isolated locations along the P-wave section was attributed to the highly altered subsurface rock and bed terminations associated with the mineralized zone and the location of the mine on lithological logs. This interpretation correlated to the mine geometry and consistent diffractions. The high amplitude and laterally consistent reflections in the S-wave CMP stack correlated extremely well to mine voids identified in the well's lithological logs and the depth of the drill confirmed mine voids location. The correlation of these three data sets allowed an approximation of mine location between borings to be determined and the potential highway impact defined.